

Kirigami Technique for the Design of Printed Flexible Capacitive Sensors

by

Laura MORELLI

THESIS PRESENTED TO ÉCOLE DE TECHNOLOGIE SUPÉRIEURE
IN PARTIAL FULFILLMENT FOR THE DEGREE OF
DOCTOR OF PHILOSOPHY
Ph.D.

MONTREAL, "NOVEMBER 26, 2024"

ÉCOLE DE TECHNOLOGIE SUPÉRIEURE
UNIVERSITÉ DU QUÉBEC



Laura Morelli, 2024



This Creative Commons license allows readers to download this work and share it with others as long as the author is credited. The content of this work cannot be modified in any way or used commercially.

BOARD OF EXAMINERS

THIS THESIS HAS BEEN EVALUATED
BY THE FOLLOWING BOARD OF EXAMINERS

Dr. Ricardo J. Zednik, thesis supervisor
Department of Mechanical Engineering - École de Technologie Supérieure

Dr. Ghyslain Gagnon, co-supervisor
Department of Electrical Engineering - École de Technologie Supérieure

Dr. Francois Blanchard, president of the board of examiners
Department of Electrical Engineering - École de Technologie Supérieure

Dr. Nicole R. Demarquette, member of the jury
Department of Mechanical Engineering - École de Technologie Supérieure

Dr. Eric J. Carleton , external independent examiner
Principal Technical Project Manager - Eurofins EAG Laboratories

THIS THESIS WAS PRESENTED AND DEFENDED
IN THE PRESENCE OF A BOARD OF EXAMINERS AND THE PUBLIC
ON "NOVEMBER 14, 2024"
AT ÉCOLE DE TECHNOLOGIE SUPÉRIEURE

ACKNOWLEDGEMENTS

I would like first of all to sincerely thank my thesis director, professor Ricardo J. Zednik, for choosing me for this project, providing me with guidance and support during all these years, and trusting my abilities throughout every step of the way. An important thank you, as well, goes to my co-director professor Ghyslaine Gagnon, for always being supportive and available to help whenever in need.

A special thanks to the co-authors of my articles, Arjun and Vinicius, for helping me out with some big steps of my work, and especially for giving me strength and mental support through the toughest obstacles of the last couple of years. In addition, I want to thank all the friends and the people met at ETS, either directly or indirectly involved in my project, for making these past four years such a memorable experience. A special mention goes to my dear friend, colleague, boss, personal advisor and supporter Maria, without whose help my PhD experience wouldn't have been as special and enjoyable.

A big big thank you to all my Montreal friends outside of university: the Italian gang, all the friends from the (many) gyms, the old and new friends, and all the people encountered during these years: those who left earlier, those who arrived late and those who stayed even just for a brief moment. You all made my years in Montreal a precious life experience that I will never forget. . . I will always keep you close to my heart.

Un immenso grazie a tutti gli amici, ai parenti, e alle persone care in Italia, che anche a distanza hanno saputo sostenermi e mi hanno sempre accolto a braccia aperte ad ogni mio ritorno. Un grazie speciale, ovviamente, alla mia migliore amica Ester, la mia supporter numero uno, capace di illuminare i miei momenti più bui con una semplice risata, anche da lontano.

Infine, e per questo più importante, il grazie più grande va alla mia famiglia: Mamma, Babbo e Giulia. Le persone senza la quale non sarei qui, grazie alla quale sono diventata la persona che sono oggi e ho raggiunto gli obiettivi che mi ero prefissata. Questo grande traguardo lo dedico a voi, *vi voglio bene*.

Étude de la technique de Kirigami appliquée à la conception de capteurs capacitifs flexibles

Laura MORELLI

RÉSUMÉ

Au cours de la dernière décennie, le domaine de la technologie flexible et portable s'est imposé comme un point central de la recherche et de l'innovation, captivant l'intérêt des scientifiques, des ingénieurs et des professionnels de la santé. Les capteurs et l'électronique flexibles représentent un tournant prometteur dans divers domaines tels que la surveillance médicale, l'interaction homme-machine et le suivi des performances sportives, entre autres.

Les capteurs capacitifs constituent une technique prometteuse de détection non invasive qui permet la surveillance ubiquitaire et à long terme des signaux biopotentiels sans nécessiter de préparation technique et de cadre médical. L'exploitation de l'électronique flexible et conformable pour la détection capacitive est une option prometteuse pour améliorer l'intégration transparente de ces types de capteurs dans la vie quotidienne du patient, tout en améliorant également les performances et la qualité de la technique de détection.

Dans ce travail, nous proposons la conceptualisation, la réalisation et la caractérisation d'une nouvelle méthode de conception d'électronique hybride flexible pour les capteurs capacitifs, en utilisant le Kirigami. La technique artistique japonaise est explorée comme une technique additive et facile à mettre en œuvre appliquée à l'électronique imprimée pour améliorer la flexibilité et la conformabilité des électrodes capacitives et permettre l'intégration cohérente de composants rigides sur le capteur sans affecter sa flexibilité.

Tout d'abord, différentes versions de conceptions Kirigami ont été réalisées sur une électrode capacitive imprimée. Leur comportement capacitif a été évalué lorsqu'ils étaient appliqués à des plaques secondaires non plates de dimensions diverses, et comparés à l'électrode imprimée non coupée correspondante. Un modèle analytique pour décrire le comportement capacitif de l'électrode flexible Kirigami a ensuite été défini, servant d'outil efficace pour comprendre l'effet de la structure Kirigami sur l'amélioration de la conformabilité, et par conséquent les performances capacitives, de l'électrode.

La structure de capteur nouvellement conçue est examinée dans ses caractéristiques électriques les plus importantes : capacité de couplage capacitif, amplitude de transmission du signal et fréquence de coupure. Son comportement en réponse aux artefacts de mouvement les plus courants a été évalué : l'application du capteur sur des corps de formes et de dimensions différentes, et avec différentes pressions appliquées sur le dessus ont été testées, afin de mesurer les variations du signal requis dans les différentes situations.

Le comportement triboélectrique du capteur a également été étudié. Le cas où le capteur se détache verticalement d'un corps non plat a été reproduit, et l'effet particulier de la flexibilité du capteur sur la tension triboélectrique résultante a été mesuré. Enfin, le comportement complexe

VIII

a été examiné et un modèle analytique a été défini, qui constitue un outil puissant pour aider à la compréhension générale du comportement triboélectrique des capteurs flexibles.

Mots-clés: Kirigami, Capteurs Capacitifs, Électronique Flexible

Kirigami Technique for the Design of Printed Flexible Capacitive Sensors

Laura MORELLI

ABSTRACT

In the past decade, the field of flexible and wearable technology has emerged as a focal point of research and innovation, captivating the interest of scientists, engineers, and healthcare professionals alike. Flexible sensors and electronics represent a promising turning point in various fields such as healthcare monitoring, human-computer interaction, and sports performance tracking, among others.

Capacitive sensors are a promising non-invasive sensing technique that enables ubiquitous and long-term monitoring of biopotential signals without the need for technical preparation and medical settings. The exploitation of flexible and conformable electronics for capacitive sensing is a promising option to improve the seamless integration of these types of sensors into the patient's everyday life, while also improving the performance and quality of the sensing technique.

In this work we propose the conceptualization, realization, and characterization of a novel Flexible Hybrid Electronics design method for capacitive sensors, using Kirigami. The Japanese artistic technique is explored as an additive, easy-to-implement technique applied to Printed Electronics to improve the flexibility and conformability of capacitive electrodes and allow the coherent integration of rigid components on the sensor without affecting its flexibility.

First, different versions of Kirigami designs were performed on a printed capacitive electrode. Their capacitive behavior was evaluated when applied to non-flat second plates of diverse dimensions, and compared to the corresponding non-cut printed electrode. An analytical model to describe the capacitive behavior of the Kirigami flexible electrode was then defined, serving as an effective tool to understand the effect of the Kirigami structure on the improved conformability, and consequently the capacitive performance, of the electrode.

The novel designed sensor structure is examined in its most important electrical characteristics: capacitive coupling ability, signal transmission amplitude, and cutoff frequency. Its behavior in response to the most common motion artifacts was evaluated: the application of the sensor to bodies of different shapes and dimensions, and with different pressures applied on top were tested, in order to measure the variations of the required signal in the diverse situations.

The triboelectric behavior of the sensor was also investigated. The case of the sensor detaching vertically from a non-flat body was replicated, and the peculiar effect of the flexibility of the sensor on the resulting triboelectric voltage was measured. Finally, the complex behavior was examined and an analytical model was defined, which constitutes a powerful tool to help the general understanding of the triboelectric behavior of flexible sensors.

Keywords: Kirigami, Capacitive Sensors, Flexible Electronics

TABLE OF CONTENTS

	Page
INTRODUCTION	1
0.1 Context	1
0.2 Research Problem	2
0.3 State of the Art	3
0.4 Thesis Objectives	4
0.5 Methodology	5
0.6 Thesis Outline	6
 CHAPTER 1 LITERATURE REVIEW	 9
1.1 Capacitive Sensing	9
1.1.1 Contactless Capacitive Sensor	11
1.1.2 Effect of the Capacitance on the Signal Acquisition	13
1.1.3 Effect of the Capacitance on the Frequency Response	13
1.2 State of the Art	15
1.2.1 Importance of Flexibility	15
1.2.1.1 Flexibility and Effects on Area	16
1.2.1.2 Uniformity of the Measurements and Reduced Motion Artifacts	17
1.2.1.3 Effects of Area on the Measurements	18
1.3 Printed Electronics and Flexible Hybrid Electronics	19
1.4 Flexible Structures by Surface Patterning: Kirigami	21
 CHAPTER 2 METHODOLOGY	 23
2.1 Sensor Prototype Fabrication	23
2.1.1 First Phase: Kirigami Electrode	23
2.1.2 Second Phase: Flexible Hybrid Kirigami Sensor	24
2.2 Characterization Methods	26
2.2.1 Resistive Measurements	26
2.2.2 Capacitive Measurements	26
2.2.3 Electrical Characterization	27
2.2.4 Triboelectric Measurements	28
2.2.5 Mechanical Reliability Test	28
2.3 Data Analysis and Modeling	29
 CHAPTER 3 FLEXIBLE CAPACITIVE KIRIGAMI ELECTRODE: EXPERIMENTAL INVESTIGATION AND ANALYTICAL MODEL	 31
3.1 Introduction	33
3.2 Materials and Fabrication	36
3.3 Analytical Model	39
3.3.1 Level 0	39

3.3.2	Level 1, 2 and 3	44
3.4	Experimental Set Up	46
3.5	Results and Discussion	47
3.6	Conclusions	52
CHAPTER 4	PRINTED HYBRID CAPACITIVE KIRIGAMI SENSOR: ENHANCING FLEXIBILITY AND CONFORMABILITY FOR IMPROVED MOTION ARTIFACTS	55
4.1	Introduction	57
4.2	Materials and Methods	62
4.2.1	Kirigami Electrode and Connecting layers	62
4.2.1.1	Printing Phase:	62
4.2.1.2	Laser Cutting Phase	63
4.2.2	Analog Front-End (AFE)	65
4.2.3	Experimental Set Up	66
4.3	Results	70
4.3.1	Capacitive Measurements	70
4.3.2	Electrical Measurements	71
4.4	Discussions	74
4.5	Conclusions	77
CHAPTER 5	ANALYTICAL MODELING AND EXPERIMENTAL VALIDATION OF TRIBOELECTRIC BEHAVIOR IN KIRIGAMI FLEXIBLE CAPACITIVE SENSORS	79
5.1	Introduction	81
5.2	Analytical Model	83
5.2.1	Phase 1: Full contact	85
5.2.2	Phase 2: Gradual loss of contact	86
5.2.3	Phase 3: Completely detached	89
5.2.4	Analytical Model	90
5.3	Materials and Methods	91
5.4	Experimental Results and Discussion	94
5.5	Conclusions	100
CONCLUSION AND RECOMMENDATIONS		103
LIST OF REFERENCES		109

LIST OF TABLES

	Page
Table 1.1 Table of frequencies and amplitude values for different types of biosignals.	14
Table 3.1 Comparison of total area and theoretical capacitance for the different hierarchical levels	37
Table 3.2 Different analytical model parameters for the different hierarchical levels	46
Table 3.3 Error Between Analytical Model and Measured Values	49
Table 4.1 Examples of other research groups employing FHE to implement flexible capacitive sensors for biopotential monitoring, with relative sensor characteristics.	60
Table 4.2 Average measured coupled capacitance of both the Kirigami sensor and the equivalent rigid sensor, when applied to second plates of different curvatures.	70
Table 5.1 Comparison of integrated area under plots for both the plotted analytical model and experimental values	97

LIST OF FIGURES

		Page
Figure 1.1	Contactless Capacitive Biosensing	12
Figure 1.2	Simplified Electrical Model	13
Figure 1.3	Effect of mechanical stress on material dimensions	17
Figure 2.1	Electrode samples showing the four different Kirigami hierarchical structures.	24
Figure 2.2	Sensor Production Steps: a) CAD design of kirigami electrode layer and connecting layer; b) printing and laser cut result of the electrode layer and connecting layer; c) schematic representation of analog front-end of the sensor; c) final sensor appearance, with PCB and printed layers interconnected to each other.	25
Figure 2.3	Electrical measurements setup: a) second plate placed on top of the sensor, a single frequency (1 Hz) signal from the signal generator is injected into the second plate, acquired by the sensor and analyzed on the oscilloscope; b) schematic representation of sensor position on the sponge sample holder; c) second plates utilized for the measurements, and corresponding curvatures.	27
Figure 2.4	Measurement setup: a) electrode placed on a sponge holder, aluminum second plate fixed to a robot arm and placed on top of the electrode. The second plate surface was covered by a Kapton HN tape layer to reduce the charge affinity between the two surfaces. A signal generator injects a sinusoidal signal in the aluminum second plate, which is capacitively transmitted to the sensor and observed on the oscilloscope. b) Sensor placement under the second plate. c) equivalent graphic representation of sensor for comparison against analytical model.	29
Figure 3.1	Electrode samples showing the four different Kirigami hierarchical structures.	37
Figure 3.2	Process steps for the realization of printed Kirigami electrode.	38
Figure 3.3	Analytical model variables: α is the angle formed between the two non-contact sides, R_l is the contact-area portion radius and R_2 is the total radius, corresponding to the electrode half-length.	40

Figure 3.4	Capacitive Measurements Setup: a) electrode placed on a sponge sample holder and subjected to a constant 2 kg-force weight. The weight is hanging on top of the sample holder, fixed by a wooden structure and controlled by a hanging scale. The Impedance Analyzer is connected to both the conductive aluminum hemisphere and to the conductive silver electrode; b) graphical representation of the hemisphere-electrode measurement setup.	41
Figure 3.5	Blue ink print of Level 0 sample when applied to the hemisphere of $d = 6.3$ cm	42
Figure 3.6	Comparison between graphic representation as used for the analytical model and blue ink print, when applied to the hemisphere of $d = 6.3$ cm, $d = 5.5$ cm, and $d = 4.5$ cm. The dark blue area represents the contact area. Ink print test was repeated on three different samples for each Level and diameter, the figure shows one example of the three for each case.	45
Figure 3.7	Average Capacitance	47
Figure 3.8	Comparison of analytical capacitive model for all different levels, as a function of percentage of non-contact area.	48
Figure 3.9	Comparison between analytical capacitive model and measured values for all different levels, as a function of the percentage of non-contact area. The average values of measured capacitance for all levels, for each diameter, are shown as single points.	50
Figure 3.10	Comparison of non-contact capacitance for all levels of hierarchy, as a function of percentage of total contact-area. The estimated values of non-contact capacitance are shown as single points.	51
Figure 4.1	Laser-cut AutoCad design for the two different layers: a) the Kirigami electrode pattern, where the sets of hierarchical cuts are represented by $l_1 = 20$ mm (in red), $l_2 = 12$ mm (in blue), $l_3 = 4.5$ mm (in green), and the hinges by $\delta = 1.5$ mm; b) the closed-loop Kirigami connecting layer, with cuts of respectively $k_1 = 36$ mm and $k_2 = 29$ mm, distanced $\gamma = 3$ mm from each other.	64
Figure 4.2	Printed layers after laser cut: a) the Kirigami electrode layer (Kapton substrate and printed silver electrode covered by six layers of insulating ink, two circles of silver were left uncovered to allow electrical connection with the connecting layer); b) the closed-loop Kirigami connecting layer (Kapton substrate and printed silver, two	

	holes surrounded by spirals were cut through, to allow electrical and mechanical connection with the electrode layer).	66
Figure 4.3	Simplified electrical model of Analog Front-End: V_{in} is the signal acquired by the electrode, C_e is the coupled capacitance between the sensor electrode and the second plate, V_b and R_b are the bias voltage and resistor, $U1$ is the op-amp connected in a buffer configuration and V_{out} the resulting acquired signal.	67
Figure 4.4	(a) Multilayer Structure: the four corners of the Kirigami Electrode and Kirigami Connecting layers are glued together to allow a mechanical connection without affecting the Kirigami electrode structure; at the same time the central point of the two spirals at the center of the Connecting Layer are electrically connected to the center of the Electrode Layer by conductive paste; on the other side, the AFE is pasted on the silver, non-cut side of the Connecting Layer by conductive paste, ensuring both good electrical and mechanical connection with the flexible layers, without limiting the respective flexibility. (b) Final Sensor Structure: top view of rigid circuit board connected, on the bottom, to the two flexible printed Kirigami layers; side view of the sensor in its relaxed state; side view of the sensor when the electrode layer is bent.	68
Figure 4.5	Electrical measurements setup: a) second plate placed on top of the sensor, a single frequency (1 Hz) signal from the signal generator is injected into the second plate, acquired by the sensor and analyzed on the oscilloscope; b) position of the sensor on the sponge holder, with the Kirigami electrode showing on top, before the application of the second body on it; c) schematic representation of sensor and second plate setup during the measurements.	69
Figure 4.6	Measured coupled capacitance, for different second plate curvature, of Kirigami flexible sensor with weights of 1.1, 2.2 and 3.3 kgf applied on top of each second plate.	71
Figure 4.7	Measured amplitude variations of the acquired signal, for different second plate curvatures and different weights applied, comparing the performance of the Kirigami flexible sensor against the rigid sensor.	72
Figure 4.8	Measured cutoff frequency variations of the acquired signal, for different second plate curvatures and different weights applied, comparing the performance of the Kirigami flexible sensor against the rigid sensor.	73

Figure 4.9	a) Measured amplitude variations of the acquired signal, before and after 100 bending cycles, for different second plate curvatures at 1.1 kgf applied; b) Mechanical bending test setup: 100 bending cycles at 60 degrees of bend.	74
Figure 5.1	Transversal movement dynamic: on top the three phases of movement as seen from the side; on the bottom the view from the top of the electrode surface covered by the second plate.	86
Figure 5.2	Capacitive model variables for a sphere-electrode case: a) graphic representation of spherical second plate detaching from the flexible electrode, with corresponding variables; b) schematic of contact and non-contact areas on the electrode surface, as measured in (Morelli, Gagnon & Zednik (2023)).	90
Figure 5.3	Measurement setup: a) electrode placed on a sponge holder, aluminum second plate fixed to a robot arm and placed on top of the electrode. The second plate surface was covered by a Kapton HN tape layer to reduce the charge affinity between the two surfaces. A signal generator injects a sinusoidal signal in the aluminum second plate, which is capacitively transmitted to the sensor and observed on the oscilloscope. b) Sensor placement under the second plate. c) equivalent graphic representation of sensor for comparison against analytical model.	92
Figure 5.4	Sensor Production Steps: a) CAD design of kirigami electrode layer and connecting layer; b) printing and laser cut result of the electrode layer and connecting layer; c) schematic representation of analog front-end of the sensor; c) final sensor appearance, with PCB and printed layers interconnected to each other.	93
Figure 5.5	Recorded signal at the sensor output during vertical movement of the second plate, using a robotic arm, at three different available speeds: 1.7 mm/s, 3.4 mm/s and 8.5 mm/s. Each curve exhibits the same characteristic features, which correspond to the different phases of the movement. For the fastest speed of 8.5 mm/s the phases are highlighted in the figure: (A) indicates Phase 1, where the electrode is still completely attached but slowly losing pressure; (B) is Phase 2, when the electrode gradually loses contact with the second plate; (C) corresponds to Phase 3, when the two surfaces are completely detached and the sensor signal is slowly going back to zero.	95

Figure 5.6	Analytical model of flexible capacitive sensor detaching from a spherical surface: a) shows the voltage $V_{tribo}(t)$ caused by the isolated triboelectric effect; b) corresponds to the capacitance variation $C_e(t)$; c) corresponds to the combined effect of both $V_{tribo}(t)$ and $C_e(t)$ as a voltage at the sensor input.	98
Figure 5.7	Comparison of experimental and analytical results: on the left the measured voltage at the sensor output, translated to have the start of phase 2 coinciding with second 1; on the right the simulated voltage found the sensor input at the beginning of phase 2 of the analytical model.	99
Figure 5.8	Superimposition of the measured triboelectric voltages: the three curves have been divided by their respective speeds and their x-axes expanded accordingly, exhibiting matching shape and dimension.	100

LIST OF ABBREVIATIONS

AFE	analog front-end
ECG	electrocardiogram
EEG	electroencephalogram
EGG	electrogastrogram
EMG	electromyogram
EOG	electrooculogram
FHE	flexible hybrid electronics
MAs	motion artifacts
PCB	printed circuit board
PE	printed electronics
SNR	signal-to-noise ratio

INTRODUCTION

0.1 Context

The fast development of customer electronics in the last 30 years changed and improved people's lives in every aspect of their daily routines: from physical work, computing, communication, and health and medicine applications (Bryzek, 1996; Mukhopadhyay, Suryadevara & Nag, 2022). The fast societal progress and electronic advancement demand always more performing, smaller, and non-invasive devices that can be easily incorporated on any surface and be compatible with different materials and organisms (Lee, Cho & Kim, 2024; Wang, Hu, Wang, Chen, Feng, Wang, Ling & Huang, 2020a).

The development of new materials, processes, sensing techniques, and applications is increasingly focusing on the creation of novel devices that are flexible, stretchable, and can be applied to any curved surface (Corzo, Tostado-Blázquez & Baran, 2020; Gao, Ota, Kiriya, Takei & Javey, 2019; Harris, Elias & Chung, 2016).

Implementing flexible electronics and devices requires most of the components involved to be flexible. Among these, flexible dielectric capacitors are especially important devices, not only for their inclusion in electronic circuits but also as essential components for energy storage, displays, and sensors (Kim, Lee & Yun, 2011; Li, Torah, Beeby & Tudor, 2012; Liang, Liu, Shen, Lu, Ma, Lu, Lou & Jia, 2019; Yu, Yu, Zhou, Zou & Liu, 2019).

One particularly interesting application of flexible capacitor technology is its use as a capacitive sensor for biopotential acquisition (Bronzino, 2006; Kaniusas, 2019; Lee, Heo, Lee, Lim, Kim & Park, 2014): its sensing principle is based on the capacitive coupling between one single-sided capacitor plate, the electrode, and the body, representing the other side of the capacitor. In this configuration the electrophysiological signal coming from the patient's body

causes a charge displacement on the electrode surface, creating a time-varying electrical current equivalent to the signal coming from the body (Kaniusas, 2019).

SIG.NUM Preemptive Healthcare Inc. is a Montreal-based start-up company working on the development and commercialization of an innovative contactless and automated technology for both short- and long-term electrocardiogram (ECG) acquisition. At the beginning of 2020, the company was taking a step toward the commercialization of a capacitive sensor array composed of multiple rigid sensors that could easily be incorporated on rigid or semi-soft surfaces, such as chairs, car seats, hospital beds and mattresses, for the ubiquitous and long-term monitoring of ECG signal. Initially, this research project was born as a collaboration with SIG.NUM, and the main objective of the thesis was to work on the design of the electrode side of the single sensor, to improve the capacitive coupling with the body and therefore the performance of the sensing system. The arrival of COVID-19 forced a stop to the collaboration, and the project continued independently to work on the design development of contactless capacitive sensors for electrophysiological signals, without uniquely focusing on the specific SIG.NUM Sensing System.

0.2 Research Problem

In the particular case of capacitive sensors, independently of their specific application, making the electrodes flexible allows for easier implementation on non-rigid, curved surfaces and better conformability to the patient's body, improving some of the major shortcomings of the current technology (Lee *et al.*, 2014). Most recent works concern the formulation and fabrication of novel materials and processes aimed at improving the flexibility to replace the traditional solid-state elements used in the composition of an electrode. This type of approach, while allowing for a certain degree of flexibility that varies depending on the materials used, still presents many downsides caused by the stress induced in the material when bent or stretched, as well as by the variation in dimensions and non-uniformity of measurements (Ohring, 2002).

Being directly dependent on its geometry, capacitor characteristics are significantly affected by dimension variations when subjected to stress and deformations. While for many applications these problems can be overlooked and easily solved by post-processing techniques, in the particular case of contactless capacitive sensing the acquired signal properties are directly affected by this variability, resulting in poor performances of the sensor and erroneous reading of the signal.

0.3 State of the Art

The current state of the art presents extensive works that focus on improving the several limitations of capacitive sensors: introducing flexibility is a crucial aspect for improving the conformability of the electrode to the target body, maximizing the effective established capacitance and minimizing some common motion artifacts (Lee *et al.*, 2014; Lessard-Tremblay, Weeks, Morelli, Cowan, Gagnon & Zednik, 2020).

Printed electronics has emerged as a promising solution to fabricate cost-effective electronic circuits and components on flexible substrates, utilizing alternative techniques such as inkjet printing, screen printing, and aerosol jet printing. Still in development, it presents several shortcomings from both the mechanical (materials flexibility, fatigue and creep, printing resolution) and electronic (low performance compared to solid-state devices) point of view (Hussain & El-Atab, 2020; Khanna, 2019).

Flexible Hybrid Electronics constitute a valid alternative that allows the seamless integration of traditional rigid electronics on flexible printed substrate, maintaining the high performance of the first, while allowing the flexibility and conformability of the latter. The combination of rigid and flexible components still faces many challenges, primarily due to the robustness of connections between the two sides (Hao, YongAn & ZhouPing, 2022; Tuncel, Bhat & Ogras, 2020; Yan, Chen & Liu, 2024).

Kirigami, the Japanese art of paper cutting, has already been employed in different engineering applications, enabling the fabrication of flexible, stretchable, and constant area devices starting from printed electronics precursors (Brooks, Chakravarty, Ali & Yadavalli, 2022; Li, Kim, Zhou, Mills, Flewellin & Jur, 2019; Yang, Zhang, Liu, Yu, Wei & Hu, 2018). Yet not well-explored in the field of capacitive sensing, Kirigami represents a promising approach to incorporate in flexible hybrid electronics devices, improving flexibility and conformability, and at the same time decreasing the stress affecting the different components of the device.

0.4 Thesis Objectives

The objective of this thesis is the realization of a novel electrode design for contactless capacitive sensing that is flexible, conformable to any surface, and more robust to motion artifacts. In particular, the new design will focus on the modeling and fabrication of an innovative structured pattern for the electrode that will allow the device to:

- Keep its thickness and surface area constant even when stretched, bent, or subjected to other types of stress. The patterning of the surface will be designed specifically in a way that even when extended in any direction, the total area of the surface won't change. As the flexibility does not come from the material properties but from the electrode structure, the materials involved won't be subjected to excessive stress, keeping their dimension and conductive/dielectric properties unvaried when under deformation.
- Increase its conformability to non-flat surfaces, allowing the sensor to maintain a constant coupled capacitance independently from where it will be applied. This will increase uniformity in the measurements and will help reduce motion artifacts in the signal.

To meet the defined objectives, Kirigami technique will be employed for the ideation of a novel electrode and sensor design. The thesis's main objective can be subdivided into the following sub-objectives, pursued in the different steps of the research project:

- definition of a novel electrode structure based on Kirigami,
- definition of a novel complete sensor structure to allow the integration of the new electrode onto traditional rigid devices,
- evaluation of novel electrode and sensor performances, taking into consideration the most important electrical characteristics mentioned in the literature review,
- analysis of most recurring motion artifacts, comparing the flexible Kirigami structure to non-Kirigami one,
- definition of analytical models to explain and describe the behavior of the novel-designed sensor.

0.5 Methodology

The methodology applied in the different steps of the project has been specifically selected with the above-mentioned objectives in mind. The chosen techniques and methods can be identified in two subgroups, reflecting their main scope in the project: sensor fabrication techniques and sensor characterization methods.

Printed electronics was selected as fabrication technique for the development of the flexible electrode and the flexible multilayer structure connecting the flexible and rigid sides of the sensor. For the introduction of Kirigami designs on the printed layers, laser cutting technique was employed, which allowed an easy-to-implement method to incorporate the innovation of Kirigami techniques on any printed device.

Electrical and Mechanical characterization were performed on the Kirigami electrode, in the first phase of the project, and on the Kirigami sensor prototype, in the following phase. The characterization techniques used were specifically selected, and tailored to the particular case

of the Kirigami flexible sensor, to evaluate the most pivotal characteristics of the sensor, independently of the final application of the device.

0.6 Thesis Outline

With the scope of illustrating and explicating the motivations, the development and the obtained results of the carried-out research project, the thesis is divided into six main chapters:

The first chapter reports the literature review carried out at the beginning of the project and throughout its development. It aims to provide a general introduction to the working principle of the studied devices, followed by an overview of the state of the art of the technology.

The second chapter summarizes the methodology choices for the different stages of the project, including the fabrication techniques and characterization methods.

The three following chapters correspond to the three main steps of the project carried out in the last four years, which are reported as scientific publications.

The third chapter focuses on the development and characterization of a novel design approach for flexible capacitive electrodes based on the Kirigami technique. The flexibility of the electrode derives from the mechanical structure of the novel design, allowing it to adapt easily to any body shape and maintain its area and thickness constant even under different stress conditions, while not being dependent on the materials used.

In the fourth chapter, the electrode is incorporated into a complete sensor structure, composed of the sensing electrode and a traditional rigid PCB. A multilayer printed structure is introduced, to allow the integration of the flexible layer on the PCB without affecting its flexibility and conformability. The hybrid flexible sensor is then tested when applied to spherical bodies of different dimensions and under different weights, to measure its sensitivity to some of the most

frequent motion artifacts, such as the ones caused by the non-conformity of capacitive sensors to non-flat surfaces, and by the pressure variations on the sensors.

In the fourth chapter, the behavior of the novel-designed sensor in the presence of triboelectricity is evaluated. The contact-mode triboelectric effect is reproduced in-lab, detaching a spherical second plate from the electrode in a vertical motion. The behavior of the flexible sensor is recorded, for different speeds tested, and analyzed. An analytical model is introduced, to physically describe the peculiar behavior of the flexible sensor compared to traditional rigid ones.

Finally, the last chapter provides the conclusions, summarizing the results and contributions of the work, and presenting some recommendations.

CHAPTER 1

LITERATURE REVIEW

This chapter summarizes the literature review carried out in the past years for the definition of the different phases of the project. First, a general introduction to how capacitors can be applied in the sensing field, describing the basics of contactless capacitive sensing and its properties. Following, a short review of the state of the art of the technology will be provided, introducing what steps have been taken to improve the performance of current sensors and what aspects still have to be perfected. Finally, the main objectives of the project are presented.

1.1 Capacitive Sensing

Capacitive sensing is a sensing technique traditionally based on capacitance variation as a measuring method for diverse types of signals: from pressure sensors and touch screens (Klein, Karpin, Kravets, Kolych, MacSweeney, Ogirko, O’Keefe & Walsh, 2019), flow sensors (Wissman, Sampath, Freeman, & Rohde, 2019; Wrasse, Bertoldi, Santos, Morales & Silva, 2019), displacement and proximity sensors (Anandan & George, 2017) to MEMs applications such as accelerometers (Keshavarzi & Hasani, 2019; Solai, Rathnasami & Koilmani, 2020).

One particularly interesting application of capacitor physics for sensing purposes is capacitive sensing of biopotentials coming from the skin (Kaniusas, 2019; Macy): biopotentials are electrical signals generated by the electrochemical activity of excitable cells inside the body, which can be found in the nervous, muscular and glandular systems of the body; when stimulated, excitable cells generate an action potential that can be externally sensed by non-invasive electrodes placed on the skin. In general, based on the working principle through which the biosignal is acquired, electrodes can be divided into two main categories (Kaniusas, 2019; Kim, Lee & Lee, 2014; Lim, Lee, Lee, Lee & Park, 2014; Taji, Shirmohammadi, Groza & Batkin, 2013):

1. *Wet electrodes:* This type of electrode requires the use of adhesive gel between the sensor and the skin. The gel creates a conductive path through which an electrical current can flow. Thanks to the gel, the electrode can be easily fixed on the body, preventing motion artifacts and producing an accurate signal. However, wet electrodes present some issues that prevent their use for long-term monitoring:

- They require skin preparation and medical assistance, hence they can only be used in a clinical environment.
- The gel can cause discomfort and irritation to the skin.
- The quality of the signal is negatively affected by the drying out of the gel over time.

2. *Dry electrodes:* In contrast with wet electrode type, dry electrodes do not use adhesive gel. Based on the sensing mechanism used, they can be differentiated into two main subfamilies of electrode: dry contact electrodes, working in direct contact with the skin, and dry insulated electrodes, which present a layer of insulation between the electrode and the body and thus work based on the capacitive coupling between the conductive surface and the skin, and no electrical current flow is present (Fu, Zhao, Dong & Wang, 2020).

The body surface and the electrode can be respectively considered as the two sides of a capacitor: the capacitance is established by the close vicinity of the two surfaces and no direct contact is needed. The signal can be potentially acquired even with a few layers of material in between the two sides. This family of electrodes is a promising substitute for long-term applications. In addition, the electrodes can be easily used by the patient even in non-medical settings, making them ideal for future implementation in ubiquitous sensing. However, they still presents some limitations (Lim *et al.*, 2014; Taji *et al.*, 2013):

- They work under the condition of very high impedance between the body surface and the sensor, for this reason, they are very sensitive to external noise.
- As they are not fixed to the patient body, motion artifacts in dry electrodes are significantly larger compared to gel-type electrodes.

- Depending on the relative position of the body on the sensor the effective area of the capacitive coupling can vary, decreasing the SNR and affecting the uniformity of the measurements.
- Rigid sensors can cause discomfort in the patient during long-term monitoring and have limited applications in soft or flexible surfaces for ubiquitous sensing.

1.1.1 Contactless Capacitive Sensor

In Fig.1.1 a schematic example of a capacitive sensor is portrayed. The device is composed of a conductive electrode, which senses the variation in the electric potential on the skin, a dielectric layer, to increase the established capacitance between the body surface and the electrode, and the analog front-end (AFE), which include a filter and pre-amplifier acting as an impedance transformer between the high impedance stage of skin-electrode coupling and the following amplifying stages (Lim *et al.*, 2014).

The resulting impedance between the electrode and the body surface tends to be extremely high, limiting the SNR. A simplified electrical model of the skin-electrode interface is represented in Fig. 1.2.

The relation between the signal present at the skin surface and the signal arriving at the pre-amplifier is given by the equation:

$$V_{amp}(\omega) = V_{skin}(\omega) \frac{R_i}{R_i + Z(\omega)} \quad (1.1)$$

Where R_i is the input resistance of the pre-amp and $Z(\omega)$ the skin-electrode impedance (Taji *et al.*, 2013). $Z(\omega)$ can be modelled as a parallel connection of a resistance R_s and the capacitance between the skin and the sensor C_s (Lim, Kim & Park, 2007; Taji *et al.*, 2013):

$$Z(\omega) = \frac{R_s}{1 + j\omega C_s R_s} \quad (1.2)$$

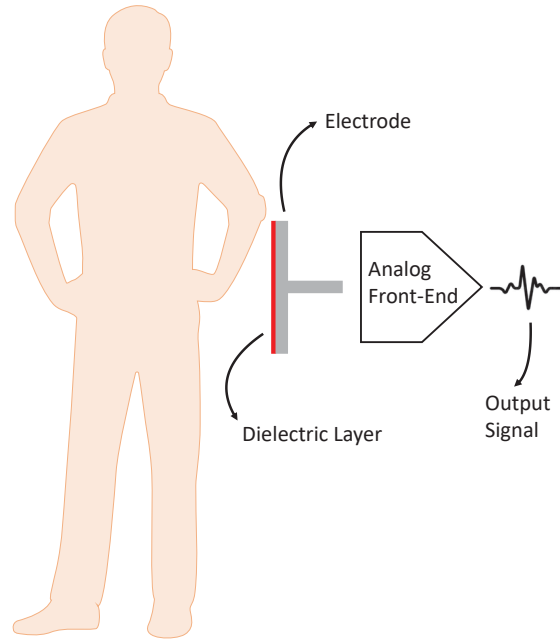


Figure 1.1 Schematic representation of a contactless sensor for electrophysiological signal acquisition.

R_s represents the resistance of the skin/electrode contact, while C_s is determined by:

$$C_s = \epsilon_0 \cdot \epsilon_r \frac{A}{d} \quad (1.3)$$

Where:

- ϵ_0 is the permittivity of free space and ϵ_r is the relative dielectric constant of the materials present between the two plates of the capacitor.
- d and A are, respectively, the distance between the two surfaces and total area of the sensor in contact with the skin.

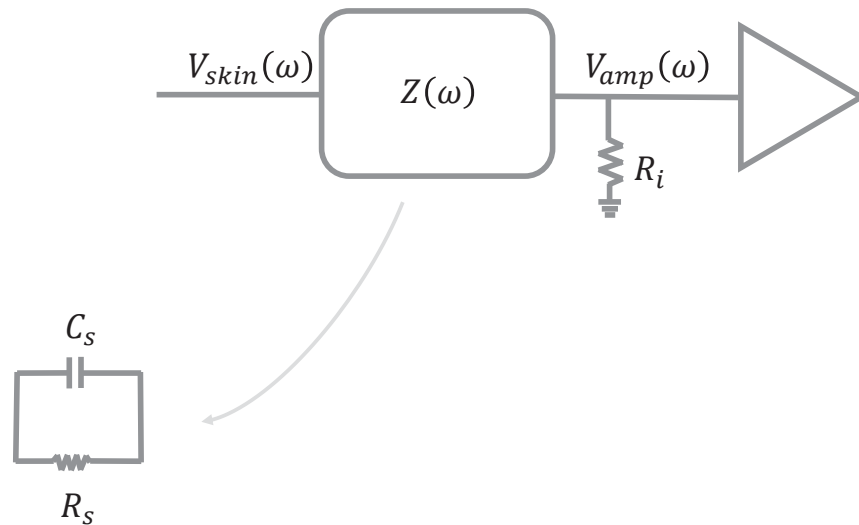


Figure 1.2 Simplified electrical model of skin-electrode interface.

1.1.2 Effect of the Capacitance on the Signal Acquisition

From the equation 1.1: the acquired signal arriving at the pre-amplifier is equivalent to the signal coming from the skin, reduced by a factor that is dependent on the total impedance $Z(\omega)$, and thus on R_s and C_s . As the R_s depends on several external factors and is not easy to control, the most effective way to minimize $Z(\omega)$ is by maximizing C_s . Given the definition of C_s in equation 1.3, there are different approaches to increase its value: working on the materials, to improve conductivity and dielectric permeability, or working on the geometry and flexibility, to increase the sensing area of the sensor establishing a capacitive coupling with the body, and reduce its distance from the skin.

1.1.3 Effect of the Capacitance on the Frequency Response

Increasing the capacitance value does not only affect the SNR. The total bandwidth of the signal is also strongly influenced by the capacitance. Considering a general sensor-amplifier system as

depicted in Fig. 1.2, its response in the frequency domain is limited in the lower part of the spectrum by the cut-off frequency, which can be defined as the frequency at which the system gain decreases by 3 dB. The cut-off frequency is dependent on the electrical parameters of the system as follows (Lee *et al.*, 2014; Lessard-Tremblay *et al.*, 2020):

$$f_c = \frac{1}{2\pi R_i C_s} \quad (1.4)$$

By increasing the capacitance the resulting cut-off frequency decreases. A low cut-off frequency value is crucial for lossless signal acquisition: in the case of biosignals, many of them present a bandwidth in the very lower frequency spectrum (Bronzino, 2006; Kaniusas, 2019). Some characteristic values are listed in Table 1.1.

The loss of information is not the only problem related to an inadequate cut-off frequency. While using a slightly higher cut-off, with the right filtering, usually results in a still legible and satisfactory signal output, it can also introduce artifacts in the recordings that may lead to erroneous signal interpretation (Berson & Pipberger, 1966; Driel, Olivers & Fahrenfort, 2021).

Table 1.1 Table of frequencies and amplitude values for different types of biosignals.

Biosignal	Bandwidth (Hz)	Amplitude (mV)
EMG	2 - 500	0.05 - 5
ECG	0.05 - 100	1 - 10
EEG	0.5 - 100	0.002 - 5
Respiratory Activity	0.12 - 0.5	-
EOG	DC - 100	0.0005 - 5
EGG	0.015 - 0.3	0.1 - 0.3

1.2 State of the Art

1.2.1 Importance of Flexibility

Most of the recent works on capacitive sensing focus on developing flexible electrodes that can be applied to different parts of the body improving the sensor performance and reducing the discomfort for the patient (Babusiak, Borik & Balogova, 2018; Babusiak *et al.*, 2018; Baek, Lee, Lim & Park, 2012; Bilent, Hong, Dinh, Martincic & Joubert, 2019; Chamadiya, Mankodiya, Wagner & Hofmann, 2013; Fuhrhop, Lamparth & Heuer, 2009; Kang, Merritt, Karaguzel, Wilson, Franzon, Pourdeyhimi, Grant & Nagle, 2006; Lee *et al.*, 2014; Lee, Sim, Kim, Lim & Park, 2010; Lessard-Tremblay *et al.*, 2020). The body is, in general, not a flat surface, and to ensure a good quality, precise and uniform measurement it is important for the electrode to conform at best to the body surface, and thus to be flexible and compliant.

Flexibility is a crucial aspect in the development of novel capacitive sensors for several reasons:

- Adapting to any body shape allows the whole surface of the sensor to establish a capacitive coupling with the body, maximizing the effective capacitance and consequently the SNR.
- Conformability also reduces the effect of motion artifacts, such as the one resulting from the movement of the body during respiratory activity. Motion artifacts represent one of the major problems of capacitive sensing, caused by the contactless nature of capacitive sensors (Lee *et al.*, 2014).
- By conforming evenly to different parts of the body the sensing area is ideally constant, regardless of the point of application of the sensor on the body. This allows a uniform signal acquisition, especially in multi-sensor array systems, which translates into reduced active filtering in the signal post-processing phase, and thus less susceptibility to data attenuation (Lessard-Tremblay *et al.*, 2020).

1.2.1.1 Flexibility and Effects on Area

Most works focus on the fabrication of novel flexible materials for the different parts of the electrode (electrode, dielectric layer, substrate). Many materials and composites have been developed which exhibit good electric or dielectric properties while being flexible (Baek, An, Cho, Park & Lee, 2008; Cai, Cizek, Long, McAferty, Campbell, Allee, Vogt, Belle & Wang, 2009; Chen, Zhang, Liang, Cao, Han & Feng, 2020; Chu, Tsai & Sun, 2012; Hasan, Rho, Kang & Ahn, 2010; Kim, Jung, Oh & Kim, 2017; Najafabadi, Tamayol, Annabi, Ochoa, Mostafalu, Akbari, Nikkhah, Rahimi, Dokmeci, Sonkusale, Ziaie & Khademhosseini, 2014; Wang, Guo, Li, Lu, Liu, Xiao, Zhang & Tong, 2012; Wu & Yao, 2017).

However, when applied to capacitive sensing the resulting flexibility is only partial and does not allow a complete conformability to the body (Lessard-Tremblay *et al.*, 2020).

In addition, many material properties change when subjected to mechanical stress such as stretching or bending, with the most significant change represented by the variability of dimensions (Ohring, 2002). Depending on its Poisson's ratio, when under stress a material tends to elongate in one direction while shortening in the others, as represented in Fig. 1.3.

Bending a flexible material, will necessarily elongate it in the bending axis direction and shrink it in the remaining directions. The described effect does not only result in a variation of area but also of thickness. Both area and thickness directly affect the value of the established capacitance, and while this might not be a significant problem for many applications, in capacitive sensing the sensing parameters are directly dependent on its capacitance value. If a sensor applied to a non-flat body changes its dimensions to conform to the sensed surface, consequently the amplitude, SNR and cut-off frequency will be altered, affecting the uniformity of the measurements.

Dimensions are not the only factors sensitive to change under mechanical stress: conductivity and dielectric properties might also be affected, varying depending on the type/degree of stress applied, increasing the variability of the acquisition (Cai *et al.*, 2009; Lessard-Tremblay *et al.*, 2020; Ohring, 2002). The ability to conform better to the body shape translates in a smaller

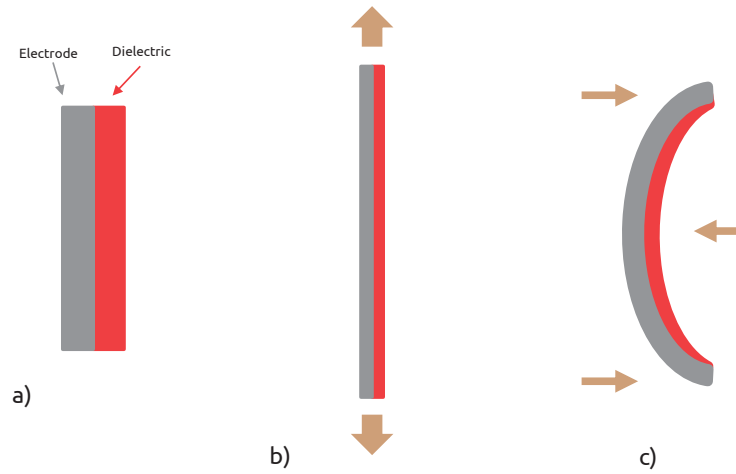


Figure 1.3 Schematic representation of the effect of mechanical stress on material dimensions: a) materials in a relaxed state, b) materials when stretched in one direction, c) materials when bent.

distance between the sensitive plate and the body, which results in a larger effective capacitance and thus a higher SNR ratio (Lessard-Tremblay *et al.*, 2020). It is thus important for the development of the next generation of capacitive electrodes to create a design that will allow the electrode to be flexible and whose flexibility does not derive from the stretching of the materials used, but from the mechanical structure of the electrode itself.

1.2.1.2 Uniformity of the Measurements and Reduced Motion Artifacts

A significant aspect usually overlooked in the development of flexible sensors is the uniformity of the measurements. While flexibility and surface area are important for good signal quality, the recordings also need to be consistent measurement after measurement, independently of the surface where the sensors are applied (Berson & Pipberger, 1966; Bragg-Remschel, Anderson & Winkle, 1982; Lee *et al.*, 2014).

For rigid or semi-rigid sensors, if positioned on different parts of the body, they usually present inconsistencies in coupled capacitance values, consequently affecting parameters such as SNR and frequency response, as explained in the previous paragraphs. The non-uniformity in the measurements is strictly related to the flexible properties of the sensor which can affect both the dimensions of the materials (Fig. 1.3) and the distance between the sensor surface and the body.

Variation of coupling surface does not only depend on the shape of the body part where the sensor is applied: on-site variations caused by the movement of the body during measuring, such as thoracic respiratory movements, variation of pressure, change in position and detaching of the body from the sensor surface are the prime cause of motion artifacts during signal acquisition. While some motion artifacts are more unpredictable than others, and therefore difficult to counteract, some of them can be mitigated by a good sensor design. A conformable electrode guarantees that, even when bent or stretched, the total area establishing a capacitive coupling with the body will ideally remain constant, and so will the effective capacitance.

1.2.1.3 Effects of Area on the Measurements

As can be deduced by (1.3), the larger the area the greater the capacitance and thus the better the performance of the sensor (Lee *et al.*, 2010). Not considering the effect, if present, of the dielectric material permittivity, the maximum value of capacitance that a sensor can achieve during coupling depends both on the ability of the sensor to adapt to the sensed surface, that is the flexibility, and on the total surface area of the electrode.

Depending on the specific application (i.e. the number of minimum electrodes required, the area to be covered, the system limits, and the cost) the perimeter of a single sensor might be fixed or subjected to constraints. It is therefore important for the single electrode to be conformable to any applied surface, to ensure no loss of coupled surface available.

1.3 Printed Electronics and Flexible Hybrid Electronics

The quest for flexible, lightweight, and cost-effective electrodes for capacitive sensing systems led to the research and development of alternative techniques to substitute the traditional bulky and solid-state technologies (Cruz, Rocha & Viana, 2018; Khan, Ali & Bermak, 2019). Printed electronics (PE) has emerged as a promising solution: by leveraging techniques such as inkjet printing, screen printing, and aerosol jet printing, PE enables the fabrication of electronic circuits and components on flexible substrates, plastics, paper, textiles, and traditional substrates (Avuthu, Gill, Sussman, Wable & Richstein, 2016; Cruz *et al.*, 2018).

Moreover, the scalable and cost-effective nature of PE, combined with the ability to rapidly prototype and customize electronic designs makes it a versatile and adapt to large-scale production technology for wearable health products (Jeerapan & Khumngern, 2023; Khan *et al.*, 2019).

PE is still a developing field of research, as the works found in literature still present several shortcomings, especially in their mechanical aspects, attributable to the properties of the materials used, the fabrication processes, and the design considerations (Hussain & El-Atab, 2020; Khanna, 2019). Some of the most common mechanical limitations are:

- **Material Flexibility and Conformability** - Functional inks and substrates do not always exhibit the flexibility required by the final application. This can lead to reduced mechanical robustness and durability, especially when subjected to bending or stretching cycles, as well as performance limitations of the final product.
- **Printed Feature Resolution** - The resolution of printed features, such as lines, traces, and electrodes, can affect the mechanical integrity of PE. Lower-resolution printing techniques may result in irregularities or discontinuities in conductive paths, leading to localized stress concentrations and potential failure points, especially under mechanical deformation.
- **Fatigue and Creep** - Repeated bending or stretching of flexible PE can induce fatigue and creep phenomena in the materials, resulting in gradual degradation of mechanical properties

over time. This can lead to delamination, cracking, or loss of conductivity in printed features, compromising device performance and longevity.

In addition, while significant steps have been made in the prototyping and production of flexible and stretchable passive electronic components and connections (Bonnassieux, Brabec, Cao, Carmichael, Chabiny, Cheng, Cho, Chung, Cobb, Distler, Egelhaaf, Grau, Guo, Haghighashtiani, Huang, Hussain, Iniguez, Lee, Li, Ma, Ma, McAlpine, Ng, Österbacka, Patel, Peng, Peng, Rivnay, Shao, Steingart, Street, Subramanian, Torsi & Wu, 2021; Mohammed & Kramer, 2017; Rim, Bae, Chen, Marco & Yang, 2016), the current PE industry is still not able to match the performance of solid-state inorganic electronics for most of the more-complex components and chips (Bonnassieux *et al.*, 2021; Chang, Facchetti & Reuss, 2017; Noh, Jung, Jung, Yeom, Pyo & Cho, 2015).

Flexible Hybrid Electronics

Flexible Hybrid Electronics (FHE) represents a sought-after alternative for the development of lightweight, conformable, and stretchable systems (Hao *et al.*, 2022; Tuncel *et al.*, 2020; Yan *et al.*, 2024): by seamlessly integrating the mechanical flexibility of flexible printed substrates with the high performance of traditional rigid electronics it promises significant advancements in developing wearable sensors that offer both comfort and performance. Compared to full PE, FHE constitutes a promising compromise between whole-flexible electronics and solid-state electronics, particularly in the field of healthcare applications, where the integration of flexible and rigid draws the most advantages for obtaining soft and conformable skin-device interfaces as well as fast and performant signal processing (Herbert, Kim, Kim, Lee & Yeo, 2018; Khan, Garg, Gui, Schadt, Gaikwad, Han, Yamamoto, Hart, Welte, Wilson, Czarnecki, Poliks, Jin, Ghose, Egitto, Turner & Arias, 2016; Lim, Kim, Qazi, Kwon, Jeong & Yeo, 2020).

Current FHE prototypes still present important challenges such as robust electrical connections between different materials and components, mechanical fatigue and failure over time, compatibility and long-term stability among diverse materials, limiting the widespread of FHE in

commercial products (Kim, Mahmood, Lee, Kim, Kwon, Herbert, Kim, Cho & Yeo, 2019; Liu, Shah & Kramer-Bottiglio, 2021; Poliks, Turner, Ghose, Jin, Garg, Gui, Arias, Kahn, Schadt & Egitto, 2016).

1.4 Flexible Structures by Surface Patterning: Kirigami

Kirigami is the traditional Japanese art of paper cutting which enables the shaping of complex 3D artistic structures by performing simple cuts on 2D paper sheets. The shape-adaptable technique is an excellent starting point for the fabrication of flexible, constant area devices (Ning, Wang, Zhang, Yu, Choi, Zheng, Kim, Huang, Zhang & Rogers, 2018; Zhai, Wu & Jiang, 2021): successful implementation of foldable and stretchable electric interconnections (Rogers, Someya & Huang, 2010), batteries (Song, Ma, Tang, Cheng, Wang, Krishnaraju, Panat, Chan, Yu & Jiang, 2014), solar cells (Tang, Huang, Tu, Liang, Liang, Song, Xu, Jiang, & Yu, 2014), foldable antennas (Nogi, Komoda, Otsukac & Suganumaa, 2013) and supercapacitors (Xu, Zverev, Hung, Shen, Irie, Ding, Whitmeyer, Ren, Griffin, Melcher, Zheng, Zang, Sanghadasa & Lin, 2018) have been demonstrated employing Kirigami. Such applications suggest Kirigami as a promising additive technique to help the evolution of FHE, improving the flexibility and conformability of current printed devices while providing increased degrees of freedom for the integration of rigid components on flexible substrates.

The flexibility and conformability of the overall Kirigami structure are induced by dividing the rigid material into rotating rigid sub-units, with the connections between these units acting as free rotational hinges. This allows macroscopic deformation to occur mainly through rotation of the sub-units, rather than by attempting to deform the rigid sub-units themselves, significantly increasing the flexibility of the whole structure while reducing the stress applied on the single sub-unit (Cho, Shin, Costa, Kim, Kunin, Li, Lee, Yang, Han, Choi & Srolovitz, 2014; Choi, Dudte & Mahadevan, 2019,2; Grima & Evans, 2000; Yang, Choi & Kamien, 2016).

Previous works made use of Kirigami technique to improve the stretchability and flexibility of electrodes for several applications, such as flexible batteries and supercapacitors, where

Kirigami structures helped achieve better capacitance stability when stretched (Diao, Woon, Yang, Chow, Wang, Lua & D'Arcy, 2021) and after being cyclically bent (Bao, Hong, Chen, Chen, Chen, Song & Fang, 2019). Single-sided Kirigami electrodes were also studied in the field of bio-sensing: multiple works employed Kirigami to improve the conformability of electrodes attached to the body (Brooks *et al.*, 2022; Li, Wang, Sun, Zhu, Liu, Tang & Xu, 2022), the increased conformability helped improve SNR, meeting high conductivity and stretchability (Gao, Elbaz, He, Xie, Xu, Liu, Su, Liu & Gu, 2018) and maintaining adhesion even under high degree of bending (Yang *et al.*, 2018). On the other hand, Kirigami capacitive electrodes are an interesting, yet not well-explored, approach to improving the flexibility and conformability of contactless devices without affecting their intrinsic characteristics.

CHAPTER 2

METHODOLOGY

In the present chapter, the methodology choices for the different stages of the project are described and justified. The techniques used are divided into two principal sections: fabrication techniques, used to produce and assemble the different parts of the sensor structure, and the characterization methods, specifically chosen to verify the mechanical and electrical advantages of the novel sensor design.

2.1 Sensor Prototype Fabrication

2.1.1 First Phase: Kirigami Electrode

In the first part of the project, the main focus was producing printed electrodes with different Kirigami structures, corresponding to different levels of hierarchy, to be compared against one another. Screen printing was chosen as fabrication method for this first phase, due to the simplicity of design and versatility of the process.

The basic printed electrode was composed of a dielectric substrate (Kapton HN, thickness of $125\text{ }\mu\text{m}$) and a conductive silver layer (LOCTITE EDAG 725A(6S54) E&C, Henkel). The conductive layer was printed by screen printing (Keko P200S - LTCC serigraphic printer) onto the dielectric substrate, and cured in an oven at $120\text{ }^{\circ}\text{C}$ for 25 minutes). The final electrode takes the shape of a square of $30\times 30\text{ mm}^2$, with a thickness of approximately $130\text{ }\mu\text{m}$.

The different Kirigami patterns were subsequently implemented on the electrode surface using laser cutting (Samurai UV Marking System — DPSS Lasers, Inc.). The final electrode samples are shown in Fig. 2.1.

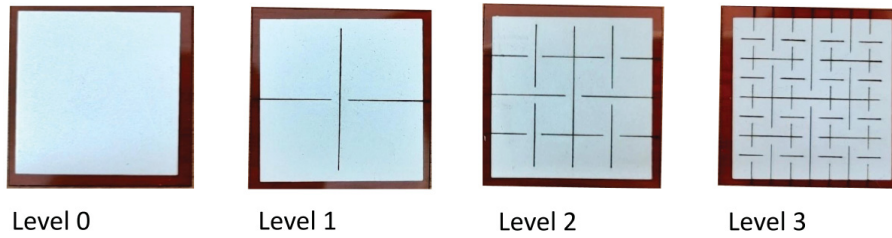


Figure 2.1 Electrode samples showing the four different Kirigami hierarchical structures.

2.1.2 Second Phase: Flexible Hybrid Kirigami Sensor

In the second phase of the project, for the realization of the printed multilayer Kirigami structure, inkjet printing was chosen as fabrication method. The change in printing technique from the first part of the project was made because of the more complex Kirigami multilayer structure design, and consequently the printed pattern, which required multiple trial and error attempts: Inkjet printing grants for significant ease of design iterations, as a result of digital CAD file input, which allows to quickly make small adjustments in design when required.

The electrode and connecting layers are based on inkjet-printed silver on a dielectric substrate. Silver nano-particle ink from ANPPPro (Silverjet P 40TE-20C) was printed using a Ceradrop X-series printer loaded into a 13 pico-liter SAMBA cartridge. Kapton FPC substrate $125\ \mu\text{m}$ from American Durafilm was selected and first cleaned with 99 % acetone solvent. Four layers of the silver ink were printed in the form of $3 \times 3\ \text{cm}^2$ squares. Intermittent drying steps using an Adphos near infrared drying lamp integrated into the Ceradrop system were performed to allow uniform drying of the printed ink. The printed structures were then sintered in a Mancorp MC301N reflow oven for 1 hour at $300\ ^\circ\text{C}$ in air. Dycotech DM-INI-7003 ink was chosen as insulating layer. Six layers of the insulating ink were inkjet printed atop the sintered silver

electrodes, via Ceradrop printer, in the form of $4 \times 4 \text{ cm}^2$, with two central holes left empty to allow an electrical connection with the silver layer below. Each layer of the printed insulator ink was UV cured in place using the built ink UV cure lamp at 5.5 mW/cm^2 and 10 mm/s conveyor velocity followed by a final cure step at 100 % power and 1 mm/s speed.

The two layers were cut into the two different Kirigami functional structures utilizing laser cutting (Samurai UV Marking System, DPSS Lasers, Inc.), with a final dimension of $5 \times 5 \text{ cm}^2$, as depicted in Fig. 2.2 a, b).

The chosen AFE is a simple pre-amplifier circuit that allows the measurements of biological signals by capacitive sensing (Sun & Yu, 2016), consisting of an op-amp in a buffer configuration and a bias resistor, as schematically represented in Fig. 2.2c).

The components are mounted on a rigid PCB of the size of $34.3 \times 34.3 \text{ mm}^2$, with an exposed copper bottom to allow the connection of the electrode to the input of the op-amp. The final sensor is depicted in Fig. 2.2d).

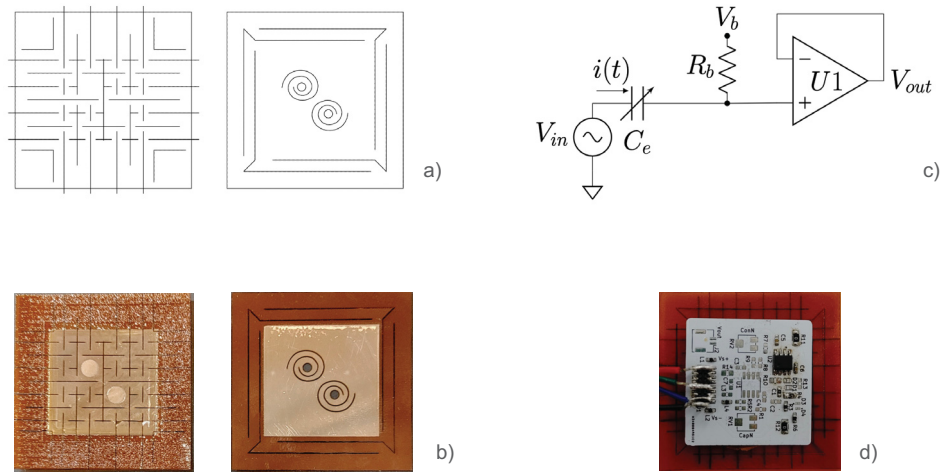


Figure 2.2 Sensor Production Steps: a) CAD design of kirigami electrode layer and connecting layer; b) printing and laser cut result of the electrode layer and connecting layer; c) schematic representation of analog front-end of the sensor; c) final sensor appearance, with PCB and printed layers interconnected to each other.

2.2 Characterization Methods

2.2.1 Resistive Measurements

To assure the quality of the printing process, the sheet resistivity of the printed electrodes was measured, before the cutting process, both for the screen printed and the inkjet printed devices.

For the screen printed electrode, the measurements were repeated on three different devices: a 4-point probe with gold coated points was used on the surface of the samples, together with a Keithley 237 as current source and Agilent 3458A as multimeter; current ranging from 1 mA to 5 mA was injected on the conductive surface and the voltage drops measured on all three samples; the results were averaged and multiplied by the shape correcting factor as indicated in (Smits, 1958); the resulting sheet resistance is $\rho_s = \frac{V}{I}C = 0.083 \Omega/sq$.

The same measurements were performed on six different inkjet printed samples: the resulting average sheet resistance is $\rho_s = \frac{V}{I}C = 0.053 \Omega/sq$

2.2.2 Capacitive Measurements

To assess the level of conformability of both the single-layer Kirigami electrodes and the final prototype of the hybrid sensor, capacitive measurements were performed analogously using an Impedance Analyzer (Keysight E4990A). The device was positioned on a conforming insulating polyester sponge sample holder, with the dielectric layer facing up, and a conductive aluminum hemispherical body of varying diameter was placed on top of it to act as the second, non-planar plate of the capacitor. The aluminum plate was pressed onto the capacitor: the different overloads for the different tests were applied by placing weights on top of the hemisphere.

The series capacitance between the aluminum plate and the silver electrode was measured on a frequency range of 20 Hz to 1 kHz, to assure the consistency of the measurement: as the measurements revealed to be constant in this range, the capacitance acquired at 100 Hz was arbitrarily chosen as representative value. Several aluminum bodies were used: hemispheres

with diameters of 15, 6.3, 5.5, and 4.5 cm, as well as a flat block (corresponding to a hemisphere of infinite diameter).

2.2.3 Electrical Characterization

The performed electrical measurements aim to provide an attentive but general characterization focused on specific electrical characteristics common to all types of electrical biosignals.

The measurements consist in the transmission of a sinusoidal signal from an arbitrary aluminum second plate to the sensor, imitating the signal acquisition of a biopotential coming from the body. The measurement set-up is the same as for the capacitive measurements, but in place of an Impedance Analyzer, a 1 Hz sinusoidal signal (Agilent 33500B - Waveform Generator) was injected in the aluminum second plate, and the output pin of the sensor was connected to an oscilloscope (Keysight InfiniiVision DSOX3014T) in order to analyze the signal acquisition (Fig. 2.3).

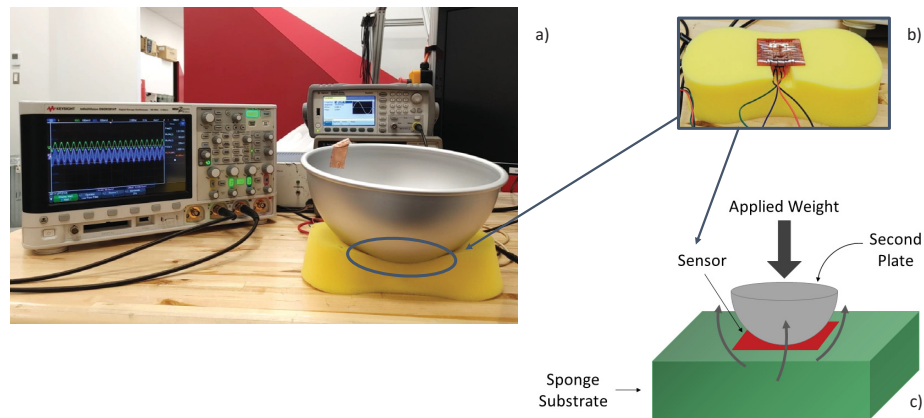


Figure 2.3 Electrical measurements setup: a) second plate placed on top of the sensor, a single frequency (1 Hz) signal from the signal generator is injected into the second plate, acquired by the sensor and analyzed on the oscilloscope; b) schematic representation of sensor position on the sponge sample holder; c) second plates utilized for the measurements, and corresponding curvatures.

The measurement results consider two main signal characteristics: the amplitude and the cutoff frequency. The amplitude of the transmitted signal is considered as a reference point to obtaining satisfactory SNR in any actual sensing application, while the cut-off frequency represents an indication of the quantity of information transmitted, and thus, the quality of the acquired signal.

The aluminum second plates considered in the experiments are one flat surface plate and different hemispheres of respectively 15 cm, 6.3 cm, 5.5 cm and 4.5 cm of diameter, corresponding to a curvature of 0, 0.13, 0.32, 0.36 and 0.44 cm^{-1} , respectively (Fig. 4.5c)). Overloads of ≈ 1.1 kgf (2.5 lbf), ≈ 2.2 kgf (5 lbf) and ≈ 3.3 kgf (7.5 lbf) were applied to both cases, to test the uniformity of the electrode under different pressure applied.

2.2.4 Triboelectric Measurements

To measure the triboelectric effect resulting from the sensor detaching vertically from a non-flat surface, electrical measurements were carried out with the aid of a robotic arm. The experimental set-up conceived to reproduce the transversal separation is composed of our hybrid flexible sensor prototype, placed on a soft sponge holder, and an aluminum hemispherical body, with a diameter of 15 cm, connected to a robotic arm (Stäubli TX2-90L) used to move the second plate in a precise vertical path on top of the sensor (Fig. 2.4).

The electrical measurements consist in the transmission of a sinusoidal signal from the aluminum second plate to the sensor, imitating the signal acquisition of a biopotential coming from the body: a single frequency (1 Hz) sinusoidal signal (Agilent 33500B - Waveform Generator) was injected in the aluminum second plate, and the output pin of the sensor was connected to an oscilloscope (Keysight InfiniiVision DSOX3014T) to monitor the acquired signal.

2.2.5 Mechanical Reliability Test

The sensor prototype has been subjected to a bending reliability test, where it has undergone 100 bending cycles at 40 degrees of bend, to monitor eventual changes in sensor response caused by the introduced stress during the repetitive bending. At the end of the 100 cycles, the sensor

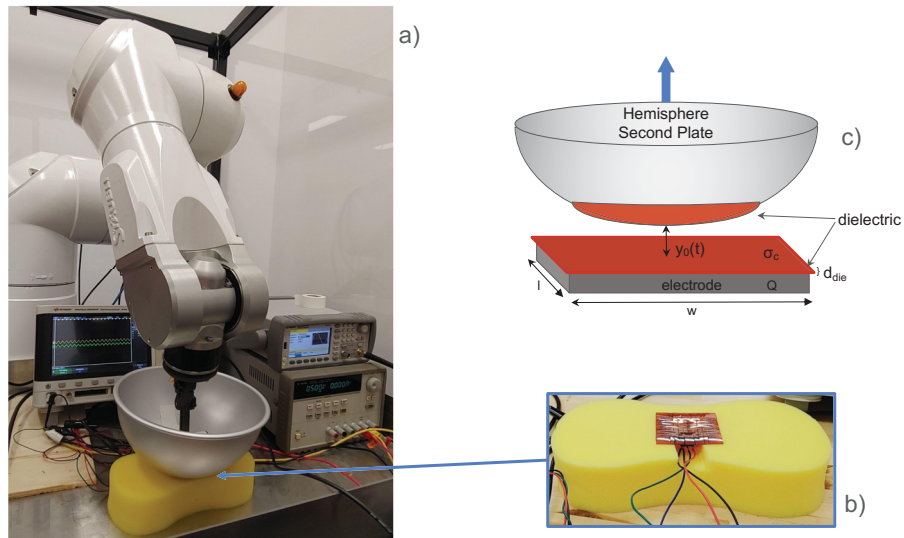


Figure 2.4 Measurement setup: a) electrode placed on a sponge holder, aluminum second plate fixed to a robot arm and placed on top of the electrode. The second plate surface was covered by a Kapton HN tape layer to reduce the charge affinity between the two surfaces.

A signal generator injects a sinusoidal signal in the aluminum second plate, which is capacitively transmitted to the sensor and observed on the oscilloscope. b) Sensor placement under the second plate. c) equivalent graphic representation of sensor for comparison against analytical model.

characteristics (amplitude, cutoff frequency) were once again re-evaluated following the same measurement set-up as above described.

2.3 Data Analysis and Modeling

All the measured data have been handled, analyzed and plotted using OriginPro (OriginLab) software. Finally, the analytical models formulated have been built and graphically visualized using Matlab.

CHAPTER 3

FLEXIBLE CAPACITIVE KIRIGAMI ELECTRODE: EXPERIMENTAL INVESTIGATION AND ANALYTICAL MODEL

Laura Morelli¹, Ghyslain Gagnon², Ricardo J. Zednik¹

¹ Département de Génie Mécanique, École de Technologie Supérieure,
1100 Rue Notre-Dame Ouest, Montréal, Québec, H3C 1K3, Canada

² Département de Génie Électrique, École de Technologie Supérieure,
1100 Rue Notre-Dame Ouest, Montréal, Québec, H3C 1K3, Canada

Article publié dans la revue
« IEEE Journal on Flexible Electronics »
le 11, July, 2023.
<https://ieeexplore.ieee.org/document/10179150>

Résumé: L'électronique flexible a récemment suscité un intérêt croissant en raison de ses promesses pour un large éventail d'applications, allant du stockage d'énergie aux écrans flexibles, en passant par les capteurs et les dispositifs portables. La tendance dans le domaine de l'électronique flexible est vers la fabrication de dispositifs composés de matériaux et de composants entièrement flexibles. Cependant, les dispositifs flexibles présentent encore de nombreuses limitations, principalement en raison du coefficient de Poisson négatif des matériaux utilisés, qui affecte les dimensions et les caractéristiques des matériaux lorsqu'ils sont pliés ou étirés.

Dans ce travail, nous proposons un nouveau design pour les électrodes capacitatives visant à améliorer la flexibilité des dispositifs sans affecter les propriétés des matériaux impliqués : le design est basé sur le Kirigami, l'art traditionnel japonais de la découpe du papier qui, lorsqu'il est appliqué à l'ingénierie, permet de façonner des structures extensibles et déformables en effectuant des coupes simples sur des substrats et des films traditionnels, garantissant ainsi la compatibilité avec les méthodes de fabrication existantes.

Nous formulons un nouveau modèle analytique pour expliquer en détail le comportement de l'électrode Kirigami appliquée à une surface non plane arbitraire. L'efficacité du nouveau design a été vérifiée au moyen de mesures capacitatives dans différentes configurations non planes:

les résultats obtenus confirment à la fois la validité du modèle analytique et la robustesse de la nouvelle approche Kirigami, avec des valeurs capacitives augmentant jusqu'à 115 % pour l'électrode Kirigami par rapport à celle sans-Kirigami.

Abstract: Flexible electronics have recently garnered increasing attention due to their promise for a wide range of applications, from energy storage to flexible screens, over sensors to wearables. The trend in flexible electronics is toward the fabrication of devices composed of fully flexible materials and components. However, flexible devices still present many limitations, primarily due to the negative Poisson's ratio of the materials used, which affects the dimensions and characteristics of the materials when bent or stretched.

In this work we propose a novel design for capacitive electrodes aimed to improve the flexibility of devices without affecting the properties of the materials involved: the design is based on Kirigami, the traditional Japanese art of paper cutting which, when applied to engineering, enables the shaping of stretchable and deformable structures by performing simple cuts on traditional substrates and films, thereby ensuring compatibility with existing manufacturing methods.

We formulate a novel analytical model to explain in detail the behavior of the Kirigami electrode applied to an arbitrary non-flat surface. The efficacy of the novel design has been verified by means of capacitive measurements in different non-flat configurations: the results obtained confirm both the validity of the analytical model and the robustness of the novel Kirigami approach, with capacitive values increasing up to 115 % for the Kirigami electrode compared to the non-Kirigami one.

Keywords: Capacitive Electrode, Contactless Sensing, Flexible Electronics, Kirigami, Printed Electronics.

3.1 Introduction

Flexible electronics have been at the center of attention in the electronics field for the past decade. The development of new materials, processes, sensing techniques, and applications focuses on the study and production of novel devices that are flexible, stretchable, and can be applied or integrated on any curved surface (Corzo *et al.*, 2020; Gao *et al.*, 2019; Harris *et al.*, 2016). The fabrication of flexible devices in particular is focusing on the development of fully flexible materials and components. Among these, flexible dielectric capacitors are especially important devices, as they are essential for energy storage, displays, and sensors (Kim *et al.*, 2011; Li *et al.*, 2012; Liang *et al.*, 2019; Wang, Zhang & Lin, 2020b; Yu *et al.*, 2019).

Most of the previous works focus on the fabrication of novel flexible materials for the different parts of electronic devices (electrode, dielectric layer, substrate). Numerous materials and composites have been developed which exhibit good electric or dielectric properties while being flexible (Chen *et al.*, 2020; Chu *et al.*, 2012; Kim *et al.*, 2017; Najafabadi *et al.*, 2014; Wu & Yao, 2017). However, when flexed or stretched, these materials change in dimension depending on their Poisson's ratio (Ohring, 2002) and, when subjected to mechanical stress, their electric and dielectric properties are affected (Cai *et al.*, 2009), making the consistent performance of a flexible electronic device a particular challenge. In addition, these materials are incompatible with conventional semiconductor or electronic device manufacturing processes (including lithography).

Some important sensing applications include the use of capacitive electrodes for contactless sensing of electrophysiological signals, such as electrocardiogram (ECG), electroencephalogram (EEG) and electromyogram (EMG) (Baek, Lee, Lim & Park, 2013; Lee *et al.*, 2014; Roland, Wimberger, Amsuess, Russold & Baumgartner, 2019; Uguz, Dettori, Napp, Walter, Marx, Leonhardt & Antink, 2020). For these specific applications, the sensing mechanism is based on the working principle of the capacitor: the electrode, corresponding to a single plate of a capacitor, is placed in close proximity to the human body, which equates to the second plate of

the capacitor, and the electrical signal generated from the organs can be capacitively captured by the electrode, without need of direct current flowing between the two sides.

The efficiency and uniformity of the device is of particular importance for such sensing applications: characteristics of the acquired signal such as Signal-to-Noise Ratio (SNR)(Lim *et al.*, 2007,1; Taji *et al.*, 2013) and cut-off frequency (Bronzino, 2006; Kaniusas, 2019) are strongly dependent on the capacitance between the body and the sensor. An electrode that is able to conform to the body allows all its surface to establish a capacitive coupling with the body, maximizing the capacitance and assuring a good quality signal acquisition (Berson & Pipberger, 1966; Bragg-Remschel *et al.*, 1982; Lee *et al.*, 2014; Lessard-Tremblay *et al.*, 2020).

A promising alternative to flexible materials is therefore the design of novel mechanical structures that will allow electronic components to be flexible and conformable, while maintaining the physical and electrical properties of established conventional materials (McIntosh, Mauger & Patterson, 2006; Montero, Laurila & Mäntysalo, 2022; Yang, Chen, Wu, Chen & Lon, 2021; Zhou, Sharma, Lüttgen & Sarr, 2020a). In this spirit, a Kirigami approach is explored to improve flexibility of traditional printed capacitor structures manufactured from conventional materials.

Kirigami metamaterials

Kirigami is the traditional Japanese art of paper cutting which enables the shaping of complex 3D artistic structures by performing simple cuts on 2D paper sheets. The shape-adaptable technique is an excellent starting point for the fabrication of flexible, constant area devices (Ning *et al.*, 2018; Zhai *et al.*, 2021). The flexibility and conformability of the overall structure is realized by dividing the rigid material into rotating rigid sub-units, with the connections between these units acting as free rotational hinges. This allows macroscopic deformation to occur mainly through rotation of the sub-units, rather than by attempting to deform the rigid sub-units themselves (Cho *et al.*, 2014; Choi *et al.*, 2019,2; Grima & Evans, 2000; Yang *et al.*, 2016).

Capacitors are some of the most simple and fundamental components used in flexible electronics, and were therefore selected as a model device to explore the Kirigami technique. Previous works

made use of Kirigami technique to improve the stretchability and flexibility of electrodes for several applications, such as flexible batteries and supercapacitors, where kirigami structures helped achieve better capacitance stability when stretched (Diao *et al.*, 2021) and after being cyclically bent (Bao *et al.*, 2019).

Single sided electrodes also find extensive application in the field of bio-sensing: multiple works employed Kirigami to improve the conformability of electrodes attached to the body (Brooks *et al.*, 2022; Li *et al.*, 2022), the increased conformability helped improving SNR, meeting high conductivity and stretchability (Gao *et al.*, 2018) and maintaining adhesion even under high degree of bending (Yang *et al.*, 2018).

For contactless capacitive sensors, particularly in the case of electrophysiological sensors, the electrode does not require to be attached to the skin by means of gel or adhesive. However, good conformability to the body is important in order to obtain high SNR, enhanced uniformity and good signal quality. Most of the works found in literature tend to focus on the employment of flexible materials to improve the flexibility of contactless capacitive electrodes (Herbert *et al.*, 2018; Lee *et al.*, 2014; Lessard-Tremblay *et al.*, 2020; Ng & Reaz, 2019).

Making use of Kirigami in the realization of capacitive electrodes is an interesting, yet not well explored, approach to improve the flexibility and conformability of contactless devices without affecting its performance. In this work, we therefore propose a novel design approach for capacitive electrodes based on Kirigami: the patterned design can be easily implemented by traditional techniques such as laser cutting, assuring compatibility with any material and process used for the fabrication of the electrode.

In order to assess how Kirigami impacts the device characteristics, three different patterns are studied, corresponding to three hierarchical levels of cuts (Yang *et al.*, 2016). To better comprehend the capacitive behavior of the electrode when coupled to an arbitrary surface, an analytical model is introduced, which takes into consideration the non-idealities of the Kirigami configuration. This analytical description is finally compared to the experimental results.

3.2 Materials and Fabrication

Kirigami patterns are numerous and can assume very different shapes: the size, lengths and disposition of cuts on the surface can be tailored depending on the target shape required for a specific application (Choi *et al.*, 2019). In the case of capacitive electrodes, in particular if we take the example of electrophysiological sensing, the electrode must be conformable to any target part of the body: our goal is to create a flexible electrode that will be able to follow the arbitrary curvature of the body, therefore maximizing the surface area of the electrode that will be able to establish a capacitive coupling with the target surface.

As different parts of the body can vary in shapes and dimensions, the chosen Kirigami pattern consists of standard, equally distanced, perpendicular cuts, which allows the electrode to bend easily in all directions. Specifically, three different Kirigami structures were chosen and compared to the equivalent conventional non-cut electrode. The three structures correspond to three different hierarchy levels of cuts (Yang *et al.*, 2016) as seen in Fig. 3.1:

- *Level 0*: intact electrode with no cuts on the surface.
- *Level 1*: three perpendicular cuts are introduced on the surface of the Level 0 structure, dividing the electrode into four equal rotating sub-units.
- *Level 2*: the same pattern is repeated on each sub-square, dividing the electrode surface into a total of 16 rotating sub-units.
- *Level 3*: the same process is repeated to create a total of 64 smaller square sub-units.

The introduction of cuts on the surface would be expected to affect the remaining area of the electrode: the effective area was therefore calculated by subtracting the area lost due to the cuts, where the cut dimensions were measured by means of an optical microscope (Laser Confocal Microscope LEXT4100) (See Table 3.1).

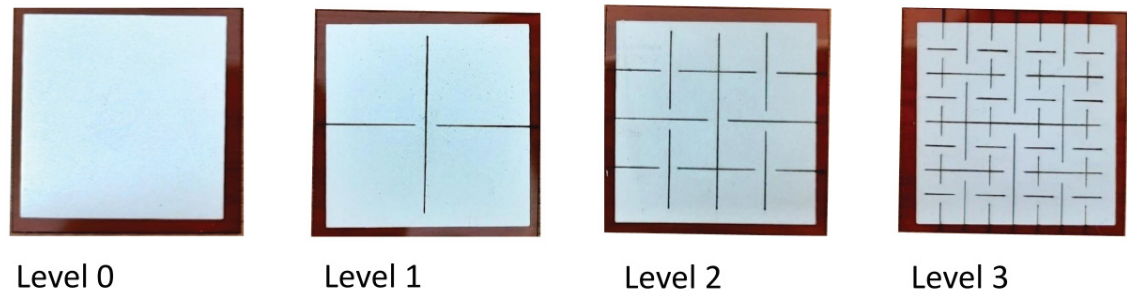


Figure 3.1 Electrode samples showing the four different Kirigami hierarchical structures.

The corresponding effect on the total surface area was found to be almost negligible, corresponding to $\approx 1\%$ from Level 0 to Level 3, as noted in Table 3.1. This confirms the high quality of the laser cutting process employed.

Table 3.1 Comparison of total area and theoretical capacitance for the different hierarchical levels

Hierarchy Level	Total Area	Removed Area
Level 0	$9.00 \times 10^{-4} \text{ m}^2$	0 %
Level 1	$8.98 \times 10^{-4} \text{ m}^2$	0.22 %
Level 2	$8.95 \times 10^{-4} \text{ m}^2$	0.55 %
Level 3	$8.90 \times 10^{-4} \text{ m}^2$	1.11 %

One of the most simple and fundamental electronic components is a capacitor electrode device. In the present case, the capacitor electrode corresponds to a single side of a capacitor and is composed of a dielectric substrate (Kapton HN, thickness of $125 \mu\text{m}$) and a conductive silver layer (LOCTITE EDAG 725A(6S54) E&C, Henkel). The conductive layer was printed by screen printing (Keko P200S - LTCC serigraphic printer) onto the dielectric substrate, and cured in an

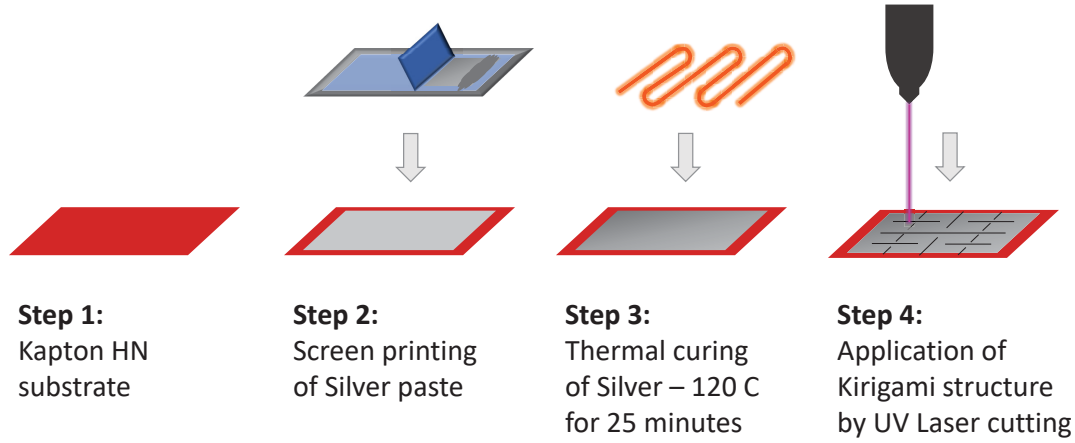


Figure 3.2 Process steps for the realization of printed Kirigami electrode.

oven at 120 °C for 25 minutes (see Fig. 3.2). The final electrode takes the shape of a square of 30x30 mm², with a thickness of approximately 130 μm.

To assure the quality of the process, sheet resistivity of the printed electrode was measured on 3 different samples: a 4-point probe with gold coated points was used on the surface of the samples, together with a Keithley 237 as current source and Agilent 3458A as multimeter; current ranging from 1 mA to 5 mA was injected on the conductive surface and the voltage drops measured on all three samples; the results were averaged and multiplied by the shape correcting factor as indicated in Smits (1958); the resulting sheet resistance is $\rho_s = \frac{V}{I}C = 0.053 \, \Omega/cm$.

The Kirigami pattern was ultimately implemented on the electrode surface by means of laser cutting (Samurai UV Marking System — DPSS Lasers, Inc.). All the materials used and the manufacturing methods employed are conventional and well-established - the Kirigami patterning represents an innovative and easy-to-apply technique to enhance the flexibility of the device.

3.3 Analytical Model

Choosing an arbitrary surface as second electrode, a flexible capacitive electrode must be able to conform to the given surface in order to establish the highest obtainable capacitance. To estimate the capacitance for an arbitrary non-flat configuration, the conventional parallel plate model is inadequate.

We therefore must develop a generalized model which takes into consideration both the conforming and nonconforming surfaces. In the present case, an hemisphere shaped second plate was chosen to simulate a generic non-developable surface.

3.3.1 Level 0

When the second electrode assumes a non-developable, arbitrarily curved surface, the Level 0 electrode is not able to conform to its surface, creating creases and folds (Hure, Roman & Bico, 2011; Sageman-Furnas, Goswami, Menon & Russell, 2014). The nonconformity results in a non-uniform distance between the two plates, affecting the capacitance.

The following analytical model consists of a hybrid between the classical parallel plate equation and the inclined parallel plate model applied to our specific case (Xiang, 2006,0). The resulting equation divides the electrode surface into different sections:

- The electrode area that evenly conforms to the second plate, described by the ideal parallel-plate capacitor relation:

$$C_c = \epsilon\epsilon_0 \frac{A_c}{t} \quad (3.1)$$

Where t is the thickness of the dielectric layer, ϵ the relative permittivity of Kapton and A_c , in this case, is the total surface area conforming to the second plate of the capacitor.

- The remaining area represented by the creases of the crumpled electrode, which can be locally described by the non-parallel plate relation (Feng, Zhou, Wang, Rao & Han, 2021;

Xiang, 2006,0):

$$C_{nc} = \frac{\epsilon\epsilon_0}{\sin(\alpha)} \int_0^{2\pi} W(\theta) \cdot \ln \frac{R_2(\theta)}{R_1(\theta)} d\theta \quad (3.2)$$

Where α is the angle formed between the two non-conforming sides, $W(\theta)$ is the perimeter function delimiting the the contact area on the electrode surface, which may vary case by case, $R_2(\theta)$ is the total radius, corresponding to the half-length of the electrode, and $R_1(\theta)$ is the portion of radius corresponding to the conforming portion, as defined in Fig. 3.3.

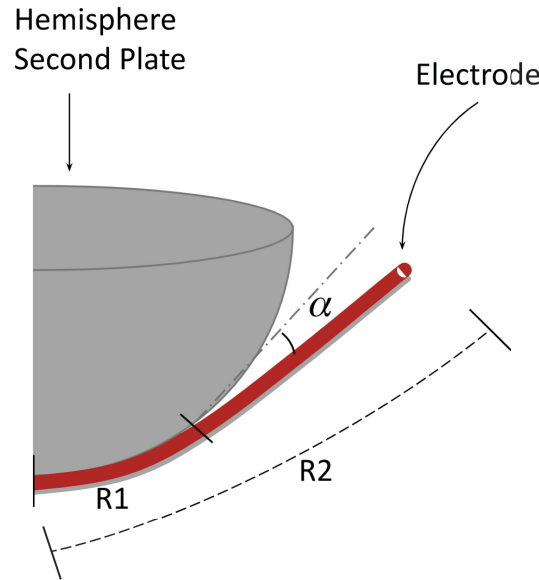
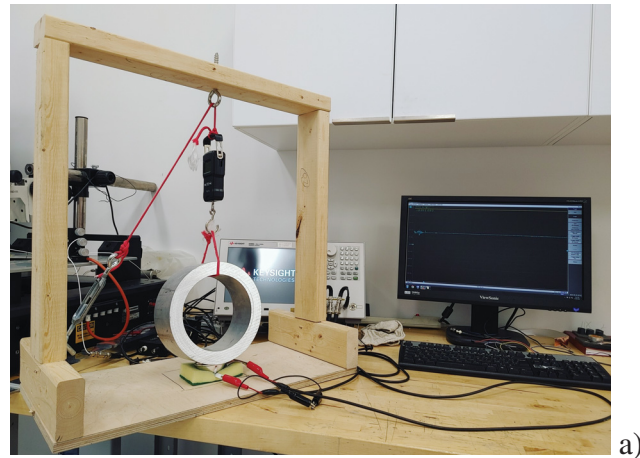


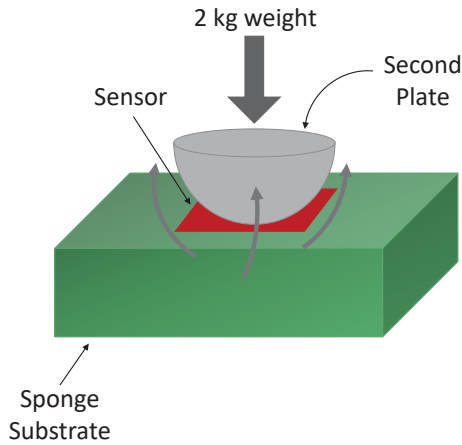
Figure 3.3 Analytical model variables: α is the angle formed between the two non-contact sides, R_1 is the contact-area portion radius and R_2 is the total radius, corresponding to the electrode half-length.

The equations can be readily applied to any arbitrary non-parallel capacitance case, as long as the contact and non-contact section of the surfaces can be analytically defined and described.

In the case of the aluminum hemispheres, when the Level 0 electrode is subjected to the weight of the spherical bodies (see Fig. 3.4), only part of the surface is able to conform to the hemisphere. To differentiate between the contact, parallel surface and the non-contact one, the hemispherical aluminum bodies have been coated with blue ink before being positioned on the surface of



a)



b)

Figure 3.4 Capacitive Measurements Setup: a) electrode placed on a sponge sample holder and subjected to a constant 2 kg-force weight. The weight is hanging on top of the sample holder, fixed by a wooden structure and controlled by a hanging scale. The Impedance Analyzer is connected to both the conductive aluminum hemisphere and to the conductive silver electrode; b) graphical representation of the hemisphere-electrode measurement setup.

the electrode and subjected to a 2 kg-force weight. The portion of the area able to conform to the sphere is clearly noticeable in Fig. 3.5a). The non-contact remaining area can be thus approximated by symmetrical semicircles at the four edges of the sample (Fig. 3.5b)).

Before applying (3.1) and (3.2) to this specific case, it is necessary to introduce a few conjectures:

1. The border and fringing effects are not taken into account.

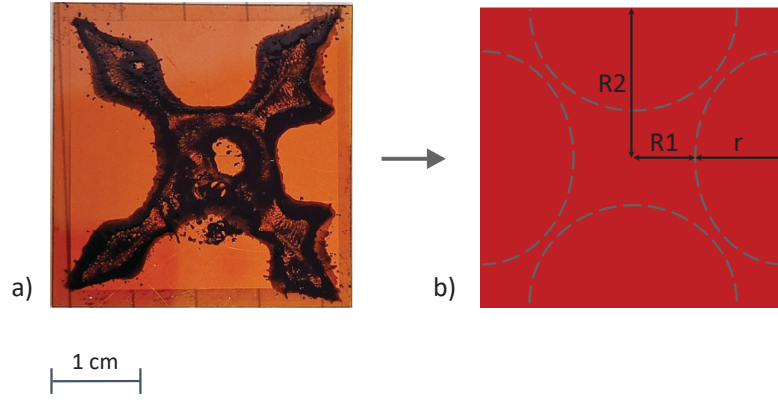


Figure 3.5 Blue ink print of Level 0 sample when applied to the hemisphere of $d=6.3$ cm:
a) Image of blue ink print left by the weight application. The dark blue area represents the conformal area; b) Graphic approximation of ink print as used in the analytical model, where R_1 is the contact-area portion radius, R_2 is the total radius, corresponding to the electrode half-length, and r is the non-contact area radius. Ink print test was repeated on three different samples, the figure shows one example of the three.

2. The angle α is considered constant and is approximated by $\frac{\pi}{12}$ as the constraints of the sponge sample holder do not allow for larger angles (small variations of the angle were tested and the results were not noticeably affected by the changes).
3. Both the surfaces are considered as flat and not curved, so that the electrical field between the two is always perpendicular to both the plates (Landau, 2013).

The final equation coincides with a series of two capacitors. Both terms of the equation vary depending on the geometrical configuration of the contact between the two plates.

The first capacitance, corresponding to the capacitance accumulated in the dielectric layer, can be written as a parallel plate capacitance adjacent to the electrode:

$$C_{nc(dielectric)} = \epsilon\epsilon_0 \frac{A_{nc}}{t} \quad (3.3)$$

where A_{nc} is the total non-contact area.

The second capacitance, corresponding to the air gap between the two sides, can be calculated starting from (3.2). In the case of the hemisphere, the non-contact portion of the surface can be approximated by 4 semicircles, as depicted in Fig. 3.5b).

To better describe this particular configuration, it is useful to introduce an additional parameter:

$$r = R_2 - R_I \quad (3.4)$$

which corresponds to the non-contact area radius of the four semicircles defined in Fig. 3.5(b).

The perimeter function can then be rewritten as:

$$W(\theta) = 4 \int_0^\pi r \, d\theta \quad (3.5)$$

The contact area radius R_I , being not constant, can also be rewritten as a function of θ :

$$R_I = R_2 - r \cdot \sin(\theta) \quad (3.6)$$

So that:

$$C_{nc(airgap)} = 4 \cdot \frac{\epsilon_0}{\sin(\alpha)} \int_0^\pi r \cdot \ln \frac{R_2}{R_2 - r \cdot \sin(\theta)} d\theta \quad (3.7)$$

Equation (3.2) can finally be rewritten as:

$$\begin{aligned}
C_{nc} &= \left(\frac{1}{C_{nc(dielectric)}} + \frac{1}{C_{nc(airgap)}} \right)^{-1} = \\
&= \left(\frac{1}{\epsilon \epsilon_0 \frac{A_{nc}}{t}} + \frac{1}{4 \cdot \frac{\epsilon_0}{\sin(\alpha)} \int_0^\pi r \cdot \ln \frac{R_2}{R_2 - r \cdot \sin(\theta)} d\theta} \right)^{-1}
\end{aligned} \tag{3.8}$$

The total capacitance is the sum of the parallel and non-parallel portions:

$$C_{tot} = C_c + C_{nc} \tag{3.9}$$

In the case of Level 0, the R_2 value is constant and equal to the electrode half-length $R_2 = 1.5$ cm. Depending on the diameter of the hemisphere, the value of R_l (contact area radius) and the value of r (non-contact area radius) change, affecting the total capacitance value.

3.3.2 Level 1, 2 and 3

Introducing cuts to the surface allows the electrode to bend more easily and to better conform to non-developable surfaces (Lee, Xi, Lee, Kim, Hao, Choi, Lee, Joo, Kim, Lien & Choi, 2020; Yang *et al.*, 2016). We repeated the blue ink print tests on the higher hierarchy samples and noticed a very similar trend as with Level 0, but repeated on each sub-square, as shown in Fig. 3.6.

In the cases of Levels 1, 2 and 3, (3.9) can still be used if applied to each sub-square, taking into account a few approximations:

1. All the sub-squares do not adhere to the hemisphere the same way, depending on the pressure between the sponge and the weighted hemisphere, which varies from point to point. For

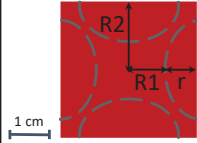
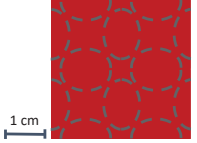
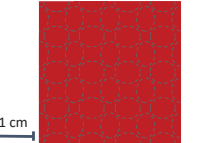
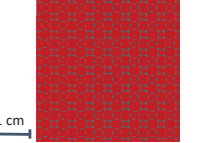
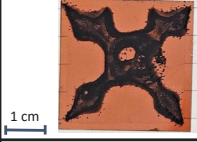
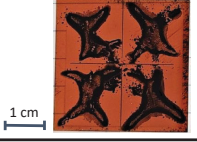
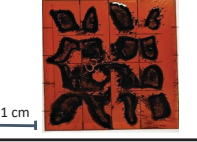

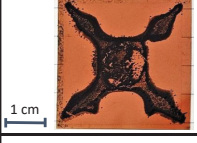
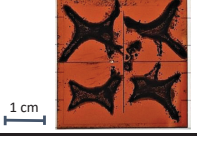
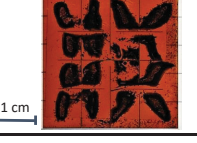

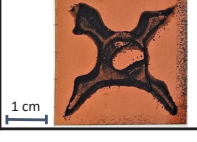
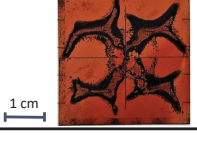
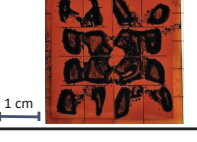
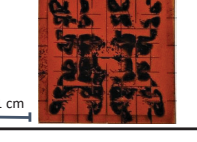
Diameter	Level 0	Level 1	Level 2	Level 3
Graphic Representation				
6.3 cm				
5.5 cm				
4.5 cm				

Figure 3.6 Comparison between graphic representation as used for the analytical model and blue ink print, when applied to the hemisphere of $d = 6.3$ cm, $d = 5.5$ cm, and $d = 4.5$ cm. The dark blue area represents the contact area. Ink print test was repeated on three different samples for each Level and diameter, the figure shows one example of the three for each case.

this reason the contact surface considered in the model is an average between all the single sub-square conformal surfaces.

2. All the hypotheses used for the Level 0 case are the same for the following cases, but applied singularly to each sub-square.

The general equation to estimate the total capacitance for a Kirigami electrode can be thus rewritten as follows:

$$C_{tot} = \sum_{i=1}^N (C_c(i) + C_{nc}(i)) \quad (3.10)$$

Where N is the total number of squares introduced by the Kirigami pattern ($N = 4, 16, 64$, corresponding respectively to Level 1, 2, and 3).

As a consequence, the other parameters of (3.1) and (3.8) also change depending on the hierarchy level, as listed in Table 3.2.

Table 3.2 Different analytical model parameters for the different hierarchical levels

Hierarchy Level	no. of Squares	Area of Square	R_2
Level 0	1	$9.00 \cdot 10^{-4} \text{ m}^2$	15.00 mm
Level 1	4	$2.25 \cdot 10^{-4} \text{ m}^2$	7.50 mm
Level 2	16	$5.62 \cdot 10^{-5} \text{ m}^2$	3.75 mm
Level 3	64	$1.41 \cdot 10^{-5} \text{ m}^2$	1.87 mm

3.4 Experimental Set Up

To assess the level of conformability of the four electrode designs, capacitive tests were performed by means of an Impedance Analyzer (Keysight E4990A). The device was positioned on a conforming insulating polyester sponge sample holder, with the dielectric layer facing up, and a conductive aluminum hemispherical body of varying diameter was placed on top of it to act as the second, non-planar plate of the capacitor. The aluminum plate was pressed onto the capacitor so as to apply a consistent total weight of 2 kg-force, as in Fig. 3.4a): the overload was applied by placing a weight on top of the hemisphere, controlled by hanging scale to keep it constant to 2 kg.

The series capacitance between the aluminum plate and the silver electrode was measured on a frequency range of 20 Hz to 1 kHz, to assure the consistency of the measurement: as the measurements revealed to be constant in this range, the capacitance acquired at 100 Hz was arbitrarily chosen as representative value. 4 distinct aluminum bodies were used: hemispheres with diameters of 6.3, 5.5, and 4.5 cm, as well as a flat block (corresponding to a hemisphere of infinite diameter).

The measurements, for each level, were repeated on 8 different samples, and the average over the 8 measurements was considered for each configuration.

3.5 Results and Discussion

The average capacitive values for each configuration are reported in Fig. 3.7.

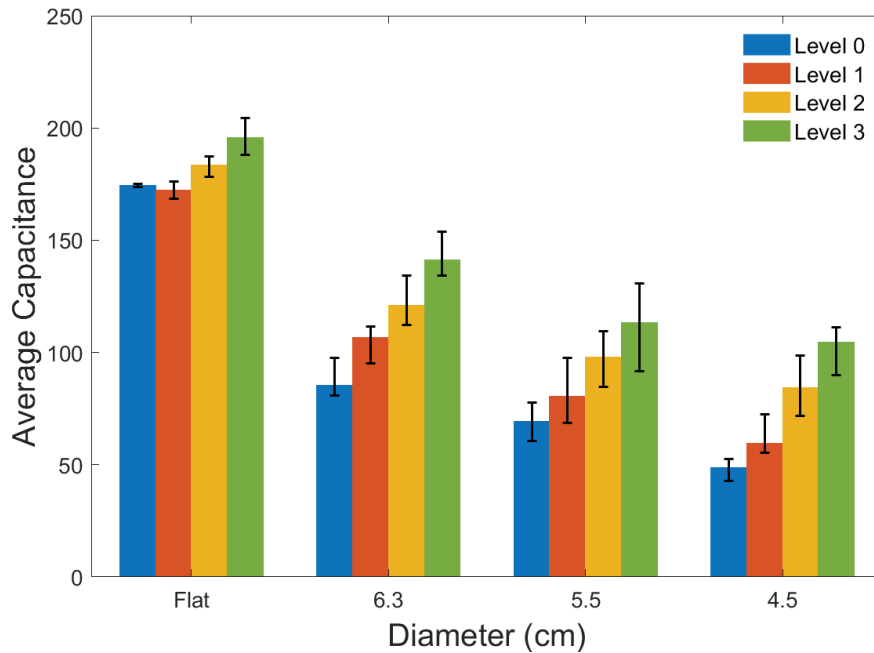


Figure 3.7 Average measured capacitance, at 100 Hz, for each of four different hierarchy levels and hemisphere diameters.

For the flat aluminum body, the difference in measured capacitance varies within $< 10\%$ between hierarchies, associated with the different levels of adhesion and the different surface roughness caused by the introduction of cuts (Albina, Taberna, Cambronne, Simon, Flahaut & Lebey, 2006; Zhang, Liu, Li, Chen & Fu, 2013). However, in the case of curved surfaces (aluminum hemispheres), the increase in capacitance from Level 0 to Level 3 is substantial. As an example: for the smallest diameter of 4.5 cm, the increment in capacitance from Level 0 to Level 1 is of 23 % on average, increasing to 74 % for Level 2 and up to 115 % for Level 3.

The measurements demonstrate how the implementation of a Kirigami pattern on a generic printed electrode can significantly improve the conformability and flexibility of the device, allowing more of its surface to establish a capacitive coupling with the second plate. Despite the

minor reduction in total surface area caused by the cuts on the electrode, the overall measured capacitance significantly increases.

The results obtained were thereafter compared with the introduced analytical model: in the case of non-developable surfaces, the model defined in section II.C accurately describes the capacitive behavior of the electrode, in particular for the Kirigami ones (Level 1, 2 and 3), where the analytical model helps understanding how the different structures affect the capacitive coupling of both the conformal and non-conformal portion of the electrode surface. In Fig. 3.8 the plots for the analytical model are shown as a function of percentage of non-contact area of the electrode for all four levels of hierarchy, where 0% corresponds to the entire surface being perfectly conformal and 100% corresponds to zero conformity.

As it can be noticed from Fig. 3.8 the trends are similar in the lower and higher part of the spectrum (0 – 20% and 80 – 100%) of non-contact area but diversify in the central part, with the plot shifting to the right for increasing level of hierarchy.

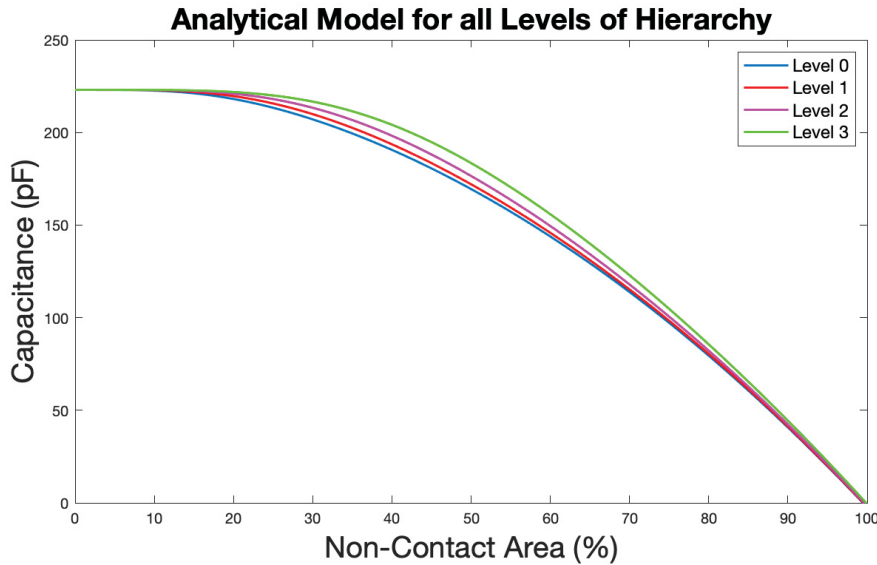


Figure 3.8 Comparison of analytical capacitive model for all different levels, as a function of percentage of non-contact area.

In Fig. 3.9 the analytical models for each level are plotted separately and the average measured values are added to the plots as single points of different shapes, corresponding to the different hemisphere diameters, where the percentage of non-contact area associated to each measurements was extrapolated from the ink prints in Fig. 3.6. All the measured values follow the trend of the analytical model, with an average error of 18%.

Considering, in our case, that the force applied to the two surfaces is constant, resulting from both the constant weight on the second plate and the sponge substrate surrounding the electrode, the ratio between parallel and non-parallel coupled capacitance for each level depends uniquely on the diameter of the hemisphere used as second plate.

Comparing the measured values for each diameter from Level 0 to Level 3, it can be appreciable from Fig. 3.9 that to every increase in average measured capacitance corresponds a decrease in percentage of non-contact area, i.e. for $d = 6.3$ cm the average non-contact area changes from around 71 % for Level 0 to circa 58 % for Level 3, as indicated in Table 3.3. This trend can indicate an improved conformity for the Kirigami structures: the enhanced flexibility of the electrode allows for more surface area to be perfectly conformable to the second plate of the capacitor. As can also be observed in Fig. 3.6 the smaller the sub-square dimension, the more the area visibly covered by the ink, on average, for each square.

Table 3.3 Error Between Analytical Model and Measured Values

Hierarchy Level	Diameter (cm)	non-Contact Area (%)	Analytical Capacitance (pF)	Measured Capacitance (pF)	Error (%)
Level 0	6.3	71	111.40	93.16	23.46
	5.5	77	86.96	71.52	20.13
	4.5	81	76.60	45.15	36.62
Level 1	6.3	64	132.62	105.28	19.54
	5.5	75	98.06	78.66	17.95
	4.5	80	78.91	57.05	24.44
Level 2	6.3	63	140.11	129.36	13.64
	5.5	71	113.07	96.78	13.37
	4.5	76	95.47	78.18	11.62
Level 3	6.3	58	160.45	147.14	12.03
	5.5	67	132.81	111.02	14.70
	4.5	72	114.23	104.12	8.43

Introducing Kirigami cuts on the electrode reduces the bending force applied on each sub-unit (Lee *et al.*, 2020), and as the unit squares become smaller, the easier it is for the electrode to

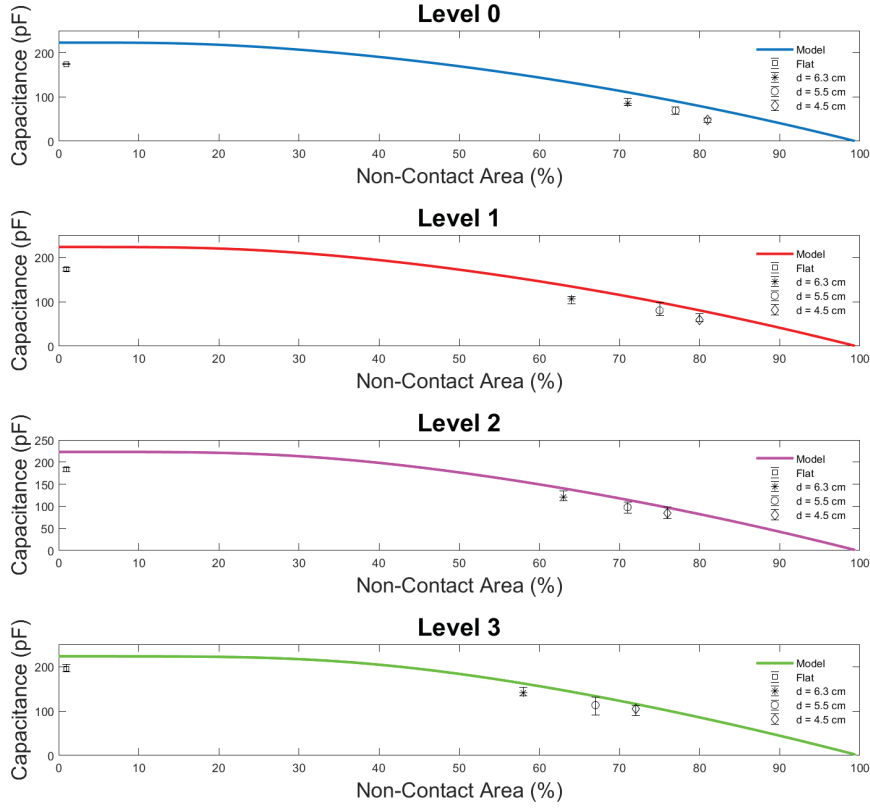


Figure 3.9 Comparison between analytical capacitive model and measured values for all different levels, as a function of the percentage of non-contact area. The average values of measured capacitance for all levels, for each diameter, are shown as single points.

adapt to the curved surface. This added to the improved flexibility, resulting in an increase of the total contact area (A_c) for increasing hierarchy level, and as a consequence an increase in total capacitance.

In addition, the contribution of the non-parallel surface portion also increases by increasing hierarchy level: in Fig. 3.10 the analytical model of the overall non-contact capacitance, described by (3.8), is plotted for each level. The single measured values of non-contact capacitance are shown as single points. In this case, the values were calculated starting from the ink prints in Fig. 3.6: the area of non-parallel coupling was extrapolated from the ink prints and the total non-contact capacitance for each case calculated using (3.8). As reported in Fig. 3.10,

the measured values follow the trend of the analytical model and, in general for any arbitrary second plate diameter, the total contribution of non-contact capacitance increases significantly from Level 0 to Level 3. Reducing the size of the squares also reduces the average distance between the non-contact surface area and the second plate. When summed up together, the equivalent non-contact capacitance (C_{nc}) is greater for the higher hierarchy levels, despite the total non-contact area actually getting smaller.

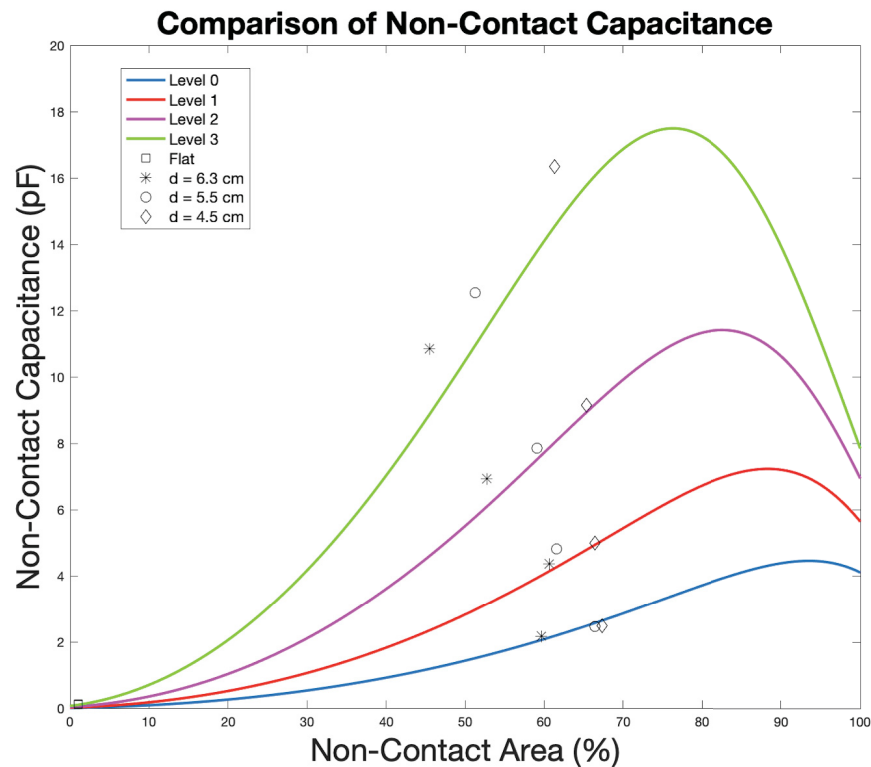


Figure 3.10 Comparison of non-contact capacitance for all levels of hierarchy, as a function of percentage of total contact-area. The estimated values of non-contact capacitance are shown as single points.

Introducing Kirigami designs on the electrode surface provides not only more flexibility to the macrostructure, compared to existing electrodes based on flexible materials, but also improves the overall performance: the total coupled capacitance, in the worst case scenario corresponding to the smallest provided diameter ($d = 4.5$ cm), exhibits an increase of 115 % from Level 0 to

level 3, combined with an improved conformability described by a reduction of - 9 % of total non-contact area.

3.6 Conclusions

In conclusion, the paper presents a novel design for flexible capacitive electrodes based on the use of the Kirigami technique to improve the flexibility and conformability of a flexible electronic device made with conventional materials and processes. Improvements up to 115 % in capacitance performance were observed, for four different hierarchy levels and curved surfaces, associated to the greater conformability of the novel design.

To explain the behavior of the Kirigami design, a novel capacitive model was developed, which considers the electrode geometry and their conformability to non-planar bodies of different sizes. The analytical model takes into account the non-contact portion of the surface, which we showed to be non-negligible when considering complex structures such as the Kirigami electrodes. The generalized model thus developed can be further applied to any arbitrary surface, as long as the contact and non-contact sections of the surface can be analytically defined and described. This is helpful for studying other flexible electronic devices beyond the structure considered in the present paper.

When applied to the present Kirigami structures, it proves to be accurate in describing the capacitive behavior of all the electrodes and consistent with the measured data, with an approximate average error of 18 %.

The presented analytical model can be easily adapted to different geometries and represents a tool to accurately describe the capacitive coupling of the electrode when applied to surfaces of different shapes and configurations.

The obtained results therefore confirm that Kirigami is a promising approach for increasing flexibility and conformability of flexible electronic devices: in particular in the case of capacitive

sensing electrode applications, the easily implemented design can significantly improve the performance of the electrode while assuring compatibility with existing materials and processes.

CHAPTER 4

PRINTED HYBRID CAPACITIVE KIRIGAMI SENSOR: ENHANCING FLEXIBILITY AND CONFORMABILITY FOR IMPROVED MOTION ARTIFACTS

Laura Morelli¹, Arjun Wadhwa², Sylvain Cloutier², Martin Bolduc³, Ghyslain Gagnon²,
Ricardo J. Zednik¹

¹ Département de Génie Mécanique, École de Technologie Supérieure,
1100 Rue Notre-Dame Ouest, Montréal, Québec, H3C 1K3, Canada

² Département de Génie Électrique, École de Technologie Supérieure,
1100 Rue Notre-Dame Ouest, Montréal, Québec, H3C 1K3, Canada

³ Department of Mechanical Engineering, Université du Québec à Trois-Rivières,
Trois-Rivières (QC), Canada

Article accepté par la revue
« IOP Flexible and Printed electronics »
le 15 Octobre 2024.
<https://iopscience.iop.org/journal/2058-8585>

Résumé: La détection capacitive des signaux électrophysiologiques est une alternative prometteuse aux méthodes de détection traditionnelles par contact pour la surveillance de la santé à long terme et omniprésente. De nombreux chercheurs se concentrent sur le développement d'électrodes capacitives flexibles pour améliorer la conformabilité et la qualité de l'acquisition de cette famille de capteurs. Cependant, les dispositifs flexibles actuels présentent encore de nombreuses limitations en raison du rapport de Poisson négatif des matériaux utilisés, ce qui affecte les dimensions et les caractéristiques des matériaux sous contrainte, ainsi que leur incompatibilité avec les méthodes de fabrication traditionnelles et les dispositifs à semi-conducteurs. Nous présentons un nouveau capteur capacitif hybride, imprimé par jet d'encre, de type Kirigami. Cette structure novatrice comprend différentes couches avec des fonctionnalités différentes, afin de permettre une flexibilité et une conformabilité améliorées de l'électrode imprimée Kirigami flexible, tout en assurant son inclusion sur un PCB rigide traditionnel pour une acquisition de signal de qualité.

La conception du capteur novateur a été testée sur différentes formes et dimensions de cibles de détection et avec différentes charges appliquées. Des mesures capacitives et électriques

ont été effectuées pour obtenir les principales caractéristiques de base du capteur telles que la capacitance couplée, l'amplitude du signal acquis et la fréquence de coupure.

Comparé à un capteur analogique mais rigide, le capteur flexible hybride conçu de manière innovante a montré une amélioration significative et une uniformité accrue des mesures, avec une augmentation de la valeur d'amplitude jusqu'à +82% pour les courbures les plus importantes, tout en maintenant un bon contact électrique et l'intégrité de toutes les couches.

Abstract: Capacitive sensing of electrophysiological signals is a promising alternative to traditional contact-type sensing for long-term and ubiquitous health monitoring. Many researchers are focusing on developing flexible capacitive electrodes to improve the conformability and the quality of acquisition of this family of sensors. However, current flexible devices still present many limitations due to the negative Poisson's ratio of the materials used, which affects the dimensions and characteristics of the materials when under stress, and their incompatibility with traditional manufacturing methods and solid-state devices.

We present a novel, inkjet-printed, hybrid capacitive Kirigami sensor design. This novel structure comprises different layers with different functionalities, in order to allow improved flexibility and conformability of the flexible Kirigami printed electrode, while securing its inclusion on a traditional rigid PCB for a quality signal acquisition.

The novel sensor design has been tested on different shapes and dimensions of sensing target and with different weights applied. Capacitive and electrical measurements were performed to obtain the main basic sensor characteristics such as coupled capacitance, acquired signal amplitude and cutoff frequency.

When compared to an analog but rigid sensor, the novel designed hybrid flexible sensor showed significant improvement and enhanced uniformity of measurements, with an increase in amplitude value up to +82% for the bigger curvatures, while maintaining good electrical contact and integrity of all the layers.

Keywords: Capacitive Sensing; Printed Electronics; Inkjet Printing; Flexible Hybrid Sensors; Kirigami;

4.1 Introduction

In recent years, the interest in non-invasive and continuous monitoring of physiological signals has triggered significant advancements in sensor technologies (Bandodkar & Wang, 2014; Promphet, Ummartyotin, Ngeontae, Puthongkham & Rodthongkum, 2021; Santos, Lucena, Pinto, Júnior & Marques, 2021; Yun, Kim, Kwon, Kim, Kim, Park & Park, 2021).

Capacitive sensing, in particular, has emerged as a promising technique for contactless biopotential monitoring, offering advantages such as high sensitivity, low power consumption, and compatibility with wearable devices (Baek *et al.*, 2013; Lee *et al.*, 2014; Roland *et al.*, 2019; Uguz *et al.*, 2020). For this application, the body surface and the electrode can be respectively considered as the two sides of a capacitor: the capacitance is established by the close vicinity of the two surfaces and no direct contact is needed. This allows the electrophysiological signal coming from the body to be acquired without the need for gels or adhesives, without specific medical preparation, and including fabric between the body and sensing electrode (Kaniusas, 2019; Lim *et al.*, 2007,1).

This family of sensors is a promising substitute for long-term applications and ubiquitous sensing. However, they still present some major limitations due to their contactless nature (Lim *et al.*, 2014; Taji *et al.*, 2013): motion artifacts (MAs) are significantly larger compared to gel-type contact sensors and, depending on the relative position of the body on the sensor, the effective area of the capacitive coupling can vary, decreasing the signal-to-noise ratio (SNR) and affecting the uniformity of the measurements.

Many works can be found in the literature that use different and innovative post-processing techniques to restore the acquired signal in case of bad acquisition set-ups and MAs (Chatterjee, Thakur, Yadav, Gupta & Raghuvanshi, 2020; Sirtoli, Liamini, Lins, Lessard-Tremblay, Cowan, Zednik & Gagnon, 2023; Venkatachalam, Herbrandson & Asirvatham, 2011). However, excessive filtering and processing can result in additional artifacts and loss of information in the signal, while also increasing the total complexity, cost, and power consumption of the final

sensor (Lessard-Tremblay *et al.*, 2020; Lim *et al.*, 2007; Taji *et al.*, 2013). It is thus important to put as much emphasis on the development of the electrode side of the sensor.

As the working principle of this type of sensor is based on the parallel plate capacitance relation, $C = \epsilon_0 \epsilon_r \frac{A}{d}$, where A is the surface area of the electrode that is able to establish a capacitive coupling with the body, d is the distance between the electrode and the body (which takes into account the dielectric presence) and ϵ_0, ϵ_r are the dielectric permittivity of vacuum and of the relative dielectric constant between the two electrodes. The geometrical characteristics of the sensor electrode and the coupling mechanism between the electrode and the body are of extreme importance for a good quality signal acquisition (Wang *et al.*, 2020b): the higher the capacitance established between the electrode and the body, the higher the SNR at the input of the sensor amplifier and the lower the cutoff frequency, which is of critical importance for a lossless signal acquisition (Berson & Pipberger, 1966; Lessard-Tremblay *et al.*, 2020).

Flexibility is a crucial aspect in the development of capacitive sensors as the human body is not, in general, a flat surface:

- Adapting to any body shape allows the whole surface of the sensor to establish a capacitive coupling with the body, maximizing the effective capacitance and consequently the SNR.
- Conformability also reduces the effect of motion artifacts, such as the one resulting from the movement of the body during respiratory activity. Motion artifacts represent one of the major issues of capacitive sensing, as a direct result of the contactless nature of capacitive sensors (Lee *et al.*, 2014; Xiao, Xing, Yang, Li & Liu, 2022).
- By conforming evenly to different parts of the body, the sensing area is ideally constant, regardless of the point of application of the sensor on the body. This allows a uniform signal acquisition, especially in multi-sensor array systems, which translates into reduced active filtering in the signal post-processing phase, and thus less susceptibility to data attenuation (Lessard-Tremblay *et al.*, 2020).

Flexible Hybrid Electronics and Kirigami Electronics

The recent growth in the field of printed electronics (Khan, Thielens, Muin, Ting, Baumbauer & Arias, 2020) has fuelled fast developments in sensors ranging from capacitance, pressure, temperature, and humidity detection (Wiklund, Karakoç, Palko, Yiğitler, Ruttik, Jäntti & Paltakari, 2021). Printed electronics utilize conductive, semi-conductive, or insulating inks on flexible substrates (such as plastic or paper) using methods such as screen printing, inkjet printing, gravure or flexographic printing. Piezoelectric-based inkjet printing (Beedasy & Smith, 2020; Kim, Kang, Park, Hahn, Jung & Joung, 2009) has been successfully employed to rapidly prototype and fabricate devices such as RFID tags, temperature sensors, strain gauges, etc. The printing technique's benefits are attributed to its ease of design iterations, as a result of digital design file input, and ultra-low volume material consumption, generally in the range of 1-3 milliliters, allowing the use of small quantities for high-cost materials such as silver, copper, and gold to fabricate functional devices (Nayak, Mohanty, Nayaka & Ramadoss, 2019).

Many recent works have been focusing on the development of printed flexible devices, in particular employing flexible materials for the realization of the capacitive electrode (Baek *et al.*, 2012; Dong, Liu, Cheng, Tang, Chen, Zhong, Chen, Liu & Jiang, 2020; Lee *et al.*, 2014,1; Lessard-Tremblay *et al.*, 2020; Taccola, Poliziani, Santonocito, Mondini, Denk, Ide, Oberparleiter, Greco & Mattoli, 2021). However, when flexed or stretched, these materials change in dimension depending on their Poisson's ratio and, when subjected to mechanical stress, their electric and dielectric properties are affected (Cai *et al.*, 2009; Ohring, 2002), impacting the uniformity and the reliability of the measurements.

Flexible Hybrid Electronics (FHE) represents a sought-after alternative for the development of lightweight, conformable, and stretchable systems (Hao *et al.*, 2022; Tuncel *et al.*, 2020; Yan *et al.*, 2024): by seamlessly integrating the mechanical flexibility of flexible printed substrates with the high performance of traditional rigid electronics it promises significant advancements in developing wearable sensors that offer both comfort and performance. Several different

works have employed FHE to build flexible capacitive sensors for biopotential monitoring, with promising results, as displayed in Table 4.1.

Table 4.1 Examples of other research groups employing FHE to implement flexible capacitive sensors for biopotential monitoring, with relative sensor characteristics.

Research Group	Size (mm^2)	Electrode Type	Coupled Capacitance (pF)	Bandwidth (Hz)
Ueno et al. (Ueno, Akabane, Kato, Hoshino, Kataoka & Ishiyama, 2007)	1000-7000	Textile	39 - 59	0.05 - 100
Rachim et al. (Rachim & Chung, 2016)	900	Hybrid Textile	20	0.04 - 40
Gao et al. (Gao, Soman, Lombardi, Rajbhandari, Dhakal, Wilson, Poliks, Ghose, Turner & Jin, 2020)	400	Metal Sputter Deposition on Plastic	7 - 35	0.3 - 100
Roland et al. (Roland <i>et al.</i> , 2019)	248 - 314	Various	77 - 733	60 - 1064
Lessard-Trembley et al. (Lessard-Tremblay <i>et al.</i> , 2020)	853	Hybrid Printed	51 - 107	0.475 - 210
Takano et al. (Takano, Ishigami & Ueno, 2021)	2000	Textile	57	0.5 - 100
Ng et al. (Ng, Reaz, Crespo, Cicutin, Shapiai, Ali, Kamal & Chowdhury, 2023)	125	Hybrid Printed	127	0.01 - 312

While constituting a promising compromise between whole-flexible electronics and solid-state electronics, challenges such as robust electrical connections between different materials and components, mechanical fatigue and failure over time, compatibility and long-term stability

among diverse materials still represent major limitations to the widespread of FHE in commercial products.

Kirigami, the antique Japanese art of paper cutting, has been shown to be a simple and easy to implement technique to improve the flexibility of electronic devices, without affecting their intrinsic characteristics (Choi *et al.*, 2021; Yang *et al.*, 2016; Zhai *et al.*, 2021). Some recent works employ the advantages of Kirigami patterning combined with printed devices to enhance device performances (Li *et al.*, 2019; Yu, Hao, Zhang, Zheng, Du, Liang, Wu & Zheng, 2021; Zhang, Wang, Zheng, Yang, Dong, Lu, Xuan & Gong, 2021), thanks to its improved electro-mechanical stability with increased electrical conductivity stability over larger strain regimes (Li *et al.*, 2019). This innovative method, paired with printed electronics, represents a promising solution for many applications of capacitive sensing (Morelli *et al.*, 2023).

However, Kirigami electrodes are not easy to incorporate in traditional sensors due to their important flexibility, which results in greater difficulty of integration to create a durable and robust connection while preserving the electrode flexibility.

In this work, we present a new hybrid capacitive sensor design approach, which addresses the above-mentioned challenges and limitations of FHE, by including the whole printed circuit board (PCB), and not just single components, on the flexible device. Conceived as a novel method applicable to any printed capacitive sensor, the present work aims to improve the flexibility of FHE printed devices: the design method introduces an additional Kirigami printed layer to connect the rigid sensor PCB to the flexible Kirigami electrode, without affecting the mechanical and electrical characteristics of both sides. Achieving enhanced flexibility has the purpose of improving the robustness of the sensor to common MAs, such as the change in coupled surface area and variation in pressure between the sensor and the target body, producing a more stable and uniform signal acquisition.

To test the efficacy of the new design method, a sensor prototype was built, which comprises a traditional Analog Front-End (AFE) and a multi-layer printed Kirigami electrode, exhibiting

remarkable flexibility and conformability on the electrode side while maintaining the robustness and reliability of conventional electronic components on the sensor side.

Compared to other FHE solutions found in literature (Kim *et al.*, 2019; Liu *et al.*, 2021; Poliks *et al.*, 2016), the novel sensor hybrid structure provides a new design approach that is effective, easy to implement and compatible with conventional manufacturing methods and materials, in order to produce a robust flexible capacitive electrode that can easily adapt to any curved surface, optimizing the sensing acquisition on the electrode-side, while being adaptable and compatible with conventional technologies and materials.

4.2 Materials and Methods

The presented sensor structure includes three main functional layers: (1) the printed Kirigami electrode layer, composed of a single side capacitive electrode; (2) the printed Kirigami connecting structure, necessary to connect the flexible Kirigami layer to the PCB; (3) the sensor AFE, mounted on a rigid PCB.

4.2.1 Kirigami Electrode and Connecting layers

Kirigami technique was applied to both the electrode and connecting layers, representing the flexible side of the hybrid sensor. Their fabrication comprises two separate phases: the printing phase, to deposit the silver and insulating functional layers on a flexible dielectric substrate, and the cutting phase, to create the two different Kirigami structures by means of laser cutting.

4.2.1.1 Printing Phase:

Both the electrode layer and the connecting layer are based on inkjet printed silver on a flexible dielectric substrate: in the case of the electrode layer, the printed silver electrode corresponds to the actual capacitive electrode, while the substrate acts as dielectric layer facing the sensing target; meanwhile, for the connecting layer, the printed silver area acts as a connecting base between the PCB and the flexible electrode, allowing to create a conductive path between the

bottom of the PCB and the flexible electrode below.

Silver nano-particle ink from ANPPPro (Silverjet P 40TE-20C) was printed using a Ceradrop X-series printer loaded into a 13 pico-liter SAMBA cartridge. Kapton FPC 125 μm from American Durafilm was selected as dielectric substrate, and first cleaned with 99 % acetone solvent. Four layers of the silver ink were printed in the form of $3 \times 3 \text{ cm}^2$ squares.

Intermittent drying steps using an Adphos near infrared drying lamp integrated into the Ceradrop system were performed to allow uniform drying of the printed ink. The printed structures were then sintered in a Mancorp MC301N reflow oven for 1 hour at 300 °C in air. Dycotech DM-INI-7003 ink was chosen as insulating layer. Six layers of the insulating ink were inkjet printed atop the sintered silver electrodes, via Ceradrop printer, in the form of $4 \times 4 \text{ cm}^2$, with two central holes left empty to allow an electrical connection with the silver layer below. Each layer of the printed insulator ink was UV cured in place using the built ink UV cure lamp at 5.5 mW/cm^2 and 10 mm/s conveyor velocity followed by a final cure step at 100 % power and 1 mm/s speed.

4.2.1.2 Laser Cutting Phase

The two layers were cut into two different Kirigami structures utilizing laser cutting (Samurai UV Marking System, DPSS Lasers, Inc.), with a final dimension of $5 \times 5 \text{ cm}^2$, designed for the specific function of each layer (Fig. 4.1):

For the electrode layer, the chosen Kirigami pattern consists of standard squared, equally distanced, hierarchical perpendicular cuts, as shown in Fig. 4.1a). The starting Kirigami design was taken from the structure realized in (Morelli *et al.*, 2023): three different hierarchical levels of cuts were performed with a dimension of respectively $l_1 = 20 \text{ mm}$, $l_2 = 12 \text{ mm}$, $l_3 = 4.5 \text{ mm}$, and hinges of width $\delta = 1.5 \text{ mm}$. This type of structure allows for better conformability to any arbitrary non-flat surface, showing improved coupled capacitance compared to an equivalent, non-cut printed electrode (An, Domel, Zhou, Rafsanjani & Bertoldi, 2019; Morelli *et al.*, 2023). The flexibility and conformability of the electrode come from the subdivision of the printed

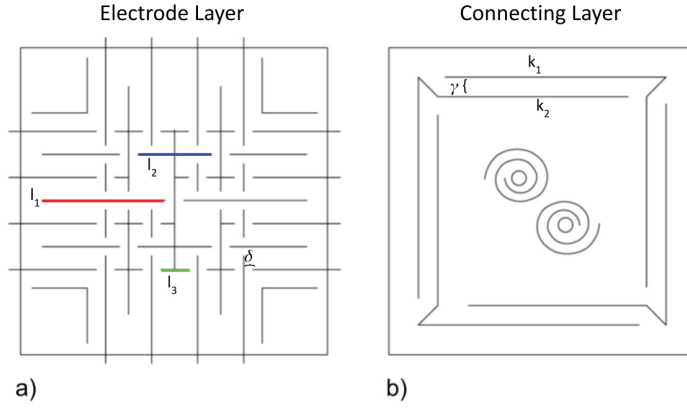


Figure 4.1 Laser-cut AutoCad design for the two different layers: a) the Kirigami electrode pattern, where the sets of hierarchical cuts are represented by $l_1 = 20 \text{ mm}$ (in red), $l_2 = 12 \text{ mm}$ (in blue), $l_3 = 4.5 \text{ mm}$ (in green), and the hinges by $\delta = 1.5 \text{ mm}$; b) the closed-loop Kirigami connecting layer, with cuts of respectively $k_1 = 36 \text{ mm}$ and $k_2 = 29 \text{ mm}$, distanced $\gamma = 3 \text{ mm}$ from each other.

layers into rotating square sub-units, with the connections between these units acting as free rotational hinges. This allows macroscopic deformation to occur mainly through rotation of the sub-units, rather than by attempting to deform the rigid sub-units themselves (Grima & Evans, 2000; Zhai *et al.*, 2021). Said mechanism allows the electrode to bend easily in all directions and adapt to any arbitrary non-flat surface, while maintaining intact its intrinsic characteristics.

Said mechanism allows the electrode to bend easily in all directions and adapt to any arbitrary non-flat surface, while maintaining intact its intrinsic characteristics. The design was slightly modified for the specific application: a portion of cuts on the central part was removed to leave enough non-cut surface available for the connection with the above connecting layer, and the external cuts were extended to reach the perimeter of the bigger electrode surface.

The connecting layer has the critical function of connecting the rigid PCB sensor to the flexible Kirigami structure of the electrode, without affecting its flexibility and while assuring a robust electrical and mechanical connection. The decision to employ a second, different, Kirigami structure as a middle layer represents a novel design approach to allow a robust but flexible connection between rigid components and flexible printed ones. For this reason, a closed-loop

Kirigami structure, corresponding to the external cuts framing the printed pattern in Fig. 4.1b), was chosen: external and internal cuts of respectively $k_1 = 36 \text{ mm}$ and $k_2 = 29 \text{ mm}$, distanced $\gamma = 3 \text{ mm}$ from each other, enable a spring-like behavior in the connecting layer, allowing the central part to extend out-of-plane while remaining flat, in response to corners and borders bending or contracting (Tao, Khosravi, Deshpande & Li, 2022).

The central silver printed part of the layer is conceived to be rigidly fixed to the PCB, while the external, cut frame is to be connected to the Kirigami electrode by its four angles exclusively. In this configuration, the Kirigami electrode is free to flex and conform to the target body, and at the same time, the central area where the PCB is attached remains flat even when the electrode below is flexed, because of the connecting layer structure that allows the motion of the central flat area out-of-plane, while the external frame bends to follow the electrode. The electrical connection between the two is assured by two central, silver-covered, spiral cuts. The spiral structure is not attached to the PCB, and is instead left free to move and elongate from the connecting layer to be linked to the central holes of the electrode layer, assuring a good electrical connection while maintaining the necessary flexibility. The contact is formed through silver epoxy paste (LOCTITE ABLESTIK 965-1L) applied manually on top of the cut-through spiral connectors, and thermally cured at 100°C for 3 hours. There are two points of contact built between the different layers: between the spirals and the prearranged dielectric holes on the electrode, and between the silver print of the connecting layer and the copper base of the PCB (Fig. 4.2).

4.2.2 Analog Front-End (AFE)

The AFE used in this work is a simple pre-amplifier circuit that allows the measurements of biological signals by capacitive sensing (Sun & Yu, 2016), consisting of an op-amp in a buffer configuration and a bias resistor, as schematically represented in Fig. 4.3.

The components are mounted on a rigid PCB of the size of $34.3 \times 34.3 \text{ mm}^2$, with an exposed copper bottom to allow the connection of the electrode to the input of the op-amp. The final multilayer structure and prototype sensor are illustrated in Fig. 4.4.

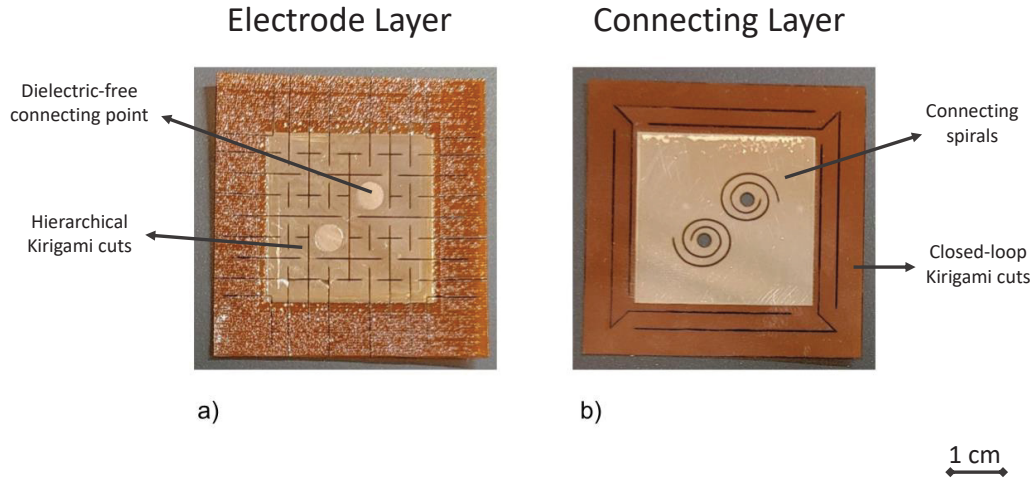


Figure 4.2 Printed layers after laser cut: a) the Kirigami electrode layer (Kapton substrate and printed silver electrode covered by six layers of insulating ink, two circles of silver were left uncovered to allow electrical connection with the connecting layer); b) the closed-loop Kirigami connecting layer (Kapton substrate and printed silver, two holes surrounded by spirals were cut through, to allow electrical and mechanical connection with the electrode layer).

4.2.3 Experimental Set Up

To quantify the improvement in electrode performance between our novel Kirigami hybrid electrode and an arbitrary rigid electrode, a series of capacitive and electrical measurements were performed in different conditions of applied weights and second plate dimensions. For direct comparison with a rigid sensor, the same PCB was used as AFE, and a printed, single-layer electrode was rigidly glued to its bottom side, made of the same materials and with the same geometrical features of the equivalent Kirigami electrode, but with no Kirigami structure applied. The goal of the performed tests is to provide an attentive but general characterization focused on specific electrical characteristics that are common to all types of electrical biosignals and are indicators of the effect of MAs on the acquisition process.

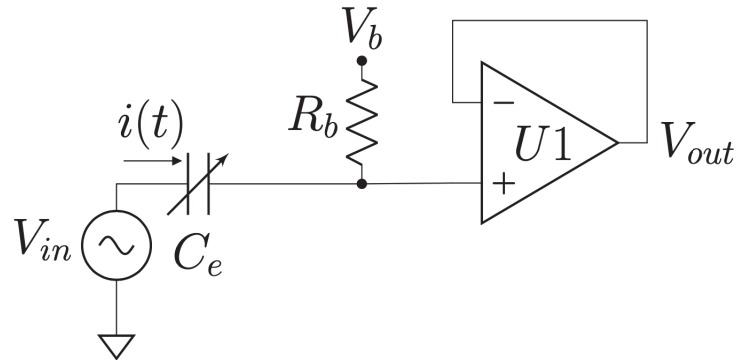
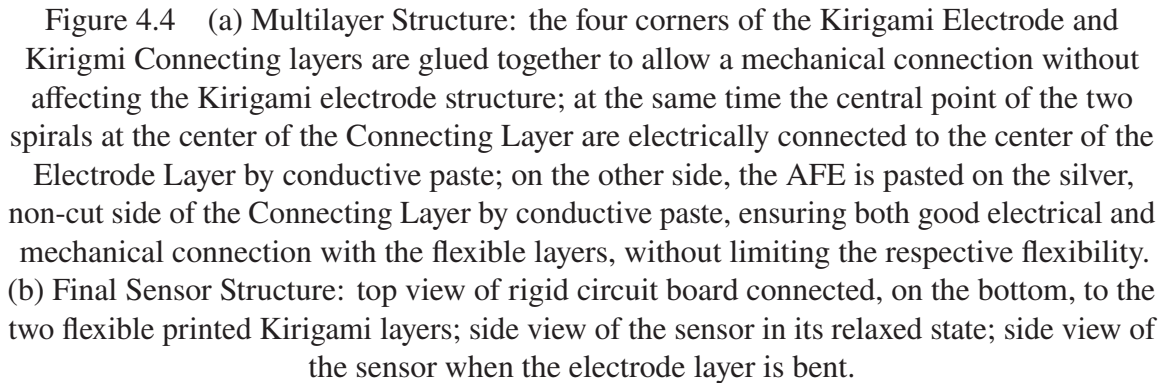


Figure 4.3 Simplified electrical model of Analog Front-End: V_{in} is the signal acquired by the electrode, C_e is the coupled capacitance between the sensor electrode and the second plate, V_b and R_b are the bias voltage and resistor, $U1$ is the op-amp connected in a buffer configuration and V_{out} the resulting acquired signal.

The capacitive measurements are performed using an Impedance Analyzer (Keysight E4990A), considering the electrode and the target body as two plates of a capacitor: the device, acting as the first plate, was positioned on a conforming insulating polyester sponge sample holder, with the dielectric layer facing up, and a conductive aluminum hemispherical body of varying diameter was placed on top of it to act as the second, non-planar plate of the capacitor (simulating different parts of the human body). The series capacitance between the aluminum plate and the Kirigami electrode connected to the sensor was measured on a frequency range of 20 Hz to 1 kHz, to assure the consistency of the measurement: as the measurements revealed to be constant in this range, the capacitance acquired at 500 Hz was arbitrarily chosen as representative value. The main goal of these types of measurements is to verify that the multi-layer design is effective in allowing the Kirigami electrode to maintain its flexibility, thus showing good capacitive coupling with the sensing target, while being integrated on the rigid PCB.



The electrical measurements consist in the transmission of a sinusoidal signal from an arbitrary aluminum second plate to the sensor, imitating the signal acquisition of a biopotential coming from the body. The measurement set-up is the same as for the capacitive measurements, but in place of an Impedance Analyzer, a 1 Hz sinusoidal signal (Agilent 33500B - Waveform Generator) was injected in the aluminum second plate, and the output pin of the sensor was connected to an oscilloscope (Keysight InfiniiVision DSOX3014T) in order to analyze the signal acquisition (Fig. 4.5a)).

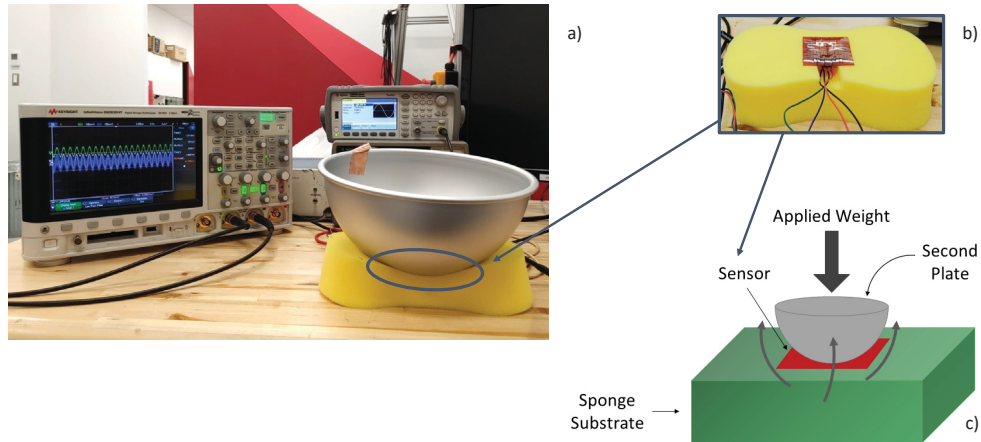


Figure 4.5 Electrical measurements setup: a) second plate placed on top of the sensor, a single frequency (1 Hz) signal from the signal generator is injected into the second plate, acquired by the sensor and analyzed on the oscilloscope; b) position of the sensor on the sponge holder, with the Kirigami electrode showing on top, before the application of the second body on it; c) schematic representation of sensor and second plate setup during the measurements.

The measurement results consider two main signal characteristics: the amplitude and the cutoff frequency. The amplitude of the transmitted signal is considered as a reference point to obtaining satisfactory SNR in any actual sensing application, while the cut-off frequency represents an indication of the quantity of information transmitted, and thus, the quality of acquired signal.

The aluminum second plates considered in the experiments are one flat surface plate and different hemispheres of respectively 15 cm, 6.3 cm, 5.5 cm and 4.5 cm of diameter, corresponding to a curvature of 0, 0.13, 0.32, 0.36 and 0.44 cm^{-1} , respectively (Fig. 4.5c)). The measurements are repeated for both the non-Kirigami and the Kirigami hybrid electrodes.

Overloads of ≈ 1.1 kgf (2.5 lbf), ≈ 2.2 kgf (5 lbf) and ≈ 3.3 kgf (7.5 lbf) were applied to both cases, to test the uniformity of the electrode under different pressure applied. Each measurement (capacitive and electrical) was repeated 10 times, and the average value was considered.

Lastly, the device was subjected to a 100 cycles bending test, at 60 degrees of bend, to evaluate the mechanical reliability of the structure. After that, the electrical measurements were repeated and the results compared with the first measured values.

4.3 Results

4.3.1 Capacitive Measurements

In Table 4.2 the average capacitance values measured for both the rigid sensor and the Kirigami hybrid sensor are listed, for different second plate curvatures. The measurements are the average of 6 measurement repetitions, with an applied weight of 2.2 kgf for each second plate.

Table 4.2 Average measured coupled capacitance of both the Kirigami sensor and the equivalent rigid sensor, when applied to second plates of different curvatures.

Average Measured Capacitance (pF)		
Second Plate Curvature (cm^{-1})	Rigid Sensor	Kirigami Sensor
0	70.69 \pm 0.62	115.53 \pm 0.69
0.13	69.96 \pm 1.46	79.98 \pm 2.08
0.32	37.63 \pm 1.45	60.75 \pm 3.87
0.36	29.23 \pm 2.67	35.8 \pm 3.34
0.44	25.97 \pm 5.25	31.82 \pm 3.77

In general, the trend for both sensors shows a decrease in value for increasing curvature. This is associated with the significant difference in second plate dimensions, which were specifically chosen to represent the behavior of the sensor in diverse situations (from flat to extremely curved). However, for all second plates considered the hybrid Kirigami sensor exhibits higher capacitance compared to the equivalent non-Kirigami one. Even in the extreme case of curvature 0.44 cm^{-1} , while still partly losing conformability due to the small dimension of the second plate, and thus significantly decreasing in capacitive value, the recorded coupled capacitance presents an increase of +32 % compared to its rigid counterpart.

The capacitive measurements of the single Kirigami hybrid sensor have been repeated, this time with different weights applied on top, and the results are represented in Fig. 4.6. Each

value corresponding to the same second plate dimension exhibits negligible difference ($\leq 8\%$), indicating a good resistance of the Kirigami electrode to variations in applied pressure.

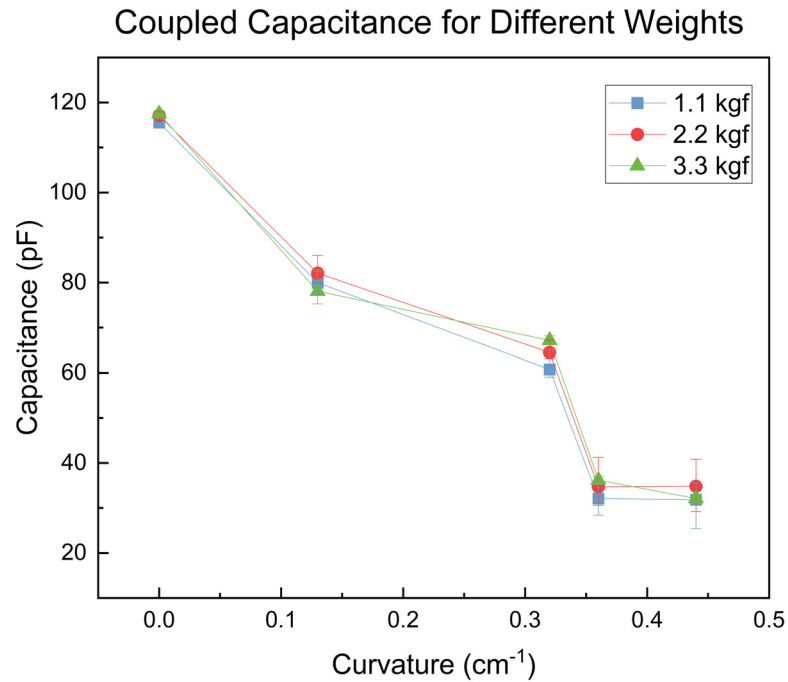


Figure 4.6 Measured coupled capacitance, for different second plate curvature, of Kirigami flexible sensor with weights of 1.1, 2.2 and 3.3 kgf applied on top of each second plate.

4.3.2 Electrical Measurements

To validate the above results, the capacitive measurements were followed by electrical measurements of a sinusoidal 1 Hz signal transmitted from aluminum second plates of varied curvatures to the sensor, with different weights applied.

In Fig. 4.7, the acquired signal amplitudes, for different second plate diameters are represented. The different colors correspond to the different weights applied on top of the second plate. Consistently with the capacitive measurements, the amplitude trend inversely follows the curvature of the plates, confirming the importance of good conformability for better signal

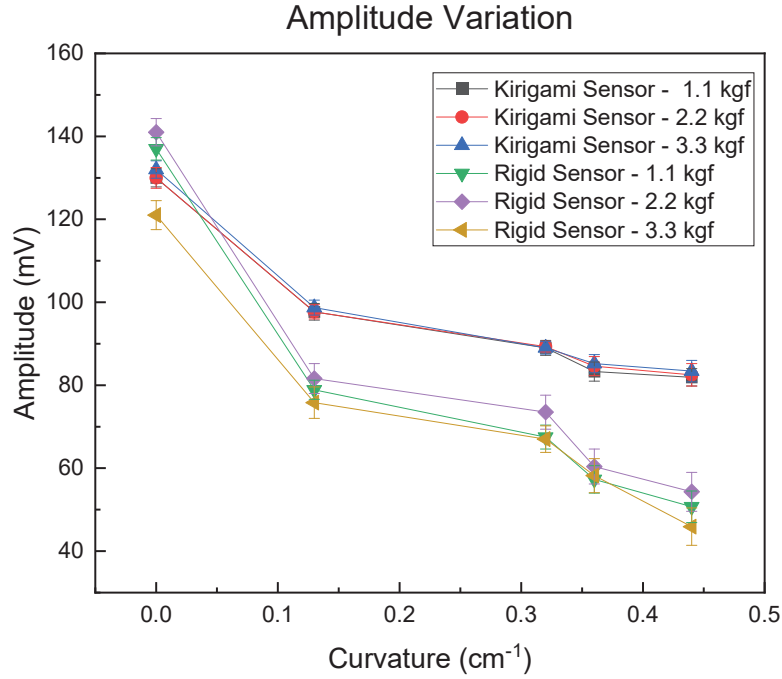


Figure 4.7 Measured amplitude variations of the acquired signal, for different second plate curvatures and different weights applied, comparing the performance of the Kirigami flexible sensor against the rigid sensor.

quality: measurements corresponding to a flat second plate exhibit a comparable signal amplitude for all weights applied; meanwhile, for increasing curvature a decrease in amplitude is recorded, as the capacitive coupling between the two sides deteriorates.

However, for a flexible Kirigami sensor, the difference in acquired signal amplitude, while still decreasing for bigger curvatures, shows a significant improvement (up to +82% for the bigger curvatures) compared to the non-Kirigami one. In addition, the Kirigami sensor exhibits little to no variation when varying applied pressure, coherently with the results obtained in the capacitive measurements above.

The cutoff frequency of the sensor bandwidth was also measured, for the different curvatures and different weights applied. The cutoff frequency ($f_c = \frac{1}{2\pi RC}$) is by standard definition the frequency corresponding to an amplitude fall of 3 dB. Starting from the measured amplitude in

Fig. 4.7, for each case the frequency of the transmitted signal was gradually decreased from 1 Hz, till the acquired signal amplitude decreased of 3dB. The frequency registered on the oscilloscope corresponding to said amplitude was recorded as the resulting cutoff frequency.

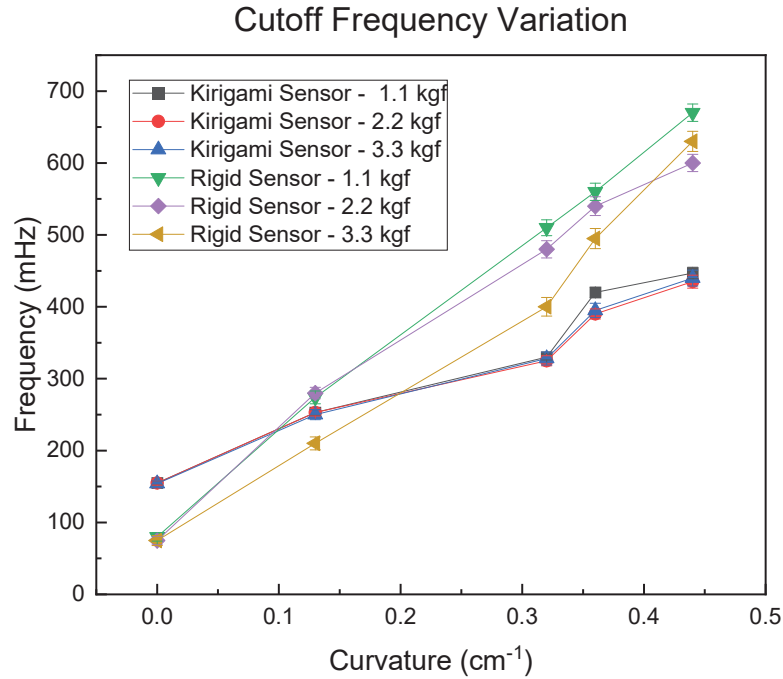


Figure 4.8 Measured cutoff frequency variations of the acquired signal, for different second plate curvatures and different weights applied, comparing the performance of the Kirigami flexible sensor against the rigid sensor.

In Fig. 4.8 the cutoff frequency variations for the different curvatures considered are plotted, divided by applied weight. For all cases, the f_c tends to grow for increasing curvature, however, for the non-flexible case the increase is significantly higher than the Kirigami case: in the case of the rigid electrode, the gap in measured cutoff frequency for the zero curvature (flat second plate) to the 0.44 cm^{-1} hemisphere case is of +738 %; meanwhile, in case of the Kirigami electrode, the total increase for the smallest second plate is significantly smaller: of +180 %. In addition, the different applied weights do not significantly affect the resulting f_c , showing good bandwidth uniformity for pressure variations during the measurements.

Finally, the sensor prototype was subjected to a mechanical reliability bending test, to monitor the effect of repetitive stress on the structure. The sensor was placed on a bending test machine and 100 bending cycles were executed consequently, at 60 degrees of bending (Fig. 4.9b)). Following, the signal amplitudes were recorded once again, for the different diameters, at 1.1 kgf applied, and the results were compared to the previous measurements in Fig. 4.9a).

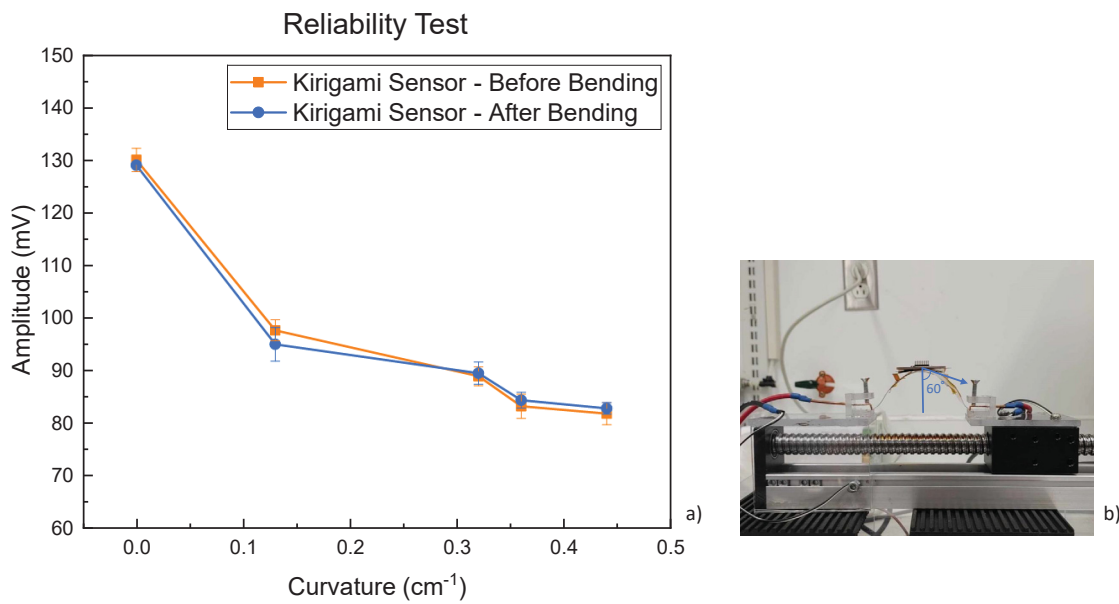


Figure 4.9 a) Measured amplitude variations of the acquired signal, before and after 100 bending cycles, for different second plate curvatures at 1.1 kgf applied; b) Mechanical bending test setup: 100 bending cycles at 60 degrees of bend.

4.4 Discussions

The designed multi-layer kirigami hybrid structure proved to be effective in allowing good flexibility and conformability of the electrode, while maintaining excellent electrical and mechanical contact throughout numerous bending and flexing tests while subjected to different weights.

The results of both the capacitive measurements and the sensor electrical measurements show consistency, indicating a direct relationship between the improved conformability brought by the novel Kirigami design and the performance of the sensor.

To better understand the effects of the electrode structure on the sensor it is useful to analyze each different aspect at time. First, as shown in both the capacitive measurements (Table 4.2) and electrical recording (Fig. 4.7), the Kirigami structure allows for a better conformability to any arbitrary non-flat surface, leading to more surface of the electrode to establish a capacitive coupling with the target surface. As a consequence, the total capacitance established by the sensor will increase, increasing the amplitude of the acquired signal and helping achieve a higher SNR.

If we consider that, for biopotential monitoring, a sensor is never used singularly but is usually part of an array of sensors that could be applied to different parts of the body, the remarkable flexibility of the Kirigami electrode favour the coupling of the different sensors of a system with the body, improving not only the performance of the single electrode but also the uniformity of the measurements for the whole system.

Moreover, a low cut-off frequency value is also extremely important for lossless signal acquisition: in the case of biosignals, many of them present a bandwidth in the very lower frequency spectrum (Bronzino, 2006; Kaniusas, 2019). The loss of information is not the only problem related to an inadequate cut-off frequency. While using a slightly higher cut-off, with the right filtering, usually results in a still legible and satisfactory signal output, it can also introduce artifacts in the recordings that may lead to erroneous signal interpretation (Berson & Pipberger, 1966; Driel *et al.*, 2021; Lessard-Tremblay *et al.*, 2020). Being able to achieve a low cut-off frequency at the point of signal acquisition is thus important to ensure no information loss and/or no added artifacts, regardless of the sensing application. As shown in Fig. 4.8, the Kirigami sensor shows a lower cutoff value compared to the rigid sensor for all curved second plates considered, even the smaller ones.

Higher conformability of the single sensor allows thus to achieve higher SNR, lower cutoff frequency and improved uniformity of the acquired signal, all before the filtering and post-processing phase.

In addition, the Kirigami multi-layer structure allows the electrode layer to be partially detached from the rigid PCB and free to bend and stretch when in contact with the body, while still maintaining good electrical contact. This added level of freedom favors the flexibility of the Kirigami electrode, allowing it to easily follow the curvature of the target body even with different pressures applied. As noticeable from Fig. 4.7 and 4.8, when varying weight from 1.1 kgf to 2.2 kgf and 3.3 kgf, for each second plate considered, the measured values vary minimally, confirming the good adaptability of the sensor to pressure variations. Other works show examples of how increasing the pressure on the electrode serves to improve the capacitive coupling and, consequently, the sensor performance (Kim, Lee & Jeong, 2020; Ng & Reaz, 2019). Being susceptible to pressure changes, however, also makes the sensor more vulnerable to some type of MAs caused, for example, by the breathing pattern of the body or any partial movement that translates into a change of pressure on the electrode.

Finally, comparing amplitude measurements before and after the reliability bending test shows no significant difference. The multilayer Kirigami structure proves to be effective in minimizing the stress applied during bending, both on the electrode side, where the cuts critically reduce the effect of the stress on the printed conductive surface (Morelli *et al.*, 2023), and on the connections between electrode and AFE, where the middle Kirigami layer secures robust contact within the two while allowing freedom of movement, even after 100 bending cycles.

The Kirigami sensor presents improved conformability and flexibility, thanks to its novel designed multi-layer hybrid structure, allowing the electrode to conform well and maintain constant contact with the body under different pressures. This results in improved SNR and cut-off frequencies, without the need of additional signal post-processing.

4.5 Conclusions

In this work we presented a novel design and structure concept for printed electrodes for biopotential capacitive sensing based on Kirigami. The design comprises different layers cut in different Kirigami structures, each specifically designed for their individual function, allowing the electrode to be flexible and stretchable while being incorporated on traditional rigid PCBs and maintaining good electrical contact.

Capacitive and electrical measurements have been performed on the sensor under different conditions of weight applied and different sizes/shapes of sensing target in order to estimate their robustness to the most common MAs. The results obtained showed substantial improvement for the presented structure when compared to an analogous rigid sensor.

Both the flexibility of the Kirigami electrode and the compliance of the multi-layer hybrid structure lead to an improved conformability to any arbitrary second plate and increased robustness to variation of pressure, thus increasing the amplitude of the acquired signal, reducing the cutoff frequency and improving the uniformity of the measurements.

The novel design represents an easy-to-implement, robust, and effective method applicable to any printed capacitive sensors, allowing the integration of flexible printed electrodes on traditional rigid PCBs, improving the first's performance while maintaining the latter's reliability.

CHAPTER 5

ANALYTICAL MODELING AND EXPERIMENTAL VALIDATION OF TRIBOELECTRIC BEHAVIOR IN KIRIGAMI FLEXIBLE CAPACITIVE SENSORS

Laura Morelli¹, Vinicius Sirtoli³, Ghyslain Gagnon², Ricardo J. Zednik¹

¹ Département de Génie Mécanique, École de Technologie Supérieure,
1100 Rue Notre-Dame Ouest, Montréal, Québec, H3C 1K3, Canada

² Département de Génie Électrique, École de Technologie Supérieure,
1100 Rue Notre-Dame Ouest, Montréal, Québec, H3C 1K3, Canada

³ Department of Electrical Engineering, Concordia University,
1455 Blvd. De Maisonneuve Ouest, Montréal, Québec, H3G 1M8, Canada

Article soumis dans la revue

« IEEE Transactions on Instrumentation and Measurement »

le 5 Août 2024.

<https://ieeexplore.ieee.org/xpl/RecentIssue.jsp?punumber=19>

Résumé: Les capteurs capacitifs flexibles ont attiré une attention considérable ces dernières années, notamment pour leur application dans la détection électrophysiologique biomédicale, car ils améliorent le confort et la flexibilité tout en étant plus robustes face à certains types d'artefacts de mouvement. En raison de leur nature sans contact, ils restent cependant sensibles à la triboélectricité, qui, en raison de leur flexibilité, semble être plus forte et plus imprévisible par rapport à leurs homologues rigides. Dans ce travail, nous proposons un nouveau modèle analytique pour prédire et justifier physiquement le comportement triboélectrique des capteurs capacitifs flexibles appliqués à des surfaces non planes. En particulier, nous considérons le cas général d'une électrode conformant à une surface sphérique, qui perd le contact à cause d'un mouvement transversal. Le modèle prend en compte à la fois l'effet de la tension triboélectrique et la capacité couplée variable, décrivant les différentes phases du mouvement. Enfin, des mesures électriques ont été réalisées sur le capteur, reproduisant en laboratoire le même dispositif et les mêmes dynamiques. Les résultats ont été comparés au modèle analytique et discutés: les résultats analytiques et expérimentaux présentent des tendances et des caractéristiques de tension similaires, avec une durée de pic pour chaque vitesse de 4.1 s, 2.1 s, 0.9 s pour l'effet modélisé et 4.6 s, 2.5 s, 1.1 s pour les résultats expérimentaux correspondants. Le modèle analytique

présenté s'est révélé précis pour décrire les artefacts de mouvement causés par le mouvement considéré et représente un outil important pour décrire et prédire des artefacts similaires pour les capteurs capacitifs flexibles.

Flexible capacitive sensors have attracted extensive attention in recent years, especially in their application for biomedical electrophysiological sensing, as they improve comfort and flexibility while being more robust to some types of motion artifacts. Due to their contactless nature, they are still susceptible to triboelectrification which, because of their flexibility, appears to be stronger and more unpredictable compared to their rigid counterparts. In this work, we propose a novel analytical model to predict, and physically justify, the triboelectric behavior of flexible capacitive sensors applied to non-flat surfaces. In particular, we consider the general case of an electrode conforming to a spherical surface, which loses contact because of a transversal motion. The model takes into account both the effect of the triboelectric voltage and the varying coupled capacitance, describing the different phases of the movement. Finally, electrical measurements were performed on the sensor, reproducing in-lab the same set-up and dynamics. The results were compared to the analytical model and discussed: both the analytical and experimental results exhibit similar trends and voltage characteristics, with spike duration for each speed of 4.1 s, 2.1 s, 0.9 s for the modeled effect and 4.6 s, 2.5 s, 1.1 s for the corresponding experimental results. The presented analytical model revealed to be accurate in describing the motion artifacts caused by the considered motion, and represents an important tool for describing and predicting similar artifacts for flexible capacitive sensors.

Keywords: Capacitive Sensing, Triboelectric Effect, Printed Electronics, Flexible Sensors, Kirigami.

5.1 Introduction

Capacitive sensing exploits the fundamental principles of a parallel plate capacitor, enabling the acquisition of various signals across a multitude of applications: from strain sensors to pressure sensors, humidity sensors, electropotential sensors, and electrophysiological sensors (Anandan & George, 2017; Baek *et al.*, 2013; Costa, Spina, Lugoda, Garcia-Garcia, Roggen & Münzenrieder, 2019; Klein *et al.*, 2019; Lee *et al.*, 2014; Uguz *et al.*, 2020; Wrasse *et al.*, 2019).

This family of devices has the advantage of being able to sense a specific signal without the need for direct contact between the sensor and the target. In the realm of electrophysiological sensors, for instance, physiological signals are captured by a single electrode through displacement current (Xiao *et al.*, 2022). The set-up is similar to traditional Ag/AgCl wet electrode, but without the need for adhesive gel, and thus no clinical nor medical preparation (Kaniusas, 2019; Lim *et al.*, 2007,1).

With the current development of novel materials and techniques to produce thinner, more flexible and wearable electrodes and sensors, capacitive sensing represents an optimal solution for long-term, ubiquitous health monitoring.

Due to the contactless nature of the electrodes, these types of sensors are significantly more sensitive to motion artifacts (MAs), which represent the prime cause of error and misreading in the acquired signal (Lim *et al.*, 2014; Taji *et al.*, 2013). MAs include all the artifacts caused by the relative movement between the sensor and the target body: undesired changes in skin potential, electrode coupling variations and peaks in current caused by contact electrification (Prabakaran & Rufus, 2021; Webster, 1977).

The prevailing MAs commonly considered in the literature are the ones caused by the coupling variations between the body and the sensor, which induce a sensitive reduction in Signal-to-Noise Ratio (SNR) and loss of information (Heuer, Martinez, Fuhrhop & Ottenbacher, 2009; Ottenbacher & Heuer, 2009). There is, however, another important source of artifacts usually

overlooked because of its unpredictability and difficulty to compensate, which is the contact electrification of the electrode caused by contact changes between the sensor and the skin, also known as the triboelectric effect (Li, Hui & Sun, 2016).

Triboelectrification is a process caused by the contact interaction of two different surfaces that leads to an exchange of charges between the two sides (Wang & Wang, 2019; Wartzek, Lammersen, Eilebrecht, Walter & Leonhardt, 2011; Zhou, Liu, Wang & Wang, 2020b), creating an electric double layer with a resulting electrostatic voltage. The consequent separation of the two surfaces, either by sliding, detaching or rolling, can thus result in an even larger potential that can easily reach several kilovolts (Wartzek *et al.*, 2011).

Although no precise quantitative estimation is possible, due to the unpredictable contact morphology of the two surfaces at microscopic scale (Shen, Wang, Sankaran & Lacks, 2016; Sobolev, Adamkiewicz, Siek & Grzybowski, 2022; Wartzek *et al.*, 2011), some works have successfully described the process of contact electrification following the separation of two electrodes, and took advantage of this physical phenomenon to generate electricity with devices known as Triboelectric Nano-Generators (TENGs) (Shao, Jiang & Wang, 2020; Sirtoli, Morelli, Zednik, Cowan & Gagnon, 2024; Zhang, Yao, Quan & Zheng, 2020; Zhou *et al.*, 2020b).

A recent work (Sirtoli *et al.*, 2024) has successfully utilized the TENGs model to predict and physically explain the MAs in biopotential monitoring. That work considered MAs caused by the electrode sliding over the skin and detaching from the body, where both skin and electrode were modeled as rigid surfaces. When detaching from the body, the motion resulted uniform throughout the area of the electrode, meaning each point on the surface of the electrode detaches simultaneously from the body and travels the same distance at the same speed. The resulting triboelectric effect was therefore directly proportional to the traveled distance.

In the studied case, the effect causes an unwanted spike in the acquired signal, that is partly compensated by the steep reduction of coupled capacitance caused by the separation of the two sides. In real-life instances, however, this model presents some limitations, an important one being considering the body as a perfectly rigid and flat surface.

In the past years significant effort has been made in the development of capacitive sensors for electrophysiology monitoring, to provide more flexibility, improved comfort and reduced sensitivity to MAs. The introduction of flexible electrodes has been shown to be effective in improving the conformability to non-flat surfaces, increasing the capacitive coupling between the electrode and the body, therefore improving the signal quality and making the sensor more robust to MAs (Berson & Pipberger, 1966; Lessard-Tremblay *et al.*, 2020; Lim *et al.*, 2014; Wang *et al.*, 2020b).

However, while allowing for better conformability and decreased capacitance variation, flexible electrodes are still subjected to contact electrification the moment that the electrode starts detaching from the body. Differently than for the rigid electrode case, the surface of the flexible electrode does not detach parallel from the body, and the relations used previously to describe both the triboelectric voltage and the capacitance variation fail to describe this more complex behavior.

In this work we propose a novel, more accurate analytical model to describe the MAs caused by the detaching of a flexible capacitive sensor from a non-planar surface, taking into consideration the combination of the triboelectric effect and capacitance variation caused by the movement in a transversal direction. The model is then verified by in-lab electrical tests reproducing the separation moment of the flexible electrode from the body, for three different speeds of movement. The analytical and experimental results are finally compared and discussed in detail.

5.2 Analytical Model

In the case of capacitive coupled sensors detaching from a target surface (e.g the body in the case of biopotential sensing), the contact electrification mechanism is the same as for TENGs, and can be thus described by the V-Q-y relationship (Niu, Wang, Lin, Liu, Zhou, Hua & Wang, 2013; Sirtoli *et al.*, 2024):

$$V = \frac{1}{wl\epsilon_0} \left\{ -Q \left[\frac{d_{die}}{\epsilon_{r_{die}}} + \frac{y(t)}{\epsilon_{r_{air}}} \right] + \sigma_c wl \left[\frac{y(t)}{\epsilon_{r_{air}}} \right] \right\} \quad (5.1)$$

which describes the voltage V on the electrode (relative to ground) equal to the sum of the voltages caused by body charges, transferred to the second plate, and dielectric charges, transferred to the dielectric layer. The constants ϵ_0 , $\epsilon_{r_{air}}$ and $\epsilon_{r_{die}}$ are the vacuum permittivity, the relative permittivity of air and the relative permittivity of the dielectric layer, w and l are, respectively, the width and length of the electrode, d_{die} is the thickness of the dielectric layer covering the electrode, σ_c is the charge density on the electrode surface, Q is the amount of charge transferred from the skin to the electrode during the contact and $y(t)$ is a numerical variable indicating the distance between the two surfaces at time t . For a rigid electrode vertically detaching from a flat, conductive surface the MAs equations describing the combined effects of triboelectric voltage and variable capacitance can be summarized, starting from the TENGs equations, as follows (Sirtoli *et al.*, 2024):

$$V_{tribo}(t) = \frac{\sigma_c y(t)}{\epsilon_0 \epsilon_{r_{air}}} \quad (5.2)$$

$$C_e(t) = \frac{Q}{V_{tribo}} = wl\epsilon_0 \left[\frac{\epsilon_{r_{air}} \epsilon_{r_{die}}}{y(t) \epsilon_{r_{die}} + d_{die} \epsilon_{r_{air}}} \right] \quad (5.3)$$

Where the triboelectric voltage $V_{tribo}(t)$ can be deduced from (5.1) considering that there is no flow-back path for Q (open-circuit test), thus $Q = 0$. Similarly, connecting the electrode and the second plate (short-circuit test), causes $V = 0$ in (5.1) from which it is possible to deduce the varying capacitance $C_e(t)$.

In this specific case, the electrode is perfectly parallel to the second plate, and during the motion each point on the surface of the electrode detaches simultaneously and creates a parallel distance from the body, where the average distance $y(t)$ corresponds to the exact distance of each point on the surface at the instant t .

This model presents some limitations, such as in real-life applications the body is never a perfectly flat surface and, as a consequence, the height variable $y(t)$ cannot be defined as a linear numeric variable.

While for rigid electrodes, in some cases assuming $y(t)$ as a number can still be considered a valid approximation, in the case of a flexible electrode the approximation is far from accurate. Flexible materials and Kirigami structures have been shown to conform easily to non-flat surfaces (Brooks *et al.*, 2022; Li *et al.*, 2022; Morelli *et al.*, 2023) reducing the average distance between the electrode and the body. When a flexible electrode detaches from the body, it happens gradually as not all points on the electrode lose contact at the same time. Moreover, the separation dynamics depend on the body part where it is applied, on where the force is applied, on its surface, and the motion direction.

Let's take as an example the arbitrary case of a flexible electrode being applied on a spherical surface (Fig. 5.1), and said electrode detaching vertically from the sphere. We can divide the motion into three distinct phases, which correspond to different equations of the model, as follows:

5.2.1 Phase 1: Full contact

In the first phase, there is a gradual loss of pressure on the electrode, but its surface is still in full contact with the body, thus $y(t) = 0$ and $V_{tribo}(t) = 0$ (Fig. 5.1a).

In this phase, the total capacitance corresponds to the equivalent parallel plate capacitance of the two coupled surfaces:

$$C_e(t) = C_c(t) = \epsilon_0 \epsilon_{air} \epsilon_{die} \frac{A_c(t)}{d_{die}} = \epsilon_0 \epsilon_{air} \epsilon_{die} \frac{wl}{d_{die}} \quad (5.4)$$

where $A_c(t)$ is the surface of the electrode in contact with the second plate which, in this phase, is equivalent to the whole electrode area $w \cdot l$.

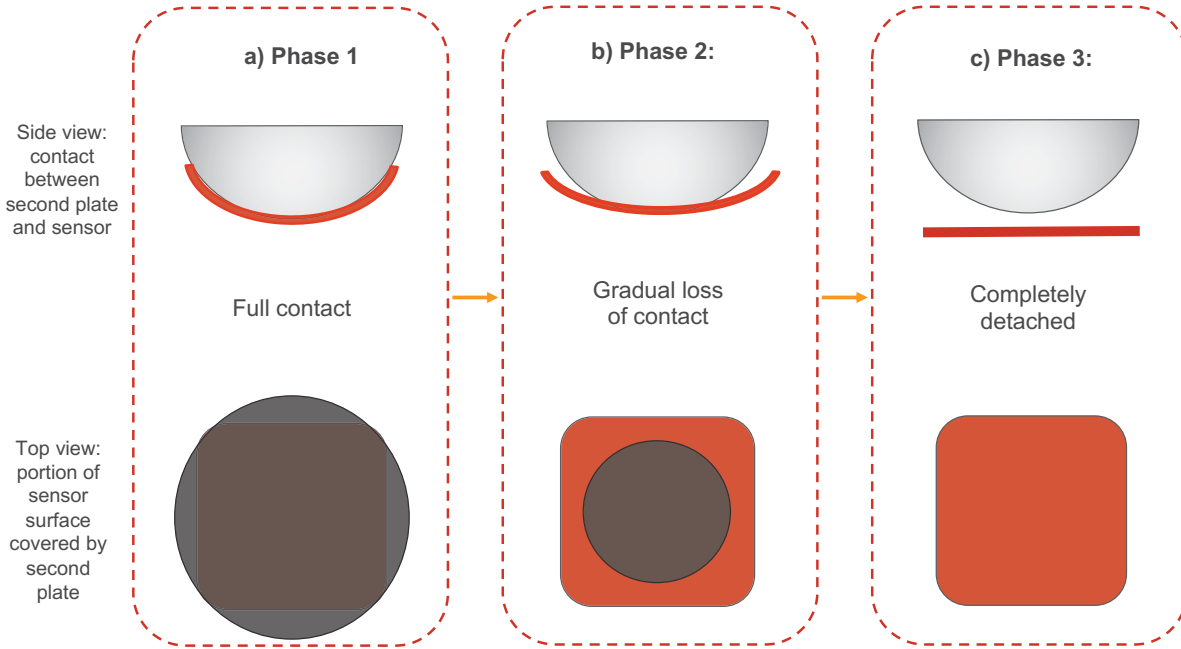


Figure 5.1 Transversal movement dynamic: on top the three phases of movement as seen from the side; on the bottom the view from the top of the electrode surface covered by the second plate.

5.2.2 Phase 2: Gradual loss of contact

The second phase corresponds to the gradual detachment of the external sides of the electrode (Fig. 5.1b), which will progressively form a gap of air with angle $\theta(t)$ with the second plate, that will increase with time from 0 to θ_f depending on the geometry of the electrode-second plate set-up.

Correspondingly, the detached surface of the electrode will take the approximate shape of a ring with a decreasing inner radius $r(t)$, which will extend with time to the point of covering the whole electrode surface, from r to 0 (defining $r = l/2$ as half the electrode length). In the last moment of this phase, the electrode is still in contact, and the last point to lose contact with the body corresponds to the center of the electrode. The average $y(t)$ in (5.2) can thus be rewritten as:

$$y(t) = \frac{(2\pi r - 2\pi r(t)) \cdot \int_0^{\theta(t)} \sin(x) dx}{\pi r^2 - \pi r(t)^2} \quad (5.5)$$

From the triboelectric effect perspective, the flexible behavior of the electrode amplifies the resulting voltage compared to the rigid case. This is caused by two main factors: the increase in speed of separation and the larger average distance between the two sides. When in full contact with the second surface, the flexible electrode is bent under the pressure of the other plate, thus not in its stable flat position. As the second plate starts to detach vertically at a constant speed, the electrode also tends to return to a flat position while gradually detaching from the second surface. The sum in speeds of the two movements results in a faster equivalent movement, which leads to a greater triboelectric effect. The same dynamic also causes a larger average distance between the two sides, given by the non-flat configuration compared to a flat one, which causes an amplified triboelectric voltage compared to an equivalent rigid case.

For the same reasons, the capacitance does not vary linearly with the increasing distance, therefore the equation (5.3) cannot be used to estimate the capacitive behavior. It has been previously investigated how flexible electrodes behave when capacitively coupled with a non-flat surface (Morelli *et al.*, 2023).

In this case, the modes are similar: the electrode starts detaching gradually from the second plate, and the external sides of the electrode introduce a gap of air with an inclination of $\theta(t)$, while the rest of the surface remains in contact. The resulting capacitance will be equivalent to the sum of both the contact portion of capacitance $C_c(t)$ and non-contact portion $C_{nc}(t)$, where

$$C_c(t) = \varepsilon_0 \varepsilon_{air} \varepsilon_{die} \frac{A_c(t)}{d_{die}} \quad (5.6)$$

and

$$C_{nc}(t) = \frac{\varepsilon_0 \varepsilon_{air} \varepsilon_{die}}{\sin(\theta(t))} \int_0^{2\pi} W(x) \cdot \ln \frac{R_2(x)}{R_1(x)} dx \quad (5.7)$$

The (5.7) describes a general case, where $\theta(t)$ is the angle formed between the non-conforming sides, $W(x)$ is the perimeter function delimiting the contact area on the electrode surface, which may vary case by case, $R_2(x)$ is the total radius, corresponding to the half-length of the electrode, and $R_1(x)$ is the portion of radius corresponding to the conforming portion.

In our more specific case of a flexible electrode applied on a spherical second plate, it has already been shown that the adhesion of the electrode on the spherical surface creates a symmetric pattern where the portion of surface gradually detaching can be described as four semicircles, each at the border of the electrode sides as shown in Fig. 5.2 b), with a radius $r_{nc}(t)$ that increases from 0 to r as the two surfaces gradually detach from each other, and an angle $\theta(t)$ that gradually increase from 0 to θ_f , depending on the specific geometry of the setup. The resulting capacitive relation for the non-contact portion of the surface can thus be rewritten as:

$$C_{nc_{air}}(t) = 4 \cdot \frac{\epsilon_0 \epsilon_{air} \epsilon_{die}}{\text{Sin}(\theta(t))} \int_0^\pi r_{nc}(t) \cdot \ln \frac{r}{r - r_{nc}(t) \cdot \text{Sin}(x)} dx \quad (5.8)$$

where the novel introduced variables are graphically represented in Fig. 5.2 a).

If, like in the described case, there are one or more layers of dielectric in between the two surfaces, the total capacitance describing the non-contact surface corresponds to a series of capacitors, where the capacitance relative to the dielectric section is:

$$C_{nc_{die}}(t) = \epsilon_0 \epsilon_{die} \frac{A_{nc}(t)}{d_{die}} \quad (5.9)$$

where A_{nc} indicates the portion of electrode surface no more in contact with the second plate.

If N is the total number of different layers of dielectric, the equivalent capacitance can therefore be calculated as the series of all the different sections:

$$C_{nc}(t) = \left(C_{nc_{air}}^{-1}(t) + \sum_{n=1}^N C_{nc_{dien}}^{-1}(t) \right)^{-1} \quad (5.10)$$

5.2.3 Phase 3: Completely detached

The third phase coincides with the complete detachment (Fig. 5.1c), when no point on the electrode surface is in contact with the second plate and the distance between the closest points on the two surfaces starts to increase ($y_0(t) > 0$), while the other parameters remain constant ($\theta(t) = \theta_f$ and $r(t) = 0$).

Once the sphere is completely detached, it will continue to move vertically, increasing its distance from the electrode in a non-planar configuration, with the closest point between the two surfaces being the center of the electrode, and the farthest points being on the perimeter of the electrode (Fig. 5.1c). The average distance between the electrode and the second plate can thus be rewritten as:

$$y(t) = y_0(t) + \frac{2 \cdot \int_0^{\theta_f} \sin(x) dx}{r} \quad (5.11)$$

where $y_0(t)$ is the closest distance between the two surfaces, corresponding to the distance between the center of the electrode and its vertical projection on the second plate.

The distance between the two surfaces causes the equivalent coupled capacitance to quickly decrease. It is important to note that at the beginning of this phase, the capacitance is not zero yet, but quickly drops to zero once the gap between the two surfaces increases. In this short period of time $A_c = 0$, therefore $C_c(t) = 0$, and the non-contact relations become:

$$C_{nc_{die}}(t) = \epsilon_0 \epsilon_{die} \frac{wl}{d_{die}} \quad (5.12)$$

$$C_{nc_{air}}(t) = 4 \cdot \frac{\epsilon_0 \epsilon_{air} \epsilon_{die}}{y_0(t) + \sin(\theta_f)} \int_0^\pi r \cdot \ln \frac{l}{l - \sin(x)} dx \quad (5.13)$$

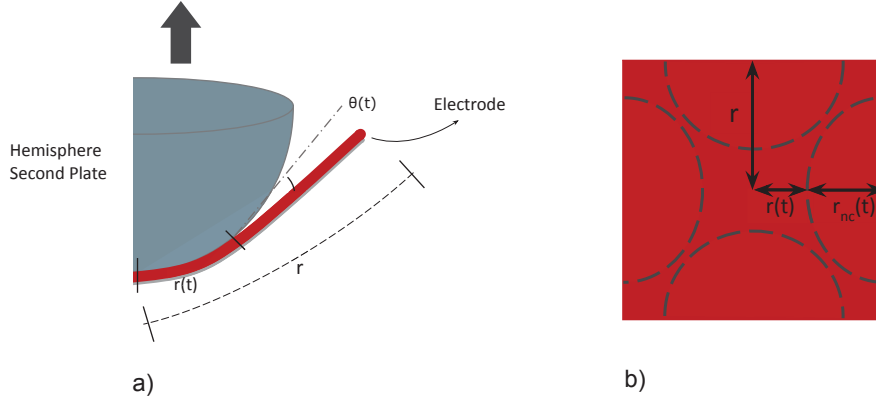


Figure 5.2 Capacitive model variables for a sphere-electrode case: a) graphic representation of spherical second plate detaching from the flexible electrode, with corresponding variables; b) schematic of contact and non-contact areas on the electrode surface, as measured in (Morelli *et al.* (2023)).

5.2.4 Analytical Model

The resulting analytical model that describes the MAs affecting a flexible capacitive sensor detaching from a non-flat surface can be summarized by the two inclusive equations:

$$V_{tribo}(t) = \frac{\sigma_c}{\epsilon_0 \epsilon_{r_{air}}} \left[y_0(t) + \frac{(2r - 2r(t)) \cdot \int_0^{\theta(t)} \sin(x) dx}{r^2 - r(t)^2} \right] \quad (5.14)$$

$$C_e(t) = C_c(t) + C_{nc}(t) \quad (5.15)$$

where $C_c(t)$ and $C_{nc}(t)$ varies depending on the movement phase as described in the above paragraphs.

The equivalent effect of both the capacitance variation C_e and triboelectric voltage V_{tribo} appears at the input of the sensor as a current (see Fig. 5.4c), quantifiable through the identity:

$$-\frac{Q}{C_e(t)} + V_{tribo}(t) = V_b + i(t)R_{in} . \quad (5.16)$$

5.3 Materials and Methods

The experimental set-up conceived to reproduce the transversal separation of a flexible capacitive sensor from a non-planar body is composed of a hybrid flexible capacitive sensor placed on a soft sponge holder, and an aluminum hemispherical body, with a diameter of 15 cm, connected to a robotic arm (Stäubli TX2-90L) used to move the second plate in a precise vertical path on top of the sensor (Fig. 5.3).

The electrical measurements consist in the transmission of a sinusoidal signal from the aluminum second plate to the sensor, imitating the signal acquisition of a biopotential coming from the body: a single frequency (1 Hz) sinusoidal signal (Agilent 33500B - Waveform Generator) was injected in the aluminum second plate, and the output pin of the sensor was connected to an oscilloscope (Keysight InfiniiVision DSOX3014T) to monitor the acquired signal.

Hybrid Flexible Capacitive Sensor

The chosen flexible capacitive sensor is a printed flexible hybrid electrode composed of a rigid PCB, containing the sensor Analog Front End (AFE), and a printed flexible Kirigami electrode, connected to the PCB using a second flexible Kirigami layer (Fig. 5.4a).

Both the electrode layer and the connecting layer are based on inkjet printed silver on a dielectric substrate: in the case of the electrode layer, the printed silver electrode corresponds to the actual capacitor electrode, while the substrate acts as a dielectric layer facing the sensing target; for the connecting layer, the printed silver layer acts as a connecting base between the PCB and the flexible electrode.

Silver nano-particle ink from ANPPPro (Silverjet P 40TE-20C) was printed, using a Ceradrop X-series printer, on top of Kapton FPC substrate 125 μm from American DuraFilm. Four layers

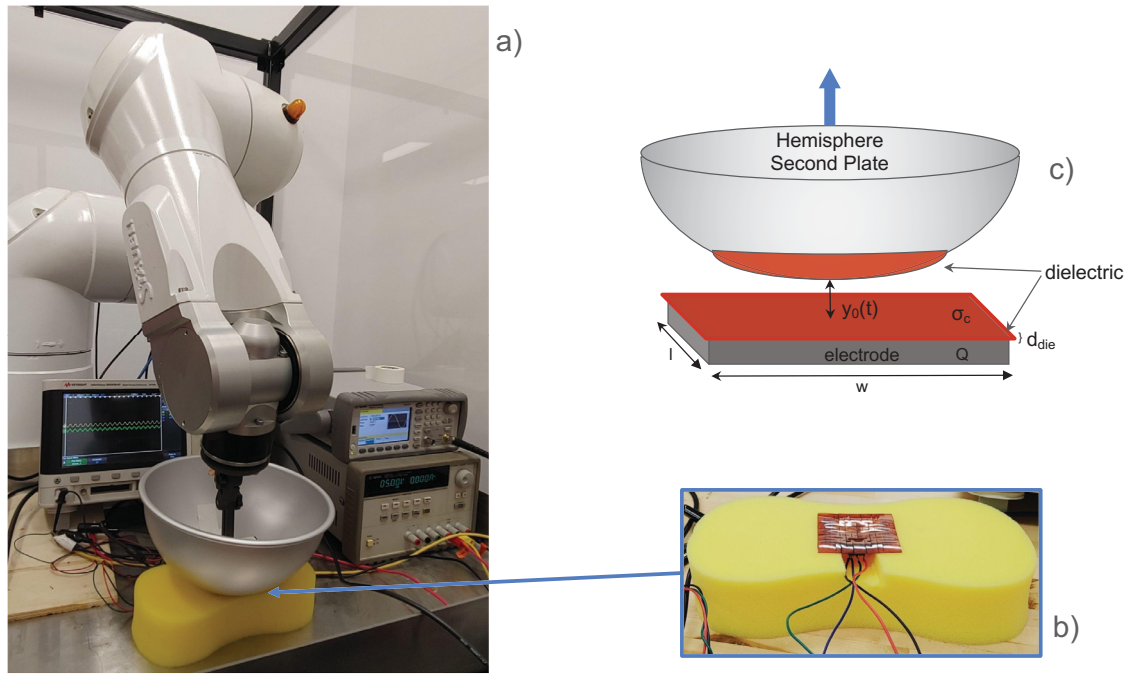


Figure 5.3 Measurement setup: a) electrode placed on a sponge holder, aluminum second plate fixed to a robot arm and placed on top of the electrode. The second plate surface was covered by a Kapton HN tape layer to reduce the charge affinity between the two surfaces.

A signal generator injects a sinusoidal signal in the aluminum second plate, which is capacitively transmitted to the sensor and observed on the oscilloscope. b) Sensor placement under the second plate. c) equivalent graphic representation of sensor for comparison against analytical model.

of the silver ink were printed in the form of $3 \times 3 \text{ cm}^2$ squares. Intermittent drying steps using an Adphos near infrared drying lamp integrated into the Ceradrop system were performed to allow uniform drying of the printed ink. The printed structures were then sintered in a Mancorp MC301N reflow oven for 1 hour at 300°C in air. Dycotech DM-INI-7003 ink was chosen as the insulating layer. Six layers of the insulating ink were inkjet printed atop the sintered silver electrodes, via Ceradrop printer, in the form of $4 \times 4 \text{ cm}^2$, with two central holes left empty to allow an electrical connection with the below silver layer. Each layer of the printed insulator ink was UV cured in place using the built ink UV cure lamp at 5.5 mW/cm^2 and 10 mm/s conveyor velocity followed by a final cure step at 100 % power and 1 mm/s speed.

In a second phase, the two layers were cut into two different Kirigami structures, designed for the specific function of each layer, through laser cutting (Samurai UV Marking System — DPSS Lasers, Inc.), with a final dimension of $5 \times 5 \text{ cm}^2$ (Fig. 5.4b).

The AFE used in this work is the simplest version of a pre-amplifier circuit that allows the measurements of biological signals by capacitive sensing (Sun & Yu, 2016), consisting of an op-amp in a buffer configuration and a bias resistor, as schematically represented in Fig. 5.4c. The components are mounted on a rigid PCB of the size of 34.3 mm^2 , with an exposed copper bottom to allow the connection of the electrode to the input of the op-amp. The contact between the flexible layers and the PCB is formed employing a silver epoxy paste (LOCTITE ABLESTIK 965-1L) applied manually on top of the cut-through spiral connectors, and thermally cured at 100°C for 3 hours. The final sensor is depicted in Fig. 5.4d.

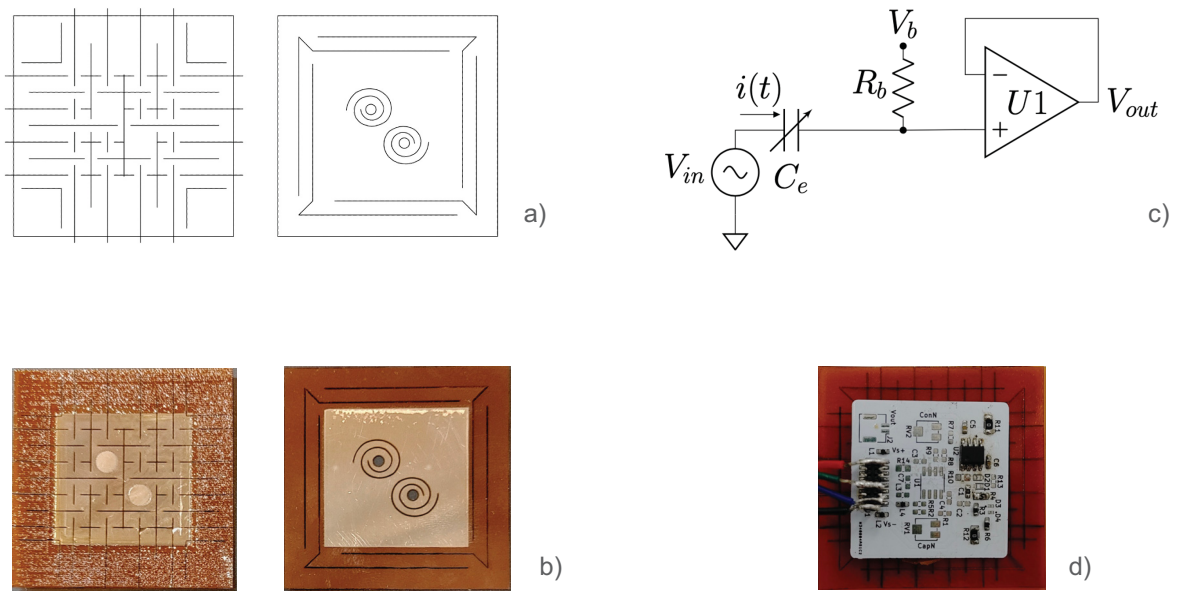


Figure 5.4 Sensor Production Steps: a) CAD design of kirigami electrode layer and connecting layer; b) printing and laser cut result of the electrode layer and connecting layer; c) schematic representation of analog front-end of the sensor; d) final sensor appearance, with PCB and printed layers interconnected to each other.

The test is organized as follows: the starting position of the hemisphere second plate is centered on top of the electrode, applying enough pressure on it so that the whole surface of the electrode

is in contact with the aluminum body (approximately 5 mm of depth on the sponge holder); the robot arm moves the second plate at constant speed in a vertical direction until the electrode results to be completely detached from the second plate, at a measured height of around 5 cm above the electrode. The movement is performed for three different speeds available by the robot: 1.7 mm/s, 3.4 mm/s, and 8.5 mm/s. As the aluminum second plate in contact with the electrode would create a triboelectric effect big enough to cause saturation of the sensor signal, even for lower speeds (Lee; Zou, Zhang, Guo, Wang, He, Dai, Zheng, Chen, Wang, Xu & Wang, 2019), a layer of Kapton HN tape of 125 μm of thickness has been fixed on the hemisphere, covering the whole surface in contact with the electrode.

5.4 Experimental Results and Discussion

The electrical measurement of the capacitive sensor output, when a motion separates the electrode from the hemisphere at three different speeds, is shown in Fig. 5.5. The output was monitored for a total of 12 s, with the motion set to start at 1 s.

As can be observed, the recorded voltage shows different trends, that coincide with the different phases of the transversal movement: in the first moment the signal exhibits a decrease in voltage corresponding to the loss of pressure on the electrode, but in this phase the electrode is still in full contact with the second plate. The triboelectric effect appears the moment that the electrode gradually detaches from the body: the signal spikes due to the effect of contact electrification, and at the same time the reducing coupled capacitance compensates the triboelectric voltage limiting the amplitude in the resulting input voltage in the sensor.

However, in all cases the recorded signal exhibits a peculiar feature: after the first peak of voltage, traceable to the overpowering effect of the reduced capacitance over the triboelectric one, a second, delayed peak appears for all speeds tested, before the signal slowly returns to zero. This unexpected result could be a consequence of the flexibility of the electrode, even though from just observing the measurements it is hard to pinpoint exactly the physical cause behind it.

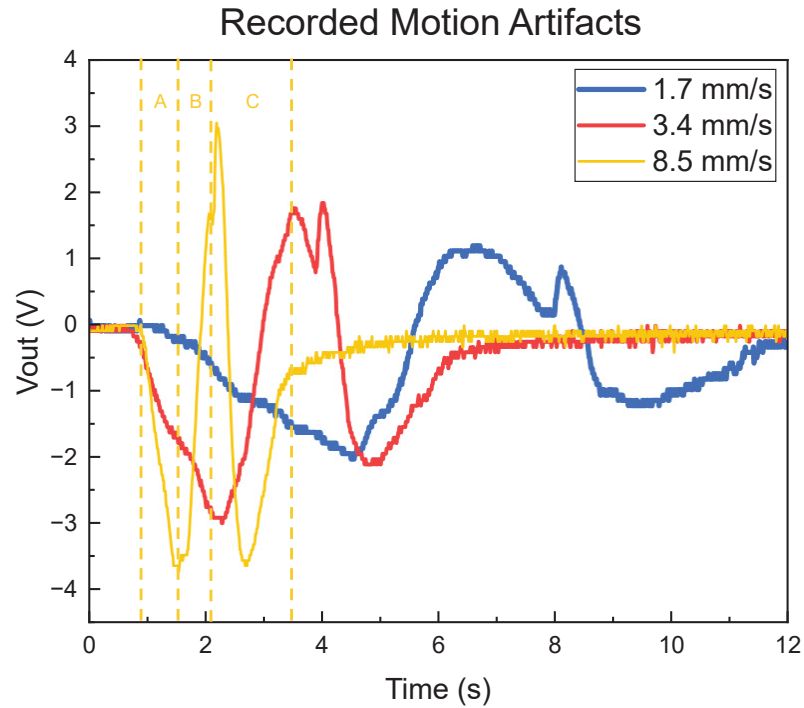


Figure 5.5 Recorded signal at the sensor output during vertical movement of the second plate, using a robotic arm, at three different available speeds: 1.7 mm/s, 3.4 mm/s and 8.5 mm/s. Each curve exhibits the same characteristic features, which correspond to the different phases of the movement. For the fastest speed of 8.5 mm/s the phases are highlighted in the figure: (A) indicates Phase 1, where the electrode is still completely attached but slowly losing pressure; (B) is Phase 2, when the electrode gradually loses contact with the second plate; (C) corresponds to Phase 3, when the two surfaces are completely detached and the sensor signal is slowly going back to zero.

The novel analytical model has been implemented using Matlab and plotted in Fig. 5.6, describing the voltage variation from the moment of the initial gradual detachment of the electrode (phases 2 and 3). A few approximations were necessarily made:

1. The border and fringing effects are not taken into account.
2. The angle θ_f has been estimated to be $\frac{\pi}{12}$, based on the geometry of the electrode-hemisphere setup (small variations of the angle were tested and the results were not noticeably affected by the changes).

3. The electrode has been considered generally flexible, and the variations due to the Kirigami pattern ignored, as the analytical model was conceived as a general model applicable to any flexible capacitive sensor. The Kirigami could be included in the capacitive model by following the steps in (Morelli *et al.*, 2023).
4. The relative movement between the sponge and the sensor during the movement dynamic was not included in the model, as it is inherent to the measurement set-up and does not define the case study considered. Both the inclined surfaces, during the detaching phase, are considered flat and not curved, so that the electrical field between the two is always perpendicular to both the plates (Landau, 2013).
5. The charge density has been estimated as

$$\sigma_c = (\eta_{sphere} - \eta_{electrode}) * \gamma \quad (5.17)$$

where γ is the energy necessary to separate the two surfaces which, in a first approximation, was arbitrarily assumed to be constant at 50 mJ (Sirtoli *et al.*, 2024), as a rough estimation accounting for reported friction force, displacement, and contact area. η is the charge affinity obtained from the triboelectric series (Lee; Zou *et al.*, 2019): in this case, since the materials in contact with each other are both polyimide, a difference $\eta_{sphere} - \eta_{electrode} = 0.025$ has been considered to take into account the eventual defects and non-predictable particles present on the respective surfaces.

The Triboelectric Voltage plot in Fig. 5.6 shows the trend of the isolated triboelectric effect. As for the case of the rigid electrode case (5.2), the voltage is directly proportional to the $y(t)$ function, but in the flexible case said function is not monotone: as described by (5.5) in the second phase of the movement, corresponding to the gradual detachment of the sensor, a faster rise in voltage is recorded due to a faster apparent speed of detachment of the conformed electrode from the curved surface; once the electrode reach a flat configuration, the third phase of the movement corresponds to the complete detachment of the two surface, where the speed corresponds to the actual speed of the moving second plate, thus slower.

The Coupled Capacitance plot in Fig. 5.6 shows the decline of coupled capacitance, which in the case of a flexible electrode is slower compared to the rigid case, thanks to the improved conformity of the electrode to the second plate. The capacitance decreases gradually until the moment of complete detachment, where the distance between the two sides causes a faster drop of C_e to 0.

Finally, the Sensor Input Voltage in Fig. 5.6 shows the resulting voltage at the sensor input, for the three different speeds considered. As it can be appreciated, the analytical modelling reflects the real current trend registered through the measurements: the gradual loss of contact described by (5.5) leads to an increase in current with a speed that depends on the speed of the movement. In all three cases, the effect of the discharging capacitance C_e compensates for the spike of the triboelectric effect, slowly reducing the resulting current till the moment of complete detachment of the two surfaces. As mentioned in the previous paragraph, the coupled capacitance does not go to zero in correspondence with the instant of complete detachment, but rapidly decreases to zero after that. At this moment, when C_e is not null yet, another spike appears, discharging rapidly after the capacitance reaches zero.

In Fig. 5.7 the measurement results and the analytical model are directly compared: in both plots all the curves have been translated to start at second 1.

Table 5.1 Comparison of integrated area under plots for both the plotted analytical model and experimental values

Speed	1.7 mm/s	3.4 mm/s	8.5 mm/s
Analytical	31.9 V · s	31.7 V · s	29.7 V · s
Experimental	40.9 V · s	38.8 V · s	34.3 V · s
Error	28.21%	22.39%	15.49%

While the magnitudes do not perfectly match between measurements and simulations, due to the introduced approximations necessary to build the analytical model, the correlation between the values confirms the validity and accuracy of the stipulated model: in both cases the spikes' duration are similar, varying from 4.1 s, 2.1 s and 0.9 s for the analytical model, while for the experimental results we measure 4.6 s, 2.5 s and 1.1 s respectively, for the three different speeds

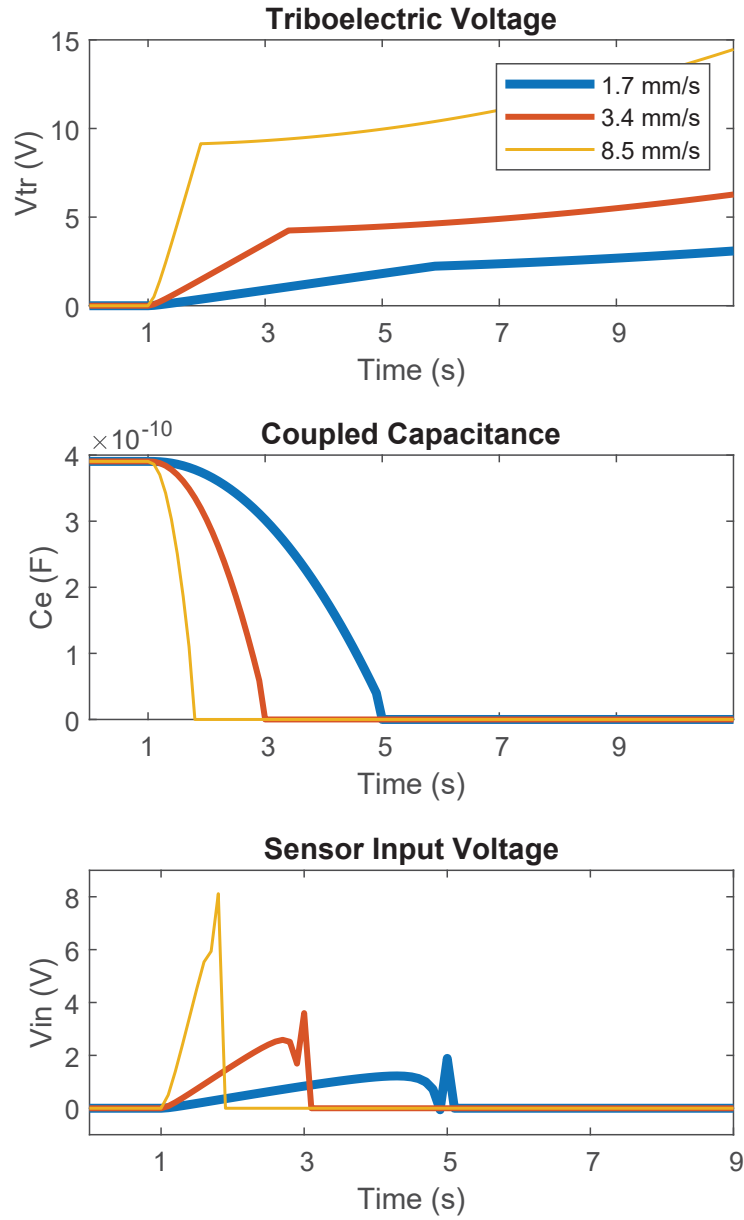


Figure 5.6 Analytical model of flexible capacitive sensor detaching from a spherical surface: a) shows the voltage $V_{tribo}(t)$ caused by the isolated triboelectric effect; b) corresponds to the capacitance variation $C_e(t)$; c) corresponds to the combined effect of both $V_{tribo}(t)$ and $C_e(t)$ as a voltage at the sensor input.

tested. Both the analytical and experimental results exhibit a trend that varies its steepness and wideness in function of the speed of movements, with peaks reaching 8.1 V, 3.8 V and 2.1 V in

the simulated plot, while in the experiments the voltage reaches 6.7 V, 4.7 V and 3.0 V for the corresponding speed.

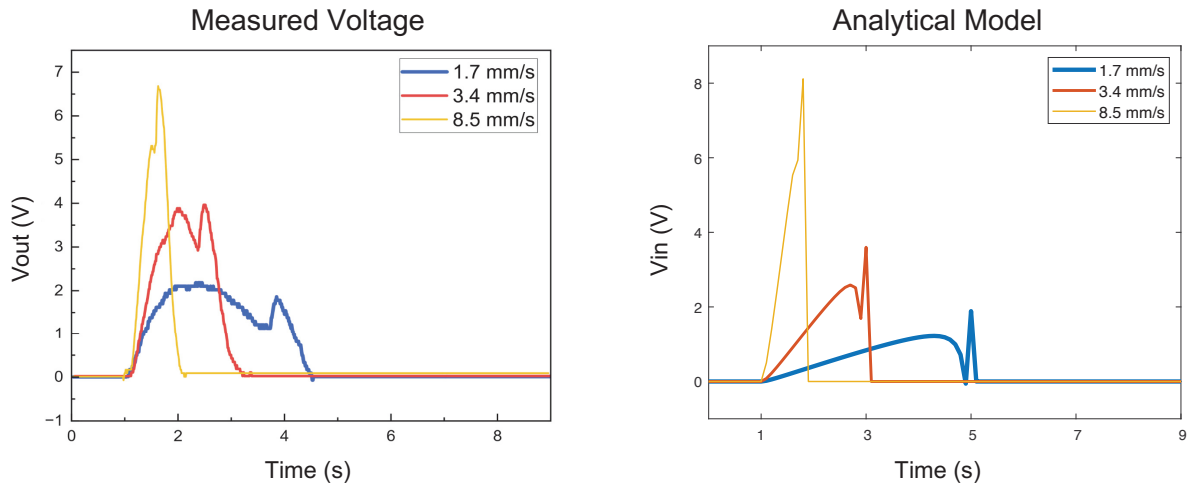


Figure 5.7 Comparison of experimental and analytical results: on the left the measured voltage at the sensor output, translated to have the start of phase 2 coinciding with second 1; on the right the simulated voltage found the sensor input at the beginning of phase 2 of the analytical model.

The total number of charges involved in the triboelectric phenomenon, while varying from case to case and hard to quantify in detail, depends on the characteristics of the two surface materials, the total area in contact and the pressure applied between the two (Wang & Wang, 2019), and should therefore be almost constant and independent on the speed used. To prove the integrity of the measurements, in Fig. 5.8 the plots of the measured voltages have been superimposed and normalized in function of their speed. The resulting curves, as expected, while varying slightly in magnitude, exhibit matching shapes and dimensions. In addition, for a direct comparison between the measured data and the analytical model, the area comprised under both the plots curves have been calculated and the results are listed in Table 5.1: both results exhibit almost constant integrated area, indicating the same amount of charges being mobilized during the movement.

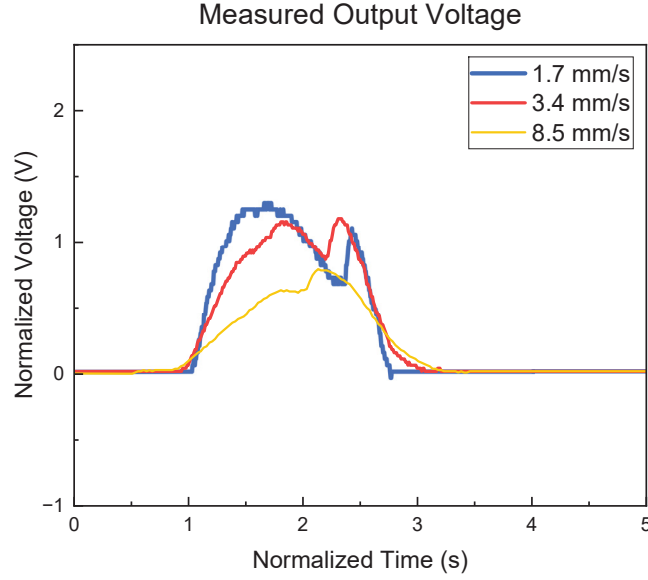


Figure 5.8 Superimposition of the measured triboelectric voltages: the three curves have been divided by their respective speeds and their x-axes expanded accordingly, exhibiting matching shape and dimension.

The obtained results confirm the accuracy of the introduced model, which can be used to explain and predict both the triboelectric and capacitive behavior of the sensor detaching from the body.

5.5 Conclusions

In conclusion, we introduced a novel analytical model aimed to describe the MAs caused by the triboelectric effect of a flexible capacitive sensor vertically detaching from a non-flat surface. The model explains the behavior of the combined triboelectric voltage, generated by separating the flexible sensor from an arbitrary spherical surface, and the coupled capacitance variation caused by the separation. First introduced as a generalized version, then applied to the specific case of a flexible electrode detaching from a spherical surface, both respectively covered by a dielectric layer, the model has been therefore plotted and compared to in-lab measurements of equivalent cases.

Three different speeds of movement have been compared: 1.7 mm/s , 3.4 mm/s and 8.5 mm/s . In all three cases the plotted data exhibit curves that differ from previously studied cases of rigid electrodes, showing a substantial difference in behavior caused by the flexibility of the electrode.

The measurements and analytical results are finally compared: while the magnitudes of the corresponding speeds tested differ slightly, the trend of the plotted model closely reflects the dynamic of the measured voltage, exhibiting the same characteristic features and correlation between the different speeds.

The differences found in measured and modelled values are due to the necessary approximations introduced into the model, which does not take into consideration external, not inherent factors such as the presence and behavior of the sponge holder in the experimental setup. The analytical model therefore demonstrates to be accurate in physically describing the flexible electrode behavior, taking into consideration both the difference in geometry and movement dynamics, representing a promising tool for the prediction of triboelectric behavior of flexible electrodes, for future applications in compensation methods of MAs in capacitive sensing.

CONCLUSION AND RECOMMENDATIONS

In conclusion, the PhD project explores the possibility of employing Kirigami to improve the flexibility and conformability of capacitive electrodes for sensing applications. Different Hierarchical levels of Kirigami structures have been implemented on same-size printed electrodes by laser cutting technique. The electrodes were evaluated when applied to non-flat surfaces, and their capacitive performance was compared to equivalent, non-Kirigami electrodes, exhibiting significant improvement in terms of both conformability and capacitive coupling. An analytical model to describe the behavior of conformable Kirigami capacitive electrodes was introduced, representing an accurate tool for estimating the capacitive coupling of a Kirigami electrode applied to arbitrary non-flat surfaces.

The best performing Kirigami structure was successively chosen and incorporated onto a capacitive sensor: to do so, a multilayer hybrid flexible Kirigami structure was realized, composed of different printed Kirigami layers with different functionalities specifically designed appositely to allow the integration of flexible components on traditional rigid PCBs and devices. The resulting sensor comprises three different structural layers: a printed Kirigami electrode, corresponding to the sensitive side of the sensor, a printed Kirigami connecting layer, to enable the integration of the flexible layer with the rigid components, ensuring good electrical and mechanical connections while not restricting the flexibility of the Kirigami electrode, and finally the rigid PCB containing the Analog Front-End for the filtering and pre-amplification of the acquired signal. The resulting sensor was tested, applied to different non-flat surfaces and subjected to different weights, to evaluate its performance in terms of uniformity and variability of measurements, as a performance metric for sensitivity against motion artifacts. The multilayer hybrid structure exhibits significant improvement compared to an equivalent rigid electrode confirming the potentials of Kirigami applications in capacitive sensing, and introducing a novel method to build hybrid flexible structures, with the use of Kirigami, that is easy to implement, cost-effective and compatible with solid-state devices and traditional fabrication techniques.

Finally, the novel hybrid structure was tested to assess the impact of the triboelectric effect on the flexible sensor performance. In particular, a non-flat second plate positioned on top of the electrode was vertically displaced until completely detached from the sensor. As expected, the flexibility of the electrode amplified the resulting triboelectric effect on the recorded signal and, in addition, exhibited a peculiar behavior that could not be predicted by the triboelectric models found in the literature. A novel analytical model was then introduced, which considers both the flexible dynamic of the movement and the capacitive behavior of the conformable electrode. The analytical model allows the prediction of the recorded voltage trend for different movement speeds and provides a physical explanation of the triboelectric effect for flexible capacitive electrodes. The model thus represents a powerful tool for future implementation of compensating methods for triboelectric artifacts in flexible capacitive sensors.

The carried out work poses promising bases for the utilization of a simple-to-implement technique such as Kirigami to significantly improve the performance of arbitrary partially flexible electrodes, underlining the advantages obtained on the electrical and mechanical characteristics thanks to the performed experiments. Future works should extend the application of Kirigami on other types of materials and production techniques, to prove compatibility with methods alternative to printed electronics. Another interesting development would include experiments with tailoring the Kirigami electrode structure for specific shape applications. The multilayer hybrid flexible sensor structure should be further improved, adding proper shielding and guarding for electromagnetic interference, and improving the AFE for specific biopotential acquisition. It should then be tested on human subjects for both short-term and long-term electrophysiological monitoring, and its application should be expanded to different types of capacitive sensing to investigate the improvement brought by Kirigami for different capacitive applications.

Contributions

The main contributions introduced in the present thesis by articles are the following:

Novel electrode design based on Kirigami technique to significantly improve the performance of a capacitive electrode.

and

Definition of a novel analytical model to describe the capacitive behavior of the Kirigami electrode.

To our knowledge, this thesis is the first example of the application of Kirigami technique on capacitive electrodes. The provided results show Kirigami to be an effective and easy-to-implement method to improve flexibility and conformability of capacitive electrodes, which can easily be introduced in the production of already existent capacitive devices to improve their mechanical and electrical performance. In addition, a novel analytical model has been introduced to explain the capacitive behavior of the Kirigami electrode compared to an equivalent non-Kirigami one, which represents an important tool for evaluating the advantages of Kirigami design for different applications.

Both contributions are published in the article in Chapter 2: "Flexible Capacitive Kirigami Electrode: Experimental Investigation and Analytical Model".

Novel sensor structure based on multilayer Kirigami design, to allow the integration of flexible Kirigami electrodes on traditional rigid and solid-state devices.

The newly introduced multilayer structure represents a first example of effective method for the integration of Kirigami flexible components onto rigid devices. The method paves the way for the use of Kirigami not only for the single main components as a technique to improve their

flexibility, but also as a structural approach to combine flexible Kirigami elements and rigid ones into hybrid flexible devices.

This contribution is described in detail in the submitted article in Chapter 3: "Printed Hybrid Capacitive Kirigami Sensor: Enhancing Flexibility and Conformability for Improved Motion Artifacts".

Analysis of the triboelectric effect of Kirigami flexible capacitive electrodes and introduction of a novel analytical model to describe the effect behavior for the case of flexible sensors applied to non-flat surfaces.

The triboelectric effect is one of the most problematic motion artifacts associated with the use of capacitive sensors. In the case of a flexible sensor, the triboelectric behavior is appreciably different compared to the case of a rigid electrode and cannot be predicted by the analytical models found in the literature. The conducted work provides a tailored analytical model to describe the specific case of flexible electrodes applied to non-flat surfaces, representing a powerful tool for the prediction and future compensation methods for this type of motion artifact.

This contribution is reported in the submitted article in Chapter 4: "Analytical Modeling and Experimental Validation of Triboelectric Behavior in Kirigami Flexible Capacitive Sensors".

Academic Accomplishments

Over the course of the PhD years, additional academic accomplishments have been attained, that were not included in the main chapters of the thesis, but still deserve to be mentioned.

Collaborations in Peer-Reviewed Articles:

- M. Lessard-Tremblay, J. Weeks, L. Morelli, G. Cowan, G. Gagnon and R. J. Zednik “Contactless Capacitive Electrocardiography Using Hybrid Flexible Printed Electrodes” *Sensors* 2020, 20, 5156; doi:10.3390/s20185156;
- V. G. Sirtoli, L. Morelli, R. J Zednik, G. Cowan, G. Gagnon “Motion Artifact Modeling of Capacitive Electrodes based on Triboelectric Nanogenerators” *IEEE Transactions on Instrumentation and Measurement*; doi:10.1109/TIM.2024.3394480;

Presentations at Academic Conferences:

- 01/03/2023 - International Exhibition and Conference for Flexible, Organic and Printed Electronics - LOPEC, Munich (Germany): Oral presentation: “Flexible Capacitive Kirigami Electrode: Experimental Investigation and Analytical Model”
- 17/05/2023 - Canada’s Flexible Printable Wearable Electronics Symposium - CPES, Montreal (Canada): Poster presentation: “Flexible Capacitive Kirigami Electrode: Experimental Investigation and Analytical Model”
- 31/05/2023 - CONGRÈS DE RECHERCHE DU LACIME, ETS, Montreal (Canada) 2nd place for best PhD poster presentation: “Flexible Capacitive Kirigami Electrode: Experimental Investigation and Analytical Model”

- 09/04/2024 - JOURNÉE DE L'INNOVATION RESMIQ, ETS, Montreal (Canada) Poster presentation: "Printed Hybrid Capacitive Kirigami Sensor: Enhancing Flexibility and Conformability for Improved Motion Artifacts"

LIST OF REFERENCES

- Albina, A., Taberna, P. L., Cambronne, J. P., Simon, P., Flahaut, E. & Lebey, T. (2006). Impact of the surface roughness on the electrical capacitance. *Microelectronics Journal*, 37(8), 752-758.
- An, N., Domel, A. G., Zhou, J., Rafsanjani, A. & Bertoldi, K. (2019). Programmable Hierarchical Kirigami. *Advanced Functional Materials*, (1906711).
- Anandan, N. & George, B. (2017). A Wide-Range Capacitive Sensor for Linear and Angular Displacement Measurement. *IEEE Transactions on Industrial Electronics*, 64(7), 5728-5737.
- Avuthu, S. G. R., Gill, M., Sussman, M., Wable, G. & Richstein, J. (2016). An Introduction to the process of Printed Electronics. *Proceedings of SMTA International*, Sep. 25-29, IL, USA, 246-252.
- Babusiak, B., Borik, S. & Balogova, L. (2018). Textile electrodes in capacitive signal sensing applications. *Measurement*, 114, 69-77.
- Baek, H. J., Lee, H. J., Lim, Y. G. & Park, K. S. (2012). Conductive Polymer Foam Surface Improves the Performance of a Capacitive EEG Electrode. *IEEE Transactions on Biomedical Engineering*, 59(12), 3422 - 3431.
- Baek, H. J., Lee, H. J., Lim, Y. G. & Park, K. (2013). Comparison of pre-amplifier topologies for use in brain-computer interface with capacitively-coupled EEG electrodes. *Biomedical Engineering Letters*, 3, 158-169.
- Baek, J. Y., An, J. H., Cho, J. M., Park, K. S. & Lee, S. H. (2008). Flexible Polymeric Dry Electrodes for The Long-term Monitoring of ECG. *Sensors and Actuators A*, 143, 423-429.
- Bandodkar, A. J. & Wang, J. (2014). Non-invasive wearable electrochemical sensors: a review. *Trends in Biotechnology*, 32(7), 363-371.
- Bao, Y., Hong, G., Chen, Y., Chen, J., Chen, H., Song, W. L. & Fang, D. (2019). Customized Kirigami Electrodes for Flexible and Deformable Lithium-Ion Batteries. *ACS Applied Materials Interfaces*, 12(1), 780-788.
- Beedasy, V. & Smith, P. J. (2020). Printed Electronics as Prepared by Inkjet Printing. *Materials*, 13(3).
- Berson, A. S. & Pipberger, H. V. (1966). The low-frequency response of electrocardiographs, a frequent source of recording errors. *American Heart Journal*, 71, 779-789.

- Bilent, S., Hong, T., Dinh, N., Martincic, E. & Joubert, P. Y. (2019). Influence of the Porosity of Polymer Foams on the Performances of Capacitive Flexible Pressure Sensors. *Sensors*, 19(1968).
- Bonnassieux, Y., Brabec, C. J., Cao, Y., Carmichael, T. B., Chabiny, M. L., Cheng, K. T., Cho, G. J., Chung, A. J., Cobb, C. L., Distler, A., Egelhaaf, H. J., Grau, G., Guo, X., Haghighashtiani, G., Huang, T. C., Hussain, M. M., Iniguez, B., Lee, T. M., Li, L., Ma, Y., Ma, D., McAlpine, M. C., Ng, T. N., Österbacka, R., Patel, S. N., Peng, J., Peng, H., Rivnay, J., Shao, L., Steingart, D., Street, R. A., Subramanian, V., Torsi, L. & Wu, Y. (2021). The 2021 flexible and printed electronics roadmap. *IOP Flexible and Printed Electronics*, 6(023001).
- Bragg-Remschel, D., Anderson, C. M. & Winkle, R. A. (1982). Frequency response characteristics of ambulatory ECG monitoring systems and their implications for ST segment analysis. *American Heart Journal*, 103(1), 20-31.
- Bronzino, J. D. (2006). *The Biomedical Engineering Handbook: Medical Devices and Systems*. TaylorFrancis Group.
- Brooks, A. K., Chakravarty, S., Ali, M. & Yadavalli, V. K. (2022). Kirigami-Inspired Biodesign for Applications in Healthcare. *Advanced Materials*, 34(18).
- Bryzek, J. (1996). Impact of MEMS Technology on Society. *Sensors and Actuators A*, (56).
- Cai, J. N., Cizek, K., Long, B., McAferty, K., Campbell, C. G., Allee, D. R., Vogt, B. D., Belle, J. L. & Wang, J. (2009). Flexible thick-film electrochemical sensors: Impact of mechanical bending and stress on the electrochemical behavior. *Sensors and Actuators B: Chemical*, 137(1), 379-385.
- Chamadiya, B., Mankodiya, K., Wagner, M. & Hofmann, U. G. (2013). Textile-based, contactless ECG monitoring for non-ICU clinical settings. *Journal of Ambient Intelligence and Humanized Computing volume*, 4, 791-800.
- Chang, J. S., Facchetti, A. F. & Reuss, R. (2017). A Circuits and Systems Perspective of Organic/Printed Electronics: Review, Challenges, and Contemporary and Emerging Design Approaches. *IEEE Journal on Emerging and Selected Topics in Circuits and Systems*, 7(1), 7-26.
- Chatterjee, S., Thakur, R. S., Yadav, R. N., Gupta, L. & Raghuvanshi, D. K. (2020). Review of Noise Removal Techniques in ECG Signals. *IET Signal Processing*, 14(9).
- Chen, Y., Zhang, Y., Liang, Z., Cao, Y., Han, Z. & Feng, X. (2020). Flexible inorganic bioelectronics. *npj Flexible Electronics*, 4(2).

- Cho, Y., Shin, J. H., Costa, A., Kim, T. A., Kunin, V., Li, J., Lee, S. Y., Yang, S., Han, H. N., Choi, I. S. & Srolovitz, D. J. (2014). Engineering the shape and structure of materials by fractal cut. *PNAS*, 111(49), 17390-17395.
- Choi, G. P. T., Dudte, L. H. & Mahadevan, L. (2019). Programming shape using kirigami tessellations. *Nature Materials*, 18, 999-1004.
- Choi, G. P. T., Dudte, L. H. & Mahadevan, L. (2021). Compact reconfigurable kirigami. *PHYSICAL REVIEW RESEARCH*, 3(043030).
- Chu, C. Y., Tsai, J. T. & Sun, C. L. (2012). Synthesis of PEDOT-modified graphene composite materials as flexible electrodes for energy storage and conversion applications. *International Journal of Hydrogen Energy*, 37(18), 13880-13886.
- Corzo, D., Tostado-Blázquez, G. & Baran, D. (2020). Flexible Electronics: Status, Challenges and Opportunities. *Frontiers in Electronics*.
- Costa, J. C., Spina, F., Lugoda, P., Garcia-Garcia, L., Roggen, D. & Münzenrieder, N. (2019). Flexible Sensors—From Materials to Applications. *Technologies*, 7(2)(35).
- Cruz, S. M. F., Rocha, L. A. & Viana, J. C. (2018). *Flexible Electronics, Chapter 3: Printing Technologies on Flexible Substrates for Printed Electronics*. Intechopen.
- Diao, Y., Woon, R., Yang, H., Chow, A., Wang, H., Lua, Y. & D'Arcy, J. M. (2021). Kirigami electrodes of conducting polymer nanofibers for wearable humidity dosimeters and stretchable supercapacitors. *Journal of Materials Chemistry A*, 9(15), 9849-9857.
- Dong, R., Liu, X., Cheng, S., Tang, L., Chen, M., Zhong, L., Chen, Z., Liu, S. & Jiang, X. (2020). Highly Stretchable Metal–Polymer Conductor Electrode Array for Electrophysiology. *Advanced Healthcare Materials*.
- Driel, J. V., Olivers, C. N. L. & Fahrenfort, J. J. (2021). High-pass filtering artifacts in multivariate classification of neural time series data. *bioRxiv*, 530220.
- Feng, Y., Zhou, Z., Wang, W., Rao, Z. & Han, Y. (2021). The 3D Capacitance Modeling of no.-parallel Plates Based on Conformal Mapping. *2021 IEEE 16th International Conference on Nano/Micro Engineered and Molecular Systems (NEMS), Xiamen, China*, 1264-1267.
- Fu, Y., Zhao, J., Dong, Y. & Wang, X. (2020). Dry Electrodes for Human Bioelectrical Signal Monitoring. *Sensors*, 20(13), 3651.

- Fuhrhop, S., Lamparth, S. & Heuer, S. (2009). A textile integrated long-term ECG monitor with capacitively coupled electrodes. *2009 IEEE Biomedical Circuits and Systems Conference*.
- Gao, B., Elbaz, A., He, Z., Xie, Z., Xu, H., Liu, S., Su, E., Liu, H. & Gu, Z. (2018). Bioinspired Kirigami Fish-Based Highly Stretched Wearable Biosensor for Human Biochemical–Physiological Hybrid Monitoring. *Advanced Materials Technologies*, 3(4).
- Gao, W., Ota, H., Kiriya, D., Takei, K. & Javey, A. (2019). Flexible Electronics toward Wearable Sensing. *Accounts of Chemical Research*, (52), 523-533.
- Gao, Y., Soman, V. V., Lombardi, J. P., Rajbhandari, P. P., Dhakal, T. P., Wilson, D. G., Poliks, M. D., Ghose, K., Turner, J. N. & Jin, Z. (2020). Heart Monitor Using Flexible Capacitive ECG Electrodes. *IEEE Transactions on Instrumentation and Measurement*, 69(7), 4314 - 4323.
- Grima, J. N. & Evans, K. E. (2000). Auxetic behavior from rotating squares. *Journal of Materials Science Letters*, 19(17), 1563–1565.
- Hao, W., YongAn, H. & ZhouPing, Y. (2022). Flexible hybrid electronics: Enabling integration techniques and applications. *SCIENCE CHINA Technological Sciences*, 65(9), 1995-2006.
- Harris, K. D., Elias, A. L. & Chung, H. J. (2016). Flexible electronics under strain: a review of mechanical characterization and durability enhancement strategies. *Journal of Materials Science*, (51), 2771 - 2805.
- Hasan, M., Rho, J. H., Kang, S. Y. & Ahn, J. H. (2010). Low Temperature Aluminum Oxide Gate Dielectric on Plastic Film for Flexible Device Application. *Japanese Journal of Applied Physics*, 49.
- Herbert, R., Kim, J. H., Kim, Y. S., Lee, H. M. & Yeo, W. H. (2018). Soft Material-Enabled, Flexible Hybrid Electronics for Medicine, Healthcare, and Human-Machine Interfaces. *Materials*, 11, 187.
- Heuer, S., Martinez, D. R., Fuhrhop, S. & Ottenbacher, J. (2009). Motion artefact correction for capacitive ECG measurement. *2009 IEEE Biomedical Circuits and Systems Conference, Beijing, Chine*, 113-116.
- Hure, J., Roman, B. & Bico, J. (2011). Wrapping an Adhesive Sphere with an Elastic Sheet. *Physical Review Letters*, 106(17).
- Hussain, M. M. & El-Atab, N. (2020). Handbook of Flexible and Stretchable Electronics. *CRC Press*.

- Jeerapan, I. & Khumngern, S. (2023). Printed Devices for Wearable Biosensors: Laboratory to Emerging Markets. *IEEE Journal on Flexible Electronics*, 2(5).
- Kang, T. H., Merritt, C., Karaguzel, B., Wilson, J., Franzon, P., Pourdeyhimi, B., Grant, E. & Nagle, T. (2006). Sensors on Textile Substrates for Home-Based Healthcare Monitoring. *IEEE - 1st Transdisciplinary Conference on Distributed Diagnosis and Home Healthcare*.
- Kaniusas, E. (2019). *Biomedical Signals and Sensors III Linking Electric Biosignals and Biomedical Sensors*. Springer, Cham.
- Keshavarzi, M. & Hasani, J. Y. (2019). Design and optimization of fully differential capacitive MEMS accelerometer based on surface micromachining. *Microsystem Technologies*, 25, 1369–1377.
- Khan, S., Ali, S. & Bermak, A. (2019). Recent Developments in Printing Flexible and Wearable Sensing Electronics for Healthcare Applications. *Sensors (Basel)*, 19(5), 1230.
- Khan, Y., Garg, M., Gui, Q., Schadt, M., Gaikwad, A., Han, D., Yamamoto, N. A. D., Hart, P., Welte, R., Wilson, W., Czarnecki, S., Poliks, M., Jin, Z., Ghose, K., Egitto, F., Turner, J. & Arias, A. C. (2016). Flexible Hybrid Electronics: Direct Interfacing of Soft and Hard Electronics for Wearable Health Monitoring. *Advanced Materials*, 26(47), 8764-8775.
- Khan, Y., Thielens, A., Muin, S., Ting, J., Baumbauer, C. & Arias, A. C. (2020). A New Frontier of Printed Electronics: Flexible Hybrid Electronics. *Advanced Materials - Special Issue: Flexible Hybrid Electronics*, 32(15).
- Khanna, V. K. (2019). Flexible Electronics, Mechanical background, materials and manufacturing. *IOP Publishings*.
- Kim, C. L., Jung, C. W., Oh, Y. J. & Kim, D. E. (2017). A highly flexible transparent conductive electrode based on nanomaterials. *NPG Asia Materials*, 9.
- Kim, H. S., Kang, J. S., Park, J. S., Hahn, H. T., Jung, H. C. & Joung, J. W. (2009). Inkjet printed electronics for multifunctional composite structure. *Composites Science and Technology*, 69(7-8).
- Kim, H., Lee, S. & Yun, K. (2011). Sensors and Actuators A: Physical. *IEEE Sensors*, 165(1), 2-7.
- Kim, J. H., Lee, S. M. & Lee, S. H. (2014). Capacitive Monitoring of Bio and Neuro Signals. *Biomedical Engineerings Letters*, 4, 142-148.

- Kim, S. Y., Lee, S. J. & Jeong, W. Y. (2020). EMG Measurement with Textile-Based Electrodes in Different Electrode Sizes and Clothing Pressures for Smart Clothing Design Optimization. *Polymers*, 12(10).
- Kim, Y. S., Mahmood, M., Lee, Y. K., Kim, N. K., Kwon, S. J., Herbert, R., Kim, D. H., Cho, H. C. & Yeo, W. H. (2019). All-in-One, Wireless, Stretchable Hybrid Electronics for Smart, Connected, and Ambulatory Physiological Monitoring. *Advanced Science*, 6(17).
- Klein, H. W., Karpin, O., Kravets, I., Kolych, I., MacSweeney, D., Ogirko, R., O’Keefe, D. & Walsh, P. (2019). *Low-Power Analog Techniques, Sensors for Mobile Devices, and Energy Efficient Amplifiers: Advanced Capacitive Sensing for Mobile Devices*. Springer, Cham.
- Landau, L. D. (2013). The classical theory of fields. *Elsevier*, 2.
- Lee, J. H., Cho, K. W. & Kim, J. K. (2024). Age of Flexible Electronics: Emerging Trends in Soft Multifunctional Sensors. *Advanced Materials*, 2310505.
- Lee, J. S., Heo, J., Lee, W. K., Lim, Y. G., Kim, Y. H. & Park, K. S. (2014). Flexible Capacitive Electrodes for Minimizing Motion Artifacts in Ambulatory Electrocardiograms. *Sensors*, 17, 14732-14743.
- Lee, S. M., Sim, K. S., Kim, K. K., Lim, Y. G. & Park, K. S. (2010). Thin and flexible active electrodes with shield for capacitive electrocardiogram measurement. *Medical Biological Engineering Computing*, 48, 447–457.
- Lee, W. B. The TriboElectric Series. *AlphaLab Inc*.
- Lee, Y. K., Xi, Z., Lee, Y. J., Kim, Y. H., Hao, Y., Choi, H. J., Lee, M. G., Joo, Y. C., Kim, C. S., Lien, J. M. & Choi, I. S. (2020). Computational wrapping: A universal method to wrap 3D-curved surfaces with nonstretchable materials for conformal devices. *Science Advances*, 6(15).
- Lessard-Tremblay, M., Weeks, J., Morelli, L., Cowan, G., Gagnon, G. & Zednik, R. (2020). Contactless Capacitive Electrocardiography Using Hybrid Flexible Printed Electrodes. *Sensors*, 20, 5156.
- Li, B. M., Kim, I., Zhou, Y., Mills, A. C., Flewellin, T. J. & Jur, J. S. (2019). Kirigami-Inspired Textile Electronics: K.I.T.E. *Advanced Materials Technologies*, 4(11).

- Li, H., Wang, Z., Sun, M., Zhu, H., Liu, H., Tang, C. Y. & Xu, L. (2022). Breathable and Skin-Conformal Electronics with Hybrid Integration of Microfabricated Multifunctional Sensors and Kirigami-Structured Nanofibrous Substrates. *Advanced Functional Materials*, 32(32).
- Li, X., Hui, H. & Sun, Y. (2016). Investigation of motion artifacts for biopotential measurement in wearable devices. *2016 IEEE 13th International Conference on Wearable and Implantable Body Sensor Networks (BSN)*.
- Li, Y., Torah, R., Beeby, S. & Tudor, J. (2012). An all-inkjet printed flexible capacitor on a textile using a new poly(4-vinylphenol) dielectric ink for wearable applications. *IEEE Sensors*, (52), 523-533.
- Liang, Z., Liu, M., Shen, L., Lu, L., Ma, C., Lu, X., Lou, X. & Jia, C. L. (2019). All-Inorganic Flexible Embedded Thin-Film Capacitors for Dielectric Energy Storage with High Performance. *ACS Applied Materials and Interfaces*, 11(5), 5247 - 5255.
- Lim, H. R., Kim, H. S., Qazi, R., Kwon, Y. T., Jeong, J. W. & Yeo, W. H. (2020). Advanced Soft Materials, Sensor Integrations, and Applications of Wearable Flexible Hybrid Electronics in Healthcare, Energy, and Environment. *Advanced Materials*, 32(15), 1901924.
- Lim, Y. G., Kim, K. K. & Park, K. S. (2007). ECG Recording on a Bed During Sleep Without Direct Skin-Contact. *IEEE Transaction on Biomedical Engineering*, 54(4), 718-725.
- Lim, Y. G., Lee, J. S., Lee, S. M., Lee, H. J. & Park, K. S. (2014). Capacitive Measurement of ECG for Ubiquitous Healthcare. *Annals of Biomedical Engineering*, 2(11), 2218-2227.
- Liu, S., Shah, D. S. & Kramer-Bottiglio, R. (2021). Highly stretchable multilayer electronic circuits using biphasic gallium-indium. *Nature Materials*, 20, 851-858.
- Macy, A. The Handbook of Human Physiological Recording. Consulted at <https://alanmacy.com/book/the-handbook-of-human-physiological-recording/>.
- McIntosh, R. B., Mauger, P. E. & Patterson, S. R. (2006). Capacitive Transducers With Curved Electrodes. *IEEE Sensors Journal*, 6(1), 125-138.
- Mohammed, M. G. & Kramer, R. (2017). All-Printed Flexible and Stretchable Electronics. *Advanced Materials*, (1604965).
- Montero, K. L., Laurila, M. M. & Mäntysalo, M. (2022). Effect of Electrode Structure on the Performance of Fully Printed Piezoelectric Energy Harvesters. *IEEE Journal on Flexible Electronics*, 1(1), 24-31.

- Morelli, L., Gagnon, G. & Zednik, R. J. (2023). Flexible Capacitive Kirigami Electrode: Experimental Investigation and Analytical Model. *IEEE Journal on Flexible Electronics*, 2(6).
- Mukhopadhyay, S. C., Suryadevara, N. K. & Nag, A. (2022). Wearable Sensors for Healthcare: Fabrication to Application. *Sensors*, 14(22), 5137.
- Najafabadi, A. H., Tamayol, A., Annabi, N., Ochoa, M., Mostafalu, P., Akbari, M., Nikkhah, M., Rahimi, R., Dokmeci, M. R., Sonkusale, S., Ziaie, B. & Khademhosseini, A. (2014). Biodegradable Nanofibrous Polymeric Substrates for Generating Elastic and Flexible Electronics. *Japanese Journal of Applied Physics*, 26(33), 5823-5830.
- Nayak, L., Mohanty, S., Nayaka, S. K. & Ramadoss, A. (2019). A review on inkjet printing of nanoparticle inks for flexible electronics. *Journal of Materials Chemistry C*, (29).
- Ng, C. L. & Reaz, M. B. I. (2019). Evolution of a capacitive electromyography contactless biosensor: Design and modelling techniques. *Measurements*, 145, 460-471.
- Ng, C. L., Reaz, M. B. I., Crespo, M. L., Cicuttin, A., Shapiai, M. I. B., Ali, S. H. B. M., Kamal, N. B. & Chowdhury, M. E. H. (2023). A Flexible Capacitive Electromyography Biomedical Sensor for Wearable Healthcare Applications. *IEEE Transactions on Instrumentation and Measurement*, 72(4007213).
- Ning, X., Wang, X., Zhang, Y., Yu, X., Choi, D., Zheng, N., Kim, D. S., Huang, Y., Zhang, Y. & Rogers, J. A. (2018). Assembly of Advanced Materials into 3D Functional Structures by Methods Inspired by Origami and Kirigami: A Review. *Advanced Materials Interfaces*, 1800284.
- Niu, S., Wang, S., Lin, L., Liu, Y., Zhou, Y. S., Hua, Y. & Wang, Z. L. (2013). Theoretical study of contact-mode triboelectric nanogenerators as an effective power source. *Energy Environmental Science*, 6(12), 3576-3583.
- Nogi, M., Komoda, N., Otsukac, K. & Suganumaa, K. (2013). Foldable nanopaper antennas for origami electronics. *Nanoscale*, 5(4395).
- Noh, J., Jung, M., Jung, Y., Yeom, C., Pyo, M. & Cho, G. (2015). Key Issues With Printed Flexible Thin Film Transistors and Their Application in Disposable RF Sensors. *Proceedings of the IEEE*, 103(4), 554-566.
- Ohring, M. (2002). *Materials Science of Thin Films, Deposition and Structure - Chapter 1: a Review of Material Science*. Elsevier Inc.

- Ottenbacher, J. & Heuer, S. (2009). Motion Artefacts in Capacitively Coupled ECG Electrodes. *World Congress on Medical Physics and Biomedical Engineering, September 7 - 12, Munich, Germany*, 25(4), 1059-1062.
- Poliks, M., Turner, J., Ghose, K., Jin, Z., Garg, M., Gui, Q., Arias, A., Kahn, Y., Schadt, M. & Egitto, F. (2016). A Wearable Flexible Hybrid Electronics ECG Monitor. *2016 IEEE 66th Electronic Components and Technology Conference (ECTC)*.
- Prabakaran, A. & Rufus, E. (2021). Review on the wearable health-care monitoring system with robust motion artifacts reduction techniques. *Sensor Review*, 42(1).
- Promphet, N., Ummartyotin, S., Ngeontae, W., Puthongkham, P. & Rodthongkum, N. (2021). Non-invasive wearable chemical sensors in real-life applications. *Analytica Chimica Acta*, 1179(338643).
- Rachim, V. P. & Chung, W. Y. (2016). Wearable Noncontact Armband for Mobile ECG Monitoring System. *IEEE Transactions on Biomedical Circuits and Systems*, 10(6), 1112 - 1118.
- Rim, Y. S., Bae, S. H., Chen, H., Marco, N. D. & Yang, Y. (2016). Recent Progress in Materials and Devices toward Printable and Flexible Sensors. *Advanced Materials*, 28(22), 4415-4440.
- Rogers, J. A., Someya, T. & Huang, Y. (2010). Materials and Mechanics for Stretchable Electronics. *Science*, 327(5973), 1603-1607.
- Roland, T., Wimberger, K., Amsuess, S., Russold, M. F. & Baumgartner, W. (2019). An Insulated Flexible Sensor for Stable Electromyography Detection: Application to Prosthesis Control. *Sensors*, 19(4).
- Sageman-Furnas, A. O., Goswami, P., Menon, G. & Russell, S. J. (2014). The Sphereprint: An approach to quantifying the conformability of flexible materials. *Textile Research Journal*, 84(8), 793-807.
- Santos, C. C. D., Lucena, G. N., Pinto, G. C., Júnior, M. J. & Marques, R. F. C. (2021). Advances and current challenges in non-invasive wearable sensors and wearable biosensors—A mini-review. *Medical Devices and Sensors*, 4(1).
- Shao, J., Jiang, T. & Wang, Z. L. (2020). Theoretical foundations of triboelectric nanogenerators (TENGs). *Science China Technological Sciences*, 63, 1087–1109.
- Shen, X., Wang, A. E., Sankaran, R. M. & Lacks, D. J. (2016). First-principles calculation of contact electrification and validation by experiment. *Journal of Electrostatics*, 82, 11-16.

- Sirtoli, V., Morelli, L., Zednik, R. J., Cowan, G. & Gagnon, G. (2024). Motion Artifact Modeling of Capacitive Electrodes Based on Triboelectric Nanogenerators. *IEEE Transactions on Instrumentation and Measurement*.
- Sirtoli, V. G., Liamini, M., Lins, L. T., Lessard-Tremblay, M., Cowan, G., Zednik, R. J. & Gagnon, G. (2023). Removal of Motion Artifacts in Capacitive Electrocardiogram Acquisition: A Review. *IEEE Transaction on Biomedical Circuits and Systems*, 17(3).
- Smits, F. M. (1958). Measurement the of Sheet Resistivities Four-Point Probe. *The Bell System Technical Journal*, 37(3), 711-718.
- Sobolev, Y. I., Adamkiewicz, W., Siek, M. & Grzybowski, B. A. (2022). Charge mosaics on contact-electrified dielectrics result from polarity-inverting discharges. *Nature Physics*, 18, 1347–1355.
- Solai, K., Rathnasami, J. D. & Koilmani, S. (2020). Superior performance area changing capacitive MEMS accelerometer employing additional lateral springs for low frequency applications. *Microsystem Technologies*, 26, 2353–2370.
- Song, Z., Ma, T., Tang, R., Cheng, Q., Wang, X., Krishnaraju, D., Panat, R., Chan, C. K., Yu, H. & Jiang, H. (2014). Origami lithium-ion batteries. *Nature Communications*, 5(3140).
- Sun, Y. & Yu, X. B. (2016). Capacitive Biopotential Measurement for Electrophysiological Signal Acquisition: A Review. *IEEE Sensors Journal*, 16(93).
- Taccola, S., Poliziani, A., Santonocito, D., Mondini, A., Denk, C., Ide, A. N., Oberparleiter, M., Greco, F. & Mattoli, V. (2021). Toward the Use of Temporary Tattoo Electrodes for Impedancemetric Respiration Monitoring and Other Electrophysiological Recordings on Skin. *Sensors*, 21(4).
- Taji, B., Shirmohammadi, S., Groza, V. & Batkin, I. (2013). Impact of Skin-Electrode Interface on Electrocardiogram Measurements Using Conductive Textile Electronics. *IEEE Transaction on Instrumentation and Measurements*.
- Takano, A., Ishigami, H. & Ueno, A. (2021). Non-Contact Measurements of Electrocardiogram and Cough-Associated Electromyogram from the Neck Using In-Pillow Common Cloth Electrodes: A Proof-of-Concept Study. *Sensors*, 21(3), 812.
- Tang, R., Huang, H., Tu, H., Liang, H., Liang, M., Song, Z., Xu, Y., Jiang, H., & Yu, H. (2014). Origami-enabled deformable silicon solar cells. *Applied Physics Letters*, 104(083501).
- Tao, J., Khosravi, H., Deshpande, V. & Li, S. (2022). Engineering by Cuts: How Kirigami Principle Enables Unique Mechanical Properties and Functionalities. *Advanced Science*.

- Tuncel, Y., Bhat, G. & Ogras, U. Y. (2020). Special Session: Physically Flexible Devices for Health and Activity Monitoring: Challenges from Design to Test. *2020 IEEE 38th VLSI Test Symposium (VTS)*.
- Ueno, A., Akabane, Y., Kato, T., Hoshino, H., Kataoka, S. & Ishiyama, Y. (2007). Capacitive Sensing of Electrocardiographic Potential Through Cloth From the Dorsal Surface of the Body in a Supine Position: A Preliminary Study. *IEEE Transactions on Biomedical Engineering*, 54(4), 759 - 766.
- Uguz, D. U., Dettori, R., Napp, A., Walter, M., Marx, N., Leonhardt, S. & Antink, C. H. (2020). Car Seats with Capacitive ECG Electrodes Can Detect Cardiac Pacemaker Spikes. *Sensors*, 20(21), 6288.
- Venkatachalam, K. L., Herbrandson, J. E. & Asirvatham, S. J. (2011). Signals and Signal Processing for the Electrophysiologist - Part I: Electrogram Acquisition. *Circulation: Arrhythmia and Electrophysiology*, 4(6).
- Wang, P., Hu, M., Wang, H., Chen, Z., Feng, Y., Wang, J., Ling, W. & Huang, Y. (2020a). The Evolution of Flexible Electronics: From Nature, Beyond Nature, and To Nature. *Annals of Biomedical Engineering*, 7(20), 2001116.
- Wang, T. W., Zhang, H. & Lin, S. F. (2020b). Influence of Capacitive Coupling on High-Fidelity no.-Contact ECG Measurement. *IEEE Sensors Journal*, 20(16).
- Wang, Z. L. & Wang, A. C. (2019). On the origin of contact-electrification. *Materials Today*, 30, 34-51.
- Wang, Z. L., Guo, R., Li, G. R., Lu, H. L., Liu, Z. Q., Xiao, F. M., Zhang, M. & Tong, Y. X. (2012). Polyaniline nanotube arrays as high-performance flexible electrodes for electrochemical energy storage devices. *Journal of Material Chemistry*, (6).
- Wartzek, T., Lammersen, T., Eilebrecht, B., Walter, M. & Leonhardt, S. (2011). Triboelectricity in Capacitive Biopotential Measurements. *IEEE Transactions on Biomedical Engineering*, 58(11), 1268-1277.
- Webster, J. (1977). Interference And Motion Artifact In Biopotentials. *IEEE 1977 Region Six Conference Record*.
- Wiklund, J., Karakoç, A., Palko, T., Yiğitler, H., Ruttik, K., Jäntti, R. & Paltakari, J. (2021). A Review on Printed Electronics: Fabrication Methods, Inks, Substrates, Applications and Environmental Impacts. *Journal of Manufacturing and Materials Processing*, 5(3).

- Wissman, J. P., Sampath, K., Freeman, S. E., & Rohde, C. A. (2019). Capacitive Bio-Inspired Flow Sensing Cupula. *Sensors*, 19(11), 2639.
- Wrasse, A. D. N., Bertoldi, D., Santos, E. N. D., Morales, R. E. M. & Silva, M. J. D. (2019). Gas–Liquid Flow Rate Measurement Using a Twin-Plane Capacitive Sensor and a Venturi Meter. *IEEE Access*, 7, 135933 - 135941.
- Wu, X. & Yao, S. (2017). Flexible Electrode Materials Based on WO₃ Nanotube Bundles for High-Performance Energy Storage Devices. *Nano Energy*, 42, 143-150.
- Xiang, Y. (2006). The electrostatic capacitance of an inclined plate capacitor. *Journal of Electrostatics*, 64(1), 29-34.
- Xiang, Y. (2008). Further study on electrostatic capacitance of an inclined plate capacitor. *Journal of Electrostatics*, 66(7-8), 366-368.
- Xiao, Z., Xing, Y., Yang, C., Li, J. & Liu, C. (2022). Non-Contact Electrocardiograms Acquisition Method Based on Capacitive Coupling. *IEEE Instrumentation Measurement Magazine*, 25(2).
- Xu, R., Zverev, A., Hung, A., Shen, C., Irie, L., Ding, G., Whitmeyer, M., Ren, L., Griffin, B., Melcher, J., Zheng, L., Zang, X., Sanghadasa, M. & Lin, L. (2018). Kirigami-inspired, highly stretchable microsupercapacitor patches fabricated by laser conversion and cutting. *Microsystem and Nanoengineering*, 4(36).
- Yan, J., Chen, A. & Liu, S. (2024). Flexible sensing platform based on polymer materials for health and exercise monitoring. *Alexandria Engineering Journal*, 86.
- Yang, C., Zhang, H., Liu, Y., Yu, Z., Wei, X. & Hu, Y. (2018). Kirigami-Inspired Deformable 3D Structures Conformable to Curved Biological Surface. *Advanced Science*, 5(12).
- Yang, E. C., Chen, Y. W., Wu, J. Y., Chen, R. & Lon, C. Y. (2021). Enhancing the Detection Sensitivity in Capacitive Tactile Sensors With Optimized Electrode Shapes. *IEEE Sensors Journal*, 21(23), 26294-26303.
- Yang, S., Choi, I. S. & Kamien, R. D. (2016). Design of super-conformable, foldable materials via fractal cuts and lattice kirigami. *MRS Bulletin*, 41, 130-138.
- Yu, H. C., Hao, X. P., Zhang, C. W., Zheng, S. Y., Du, M., Liang, S., Wu, Z. L. & Zheng, Q. (2021). Engineering Tough Metallosupramolecular Hydrogel Films with Kirigami Structures for Compliant Soft Electronics. *Small*, 17(41).

- Yu, J., Yu, H., Zhou, P., Zou, W. & Liu, L. (2019). Fabrication of a Flexible Capacitive Pressure Sensor Using Full Inkjet Printing. *2019 IEEE 9th Annual International Conference on CYBER Technology in Automation, Control, and Intelligent Systems (CYBER)*.
- Yun, S. M., Kim, M. H., Kwon, Y. W., Kim, H. B., Kim, M. J., Park, Y. G. & Park, J. U. (2021). Recent Advances in Wearable Devices for Non-Invasive Sensing. *Applied Sciences*, 11(3), 1235.
- Zhai, Z., Wu, L. & Jiang, H. (2021). Mechanical metamaterials based on origami and kirigami. *Applied Physics Reviews*, 8(041319).
- Zhang, H., Liu, X., Li, H., Chen, N. & Fu, Y. (2013). Effect of the surface roughness on the detecting capacitance. *Key Engineering Materials*, 562-565, 1461-1466.
- Zhang, H., Yao, L., Quan, L. & Zheng, X. (2020). Theories for triboelectric nanogenerators: A comprehensive review. *Nanotechnology Reviews*, 9(1), 610-625.
- Zhang, S., Wang, S., Zheng, Y., Yang, R., Dong, E., Lu, L., Xuan, S. & Gong, X. (2021). Coaxial 3D-Printed and kirigami-inspired deployable wearable electronics for complex body surfaces. *Composites Science and Technology*, 216.
- Zhou, D., Sharma, S. K., Lüttgen, A. & Sarr, C. (2020a). Systematic Design Optimization of Capacitive Touch Sensor Electrode Patterns. *IEEE Sensors Journal*, 20(4), 1962-1970.
- Zhou, L., Liu, D., Wang, J. & Wang, Z. L. (2020b). Triboelectric nanogenerators: Fundamental physics and potential applications. *Friction*, 8, 481–506.
- Zou, H., Zhang, Y., Guo, L., Wang, P., He, X., Dai, G., Zheng, H., Chen, C., Wang, A. C., Xu, C. & Wang, Z. L. (2019). Quantifying the triboelectric series. *Nature Communications*, 10(1427).